(NASA-CR-155736) HIGH RESOLUTION 10 MU SPECTROMETRY AT DIFFERENT PLANETARY LATITUDES. A PRACTICAL HADAMARD TRANSFORM SPECTROMETER FOR ASTRONOMICAL APPLICATION Final Report, 1 Sep. 1973 - (Cornell Univ., G3/91 N78-17976 Unclas 05334

CORNELL UNIVERSITY

Center for Radiophysics and Space Research

ITHACA, N.Y.

CRSR 686

FINAL REPORT

for

HIGH RESOLUTION 10μ SPECTROMETRY AT DIFFERENT PLANETARY LATITUDES

NASA Grant NGR 33-010-210

September 1, 1973 through April 28, 1977

Principal Investigator: Prof. Martin Harwit

FINAL REPORT

for

HIGH RESOLUTION 10μ SPECTROMETRY AT DIFFERENT PLANETARY LATITUDES

NASA Grant NGR 33-101-210

September 1, 1973 through April 28, 1977

Principal Investigator: Prof. Martin Harwit
CRSR
Cornell University
Ithaca, New York 14853

1. Introduction

Jupiter's bands are a clear indication of atmospheric differences at different lattitudes on the planet. The aim of the present study was to attempt infrared observations at different lattitudes in order to obtain spectra in the 10μ region. These spectra might then help one to understand differences in chemical composition or physical structure of the well known optical features.

In order to obtain such spectra of a rotating planet, it seemed well to attempt simultaneous observations at different lattitudes. We planned to use a Hadamard transform spectrometer with 15 entrance slits in order to obtain 15 simultaneous spectra, at a resolution of 0.01μ. The spectral band covered contained 255 spectral elements.

2. Results

The results obtained during the course of the study are covered in ten publications which include seven journal articles, two general review papers, and a Ph.D. thesis. These publications are listed in section 3 below. The thesis which is the best single summary of the work done under the present contract appears as the Appendix to this report.

The publications fall into two main groups: those that deal with technical aspects of the instrumentation we had to develop in order to make observations; and those that deal with observational work.

The technical difficulties encountered turned out to be rather more severe than had been initially anticipated. Many of the problems we had to solve are of a very general nature that applies to other varieties of multiplex instrumentation, as well as to other classes of Hadamard transform spectrometers. As a result, all the technically innovative work was of sufficiently general interest to warrant publication.

The astronomical observations that were undertaken are described in the thesis of Ming-Hing Tai, the graduate student who worked on the project (see Appendix). The results cited there represent the first observations undertaken with our instrument. The instrument did in fact perform with the spectral resolving power and the number of spatial and spectral elements we had anticipated in our design. Because of the above mentioned technical difficulties, we suffered considerable delays in in initiating observations. Ultimately we therefore had to content ourselves with far less observing time than we had originally hoped to obtain, and the observational side of the program had to be carried out at far more modest levels than anticipated because important technical requirements had drained a disproportionately large fraction of our available funds.

Despite these setbacks, however, we feel that the results obtained--while not precisely in line with what we had set out to do--are interesting, led to a large number of publications, and constitute a worthwhile contribution to observational planetary science.

3. Publications

1. Two asymmetric Hadamard transform spectrometers, Martin Harwit, Perry G. Phillips, Leon W. King, and Daniel A. Briotta, Jr. Applied Optics, 13, 2669 (1974).

2. Infrared astronomy and the shuttle, Martin Harwit, Astronautics and Aeronautics 12, 23 October (1974) 1.

3. Masks for Hadamard transform optics, and weighing designs, Neil J. A. Sloane and Martin Harwit, Applied Optics 15, 207 (1976).

4. A practical multi-spectrum Hadamard transform spectrometer, Ming Hing Tai, D. A. Briotta, Jr., N. Kamath and Martin Harwit, Applied Optics 14, 2533 (1975).

5. Errors in Hadamard spectroscopy or imaging caused by imperfect masks, Ming Hing Tai, Martin Harwit and Meil J. A. Sloane, Applied Optics 14, 2678 (1975).

6. Fourier and Hadamard transform spectrometers: a limited comparison, Ming Hing Tai and Martin Harwit, Applied-Optics 15, 2664 (1976).

7. "Hadamard Transform Analytical Systems", Martin Harwit, to be published in "Transformations in Analytical Chemistry," P. Griffiths, Ed., Plenum Press (1978).

8. Fourier and Hadamard transform spectrometers: a limited comparison II. M. Harwit and Ming Hing Tai, Applied Optics 16, 3070 (1977).

9. Distortion in Hadamard Transform Optics, N.J.A. Sloane, Martin Harwit and Ming-Hing Tai, accepted for publication, Applied Optics (1978).

10. A practical Hadamard transform spectrometer for astronomical application, Ming-Hing Tai, Cornell University Ph.D. thesis and Center for Radiophysics and Space Research Report CRSR 655 (1977).

4. Personnel Participating on the Grant

Prof. M. Harwit, principal investigator

Mr. Ming Hing Tai, graduate student

Mr. Gary Melnick, graduate student

Mr. Frank W. Dain, undergraduate student (part time)

Mr. Gerald Stasavage, research technician (part time)

Mr. Daniel A. Briotta, Jr., graduate student (part time)

Mr. Leon W. King, graduate student (part time)

Mr. Narayana Kameth, programmer (part time)

5. Financial Status

All funds provided under this contract have been spent by this time.

CENTER FOR RADIOPHYSICS AND SPACE RESEARCH

CORNELL UNIVERSITY

ITHACA, NEW YORK

January, 1977

A PRACTICAL HADAMARD TRANSFORM SPECTROMETER FOR ASTRONOMICAL APPLICATION

by

Ming-Hing Tai

DEDICATION

To my parents

献给 爸爸、妈妈

ACKNOWLEDGEMENTS

This project is by no means one man's product. Many people have devoted their talents to the completion of this project. I am just the one to make a summary of it.

My special thanks go to Prof. Martin Harwit, my thesis advisor. Martin set himself up as an admirable example: he always moved the heaviest equipment himself; tackled the most difficult jobs in the experiment so that he himself was responsible for any misfortunes; was earnest in discussions about problems with his student; and was modest in sharing the credit for the results. Above all, he truly expressed concern about his student, as a respectable advisor and as a warm friend.

My second thanks go to Dr. Daniel A. Briotta. Dan helped to automize the whole process and taught me the mini computer technique. Dan has shown me how to run the computer as though he were showing me how the lines in his palm run.

My thanks also go to the infrared astronomy group at Cornell. Prof. J. Houck has served on my committee and has always been available for discussion of astronomical and experimental problems. I especially thank him for his help in finishing up my degree while Martin was on sabbatical leave. Dr. Phillips built the spectrometer. The late L. King modified it. G. Stasavage built some electronic parts and H. Kondracki built the dewer. G. Melick helped with the observation, data processing and electronic parts, G. Gull with the field trip, and Drs. W. Forrest, Diward, and D. Shacck were involved in many valuable discussions. Thanks also go to Westy Dain for not only being always willing to help on chilly night's observations and tedious laboratory work, but also for proof reading my thesis.

I thank Prof. E.E. Salpeter for serving on my committee, Prof. A. Siever and Allen Chin for helping the He_3 cooled dewer, and Prof. P. Gierasch for always being available for discussing astronomical problems. I also thank G. Vincent for building many mechanical parts, B. Boettcher for figures and Eckelmaun for photographs.

The author thanks the staffs of the Kitt Peak National Observatory and McDonald Observatory for generous allotments of observing time and for assistance during the observing runs.

Finally, my thanks go to Divan Sun, Adeline Wu, and W.W. Chiu, for typing the thesis for me, and to N.H. Cheung, K.K. Mon, K.M. Lo and many of my Chinese friends for their continual help during these years.

Portions of this work were supported by the NGR 33-010-210 and NSG 1263.

TABLE OF CONTENTS

LIST OF FIGURES

LIST OF TABLES

忆 秦 娥

娄 山 关

一九三五年二月

西风烈，
长空雁叫霜晨月。
霜晨月，
马蹄声碎，
喇叭声咽。

雄关漫道真如铁，
而今迈步从头越。
从头越，
苍山如海，
残阳如血。

毛泽东主席

CHAPTER I

HISTORICAL INTRODUCTION TO HADAMARD TRANSFORM SPECTROMETRY (HTS)

The idea of modulating or encoding the optical output of a spectrometer goes back to the original work of Golay (1949) and Fellgett (1951). Its purpose is to allow many different wavelengths of radiation to fall on a detector simultaneously, and thereby to increase the signal-to-noise ratio (SNR) of the resulting spectrum. This improvement comes about because each element of the spectrum is effectively viewed a larger fraction of the total available observing time. One idea is to encode or modulate each spectral wavelength exiting the spectrometer output with an audio frequency that contains the optical wavelength information. The use of a conventional wave analyzer then allows recovery of the original optical spectrum. There are many variations of this technique.

In 1968, Ibbett *et al* and Decker *et al* independently suggested the use of sequentially stepped multiplex spectrometers. In both systems radiation enters a dispersive instrument through a single slit and is analyzed at a number of exit slits. Decker *et al* pointed out that two constraints should be imposed on the encoding scheme:

(1) To obtain the optimum signal to noise ratio, each spectral element should be viewed during exactly half the step positions.

(2) To impose the smallest dynamic range requirements on the

detector amplifier system, each step position should pass light from exactly half the spectral elements. They also worked out a scheme that satisfied the two constraints for masks having elements m=4n+2, where n is an arbitrary integer or zero. Ibbett et al introduced the Hadamard pattern for the mask. As discussed below, this is a pattern based on a set of binary orthogonal matrices first studied by the French mathematician Jacques Hadamard. Ibbett et al also described the application of their scheme to a real time computer aided measurement.

In 1969, Sloane et al worked out a number of binary cyclic coding schemes for multiplex spectrometry and evaluated the performance of each scheme in terms of a linear, least mean square, unbiased estimate. These schemes include a Hadamard matrix H, and various modified Hadamard matrices, which these authors refer to as G matrix and S matrix (Fig. 1-1).

A Hadamard matrix H of order N is an N x N matrix H_N of +1's and -1's which satisfies:

$$H_N H_N^T = N I_N$$

where I_N is an N x N unit matrix

A modified Hadamard matrix G of order M is a partitioned matrix from the H matrix:

$$\underline{H} = \begin{bmatrix} 1 & \cdots & 1 \\ \vdots & & \\ \vdots & \underline{G} & \\ \vdots & & \\ 1 & & \end{bmatrix} \qquad (M = N-1)$$

$$\underline{H} = \begin{bmatrix} + & + & + & + & + & + & + & + \\ + & + & + & - & - & - & + & - \\ + & + & - & - & - & + & - & + \\ + & - & - & - & + & - & + & + \\ + & - & - & + & - & + & + & - \\ + & - & + & - & + & + & - & - \\ + & + & - & + & + & - & - & - \\ + & - & + & + & - & - & - & + \end{bmatrix}$$

$$\underline{G} = \begin{bmatrix} + & + & - & - & - & + & - \\ + & - & - & - & + & - & + \\ - & - & - & + & - & + & + \\ - & - & + & - & + & + & - \\ - & + & - & + & + & - & - \\ + & - & + & + & - & - & - \\ - & + & + & - & - & - & + \end{bmatrix}$$

$$\underline{S} = \begin{bmatrix} 0 & 0 & 1 & 1 & 1 & 0 & 1 \\ 0 & 1 & 1 & 1 & 0 & 1 & 0 \\ 1 & 1 & 1 & 0 & 1 & 0 & 0 \\ 1 & 1 & 0 & 1 & 0 & 0 & 1 \\ 1 & 0 & 1 & 0 & 0 & 1 & 1 \\ 0 & 1 & 0 & 0 & 1 & 1 & 1 \\ 1 & 0 & 0 & 1 & 1 & 1 & 0 \end{bmatrix}$$

Figure 1-1. An 8 x 8 Hadamard matrix and two 7 x 7 cyclic matrices that can be derived from it.

where the first row and first column of H are all +1's. A feature of the G matrix is that it can be written in cyclic form-- a factor which we will show to be of considerable practical importance.

A modified Hadamard matrix S is a matrix obtained from G by replacing +1's by 0's and -1's by +1's.

The properties of H, G, and S will be discussed in section 2-6.

When we talk of encoding by means of a Hadamard matrix we have the following in mind. A mask is used to modulate - open or close - a series of entrance and exit slits in a spectrometer. If a certain slit location is open, we can designate it by a +1; if it is closed we can designate it by a 0; if it can be used to subtract from the signal incident on the detector, we designate it by -1. The sequence of +1's and -1's characterizing a mask in a given modulating position corresponds to a row of a matrix. The whole set of mask positions corresponds to the set of rows of the matrix. If the sequence of mask patterns corresponds to the rows of a Hadamard matrix we say we are encoding with a Hadamard pattern.

Sloane *et al* also introduced the idea of using a cyclic matrix for coding masks. This greatly decreases the experimental cost and facilitates operation, since any N slits of a single mask 2N-1 slits long can be used to provide one of the required mask patterns.

The first single entrance Hadamard spectrometer (HTS) was built by Decker and Harwit (1969). The spectrometer had a single entrance slit and 19 exit slits. The exit mask was stepped manually. The authors used this spectrometer to take the spectrum of the mercury vapor 1.7μ band to demonstrate the Hadamard transformed spectrum's fidelity and freedom from systematic errors.

With 19 exit slits, the HTS had a theoretical signal-to-noise advantage of 2.18 over the conventional spectrometer, which is rather hard to verify experimentally, Decker (1971) therefore proceeded to build a 255-slit HTS. In this spectrometer, the radiation, after being decoded by the exit mask, exits along the same path it comes in. This reverse pass de-disperses the beam and allows it to be brought to a focus at the entrance plane. Thus the dimensions of the focused image are roughly the same as the dimensions of the entrance aperture, and the detector size can be minimized. This is important since sufficiently large detectors sometimes do not exist, and if available tend to be noisy. Decker experimentally verified the theoretically predicted multiplex advantage of an HTS.

DeGraauw and Veltman (1970) were the first to use an HTS for astronomical work during the 1970 solar eclipse. Houck et al (1973) subsequently used an HTS to obtain near infrared spectra of Mars from airplane altitudes.

Besides putting an encoding mask at the exit plane, one can also put another encoding mask at the entrance plane of a spectrometer. In that way the radiation is modulated at both the entrance and exit apertures. Harwit et al (1970) worked out this scheme of doubly multiplexed dispersive spectrometry. The double multiplexing scheme allows one to increase the total amount of radiation that can be transmitted through a spectrometer. Furthermore, by a proper reduction of the data, one can also obtain a one dimensional picture of the source at the entrance plane. For a spectrometer of m entrance slits and n exit slits, one needs m x n data points to recover m spatial spectra, with each spatial spectrum containing n spectral elements. For a homogeneous source one does not need the spatial information, so (n + m - 1) data points will be enough to recover the spectra. Harwit et al (1974a)describe two schemes for recovering the spectrum with (n + m - 1) data points.

In 1975 Tai et al (1975a) finished the construction of a doubly coded Hadamard transform spectrometer. The spectrometer has 15 entrance slits and 255 exit slits, which can simultaneously obtain 15 spatial spectra, each having 255 spectral elements. Tai et al (1975b) went on to give an analysis of the errors in Hadamard spectrometry caused by imperfect masks.

Besides coding the radiation at both the entrance and the exit aperture, one can go one step further and use a two dimensional mask at the entrance aperture (Harwit, 1971). This yields a two dimensional picture at the entrance aperture, where each spatial point at the entrance has its own spectrum. To put it a different way, one obtains a two dimensional picture of the source at the entrance aperture for each color of the spectral elements.

Harwit (1973) experimentally verified the operation of imaging spectrometry, and Swift et al (1976) constructed the first Hadamard imaging spectrometer.

There are other discussions of Hadamard transform spectrometry in the literature, mostly of theoretical aspects. Nelson and Fredman (1970) give a more complete theoretical treatment of Hadamard matrix encoding. They also rediscovered a theorem due initially to Hotelling (1944) showing that the Hadamard matrix is the best design for a singly coding mask. Sloane and Harwit (1976) show the connection between Hadamard spectrometry and the mathematics of weighing designs in statistics.

There have been various comparisons of Hadamard transform spectrometry with other spectrometry. Larson et al (1974) makes a theoretical comparison of singly multiplexed Hadamard transform spectrometers and scanning spectrometers. They present a general mathematical framework for the comparison of relative performance and also verify their prediction by computer simulation of various characteristic spectra. Their results show that where the noise level is constant and independent of the incident photon flux, the determined multiplex advantage is $\sqrt{N/2}$, as predicted by Fellgett (1951). This is usually the case in a low energy region, such as the infrared. For a noise level that is signal-dependent, such as in the UV energy region, the detector is characterized by an output with statistics approaching a Poisson distribution and variance therefore proportional to the input signal. In that case the

HTS technique will be advantageous only for spectra that are characterized by a few well-defined and intense peaks on a very low intensity background. For spectra with high background, for dense spectra, or for spectra having very weak spectral features, the HTS will have no advantage over the conventional single slit (SS) technique.

Hirschfeld and Wyntjes (1973) compare Fourier transform and Hadamard transform spectrometry. They also describe various limitations of Hadamard transform spectrometry. This paper was followed by an exchange of notes between Decker (1973) and Hirschfeld and Wyntjes (1973) in the journal Applied Optics in which some of these limitations are disputed. These papers concern themselves with a number of practical matters on which opinions can vary. Here we mention these controversial papers mainly for completeness. Their contents will be discussed further below.

Wyatt and Esplin (1974) analyzed the effect of band width on noise equivalent power (NEP) for multiplex spectrometry with cryogenically cooled, cooled-background extrinsic long wavelength infrared detectors. They find that the NEP is directly proportional to band width, so multiplex schemes that require increased band width are not of real advantage. They further conclude that doubly encoded systems that are based on $m + n - 1$ measurements would have a real throughput advantage

Various other aspects of Hadamard matrices and Hadamard transform spectrometry which have not been mentioned above are covered in articles by: Baumert, Pratt et al (1969), Hirschy _et al_ (1971), Allen _et al_ (1972,1973), Kowalski _et al_ (1973), Planky _et al_ (1974), Oliver _et al_ (1974).

In this thesis Chapter II will describe the mathematical properties of Hadamard matrices and their application to spectroscopy. Chapter III describes the Hadamard transform spectrometer, and gives results on laboratory performance. Chapter IV gives a comparison of Hadamard transform and Fourier transform encoding in spectrometry. The output of an HTS is fed into a mini computer. The computer performs a real time inverse Hadamard transform to recover the spectrum. Chapter V describes the algorithm and programming of inverse Hadamard transform. Chapter VI discusses observational results and their interpretation.

CHAPTER II

HADAMARD MATRICES

(A) Weighing Designs

In order to understand the mathematical advantage of Hadamard transform encoding, let us look at the following examples (Sloane et al, 1976).

Suppose four objects are to be weighed, using a spring balance which makes an error e each time it is used. Assume that e is a random variable with mean zero and variance σ^2.

First suppose the objects are weighed separately. If the unknown weights are ψ_1, ψ_2, ψ_3, ψ_4, the measurements are η_1, η_2, η_3, η_4, and the errors made by the balance are e_1, e_2, e_3, e_4, then the four weighings give four equations:

$$\eta_1 = \psi_1 + e_1 \qquad \eta_2 = \psi_2 + e_2$$

$$\eta_3 = \psi_3 + e_3 \qquad \eta_4 = \psi_4 + e_4 \quad .$$

The best estimate of the unknown weights are the measurements themselves:

$$\hat{\psi}_1 = \eta_1 = \psi_1 + e_1$$

$$\hat{\psi}_2 = \eta_2 = \psi_2 + e_2$$

These are unbiased estimates:

$$E\hat{\psi}_1 = \psi_1$$

$$E\hat{\psi}_2 = \psi_2 \qquad \text{(E denotes expected value)}$$

with variance or mean square error

$$E(\hat{\psi}_1 - \psi_1)^2 = E\sigma_1^2 = \sigma^2$$

On the other hand, suppose the balance is a chemical balance with two pans, and the four weighings are made as follows:

$$\begin{aligned} \eta_1 &= \psi_1 + \psi_2 + \psi_3 + \psi_4 + e_1 \\ \eta_2 &= \psi_1 - \psi_2 - \psi_3 - \psi_4 + e_2 \\ \eta_3 &= \psi_1 + \psi_2 - \psi_3 - \psi_4 + e_3 \\ \eta_4 &= \psi_1 - \psi_2 - \psi_3 + \psi_4 + e_4 \qquad (2\text{-}1) \end{aligned}$$

This means that in the first weighing all four objects are placed in the left hand pan, and in the other weighings two objects are in the left pan and two in the right. (Note that the e are independent of the weights on the balance. This point is crucial). It is easy to solve for ψ_1, ψ_2, ψ_3, ψ_4, as long as the coefficient matrix for ψ is not singular. Thus the best estimate for ψ_1 is

$$\hat{\psi}_1 = \tfrac{1}{4}(\eta_1 + \eta_2 + \eta_3 + \eta_4)$$
$$= \psi_1 + \tfrac{1}{4}(e_1 + e_2 + e_3 + e_4)$$

The variance of Ce, here C is a constant, is C^2 times the variance of e, and the variance of a sum of independent random variables is the sum of the individuals variances. Therefore the variance of $\hat{\psi}_1$ (and also of $\hat{\psi}_2$, $\hat{\psi}_3$, $\hat{\psi}_4$) is $\frac{4\sigma^2}{16} = \frac{\sigma^2}{4}$

Weighing the objects together has reduced the mean square error by a factor of 4. In effect the signal to noise ratio (SNR), which is given by the root mean square (rms) error is reduced by a factor of 2.

Finally, suppose the balance is a spring balance with only one pan, so only coefficients 0 and 1 can be used. A good method of weighing the four objects is:

$$\begin{aligned}
\eta_1 &= \qquad\quad \psi_2 + \psi_3 + \psi_4 + e_1 \\
\eta_2 &= \psi_1 + \psi_2 \qquad\qquad\quad + e_2 \\
\eta_3 &= \psi_1 \qquad\quad + \psi_3 \qquad + e_3 \\
\eta_4 &= \psi_1 \qquad\qquad\qquad + \psi_4 + e_4 \qquad (2\text{-}2)
\end{aligned}$$

In this case the variances of ψ_1, ψ_2, ψ_3, ψ_4, are $\frac{4\sigma^2}{9}$, $\frac{7\sigma^2}{9}$, $\frac{7\sigma^2}{9}$, $\frac{7\sigma^2}{9}$ respectively, a smaller improvement than in the previous case.

The theory of weighing designs is of immediate interest to multiplex optics, since the simultaneous measurement of the intensities of different bundles of rays is completely analogous to the simultaneous weighing of different groups of weights. In measuring the intensity of radiation passed through slits in a mask, we are effectively 'weighing' that radiation.

(B) General Mathematical Formulation

One can put the problem into a more general form. Let ψ_i be the i^{th} unknown, η_j be the j^{th} measurement, e_j be the error associated with the j^{th} measurement. Let w_{ji} be the weighing coefficient of the j^{th} measurement with the i^{th} unknown. Then

$$\eta_j = w_{ji}\psi_i + e_j \qquad \begin{matrix} i=1\cdots\cdots n \\ j=1\cdots\cdots n \end{matrix} \qquad (2\text{-}3)$$

In matrix notation:

$$\underline{\eta} = \underline{W}\,\underline{\psi} + \underline{e} \qquad (2\text{-}4)$$

With the notation < > for ensemble averages, the error e_i has the following properties:

(1) $\langle e_i \rangle = 0$

(2) e_i is independent of $\underline{\psi}$

(3) $\langle e_i e_j \rangle = 0$ if errors are assumed to be uncorrelated.

$= \sigma^2$ if $i=j$

The problem now is the following: (i) For a particular coding matrix W, what should be the decoding matrix A? i.e. What is A such that $\underline{\hat{\psi}}=\underline{A}\,\underline{\eta}$ where $\underline{\hat{\psi}}$ is an unbiased estimate of $\underline{\psi}$.

(ii) What is the best choice of $\underline{W}$ (or $\underline{A}$) that will minimize the error of measurement i.e. What is $\underline{W}$ such that

$$\varepsilon = \langle \sum_{j=1}^{n} (\hat{\underline{\psi}}_j - \underline{\psi}_j)^2 \rangle$$

is a minimum.

In the absence of noise, i.e. n=0, it is clear from (2-4) that

$$\underline{\psi} = \underline{W}^{-1}\underline{n}$$

and therefore

$$\underline{A} = \underline{W}^{-1}$$

and

$$\hat{\underline{\psi}} = \underline{A}\ \underline{n} = \underline{\psi}$$

In the presence of noise,

$$\hat{\underline{\psi}} = \underline{A}\cdot\underline{n}$$

$$= \underline{A}\ \underline{W}\ \underline{\psi} + \underline{A}\ \underline{n}$$

and with the assumed properties of the noise $\langle\underline{\psi}\rangle = \underline{\psi}$, one obtains

$$\langle\hat{\underline{\psi}}\rangle = \underline{A}\ \underline{W}\ \langle\underline{\psi}\rangle + \underline{A}\langle\underline{e}\rangle$$

$$= \underline{A}\ \underline{W}\ \underline{\psi}$$

Assuming no prior knowledge of the unknowns, one may use the unbiased condition $\langle\hat{\underline{\psi}}\rangle = \underline{\psi}$. This again implies

$$\underline{A} = \underline{W}^{-1}$$

So with the assumed properties of noise and unbiased condition, the decoding matrix is just the inverse of the coding matrix.

One still has to find a coding matrix which will minimize the uncertainty, ε .

The second question can be solved in the following way: Let $\hat{\eta}_i$ be the i^{th} measurement in the absence of noise, then for each measurement

$$\begin{aligned} \eta_i &= W_{i1}\psi_1 + W_{i2}\psi_2 + \cdots + W_{in}\psi_n + e_i \\ &= \hat{\eta}_i + e_i \\ \psi_j &= A_{j1}\eta_1 + A_{j2}\eta_2 + \cdots + A_{jn}\eta_n \\ &= A_{j1}(\hat{\eta}_1 + e_1) + A_{j2}(\hat{\eta}_2 + e_2) + \cdots \\ &\quad + A_{jn}(\hat{\eta}_n + e_n) \\ &= (A_{j1}\eta_1 + \cdots + A_{jn}\eta_n) + (A_{j2}e_2 + \cdots + A_{jn}e_n) \\ &= \psi_j + \text{noise} \end{aligned}$$

The mean square of the noise term corresponding to the j^{th} unknown is therefore

$$\varepsilon_j = (A_{j1}^2 + \cdots + A_{jn}^2)\,\sigma^2$$

$$= \Delta_j^2\,\sigma^2 \qquad (2\text{-}7)$$

where

$$\Delta_j = (A_{j1}^2 + \cdots + A_{jn}^2)^{1/2} \qquad (2\text{-}8)$$

and Δ_j represents the improvement in the SNR for the weighing design, compared to the SNR for individual weighings.

Hence, the problem of maximizing the signal to noise ratio becomes the problem of minimizing ε_j; or Δ_j (Nelson and Fredman (1970)).

Sloane et al (1969) independently developed an expression for ε/σ^2 where

$$\varepsilon/\sigma^2 = \text{Trace } \underline{W}^{-1}(\underline{W}^{-1})^T$$
$$= \text{Trace } \underline{A}\,\underline{A}^T \qquad (2\text{-}9)$$

Equation (2-8) and (2-9) amounts to the same thing because it can be seen very easily that

$$\text{Trace } \underline{A}\,\underline{A}^T = \sum_{j=1}^{n} \Delta_j^2$$

The question of minimizing ε had been answered by Hotelling (Hotelling, 1944) and rediscovered by Nelson and Fredman. Hotelling has shown that for any choice of mask W with $|W_j| \leq 1$, the ε_i are bounded by $\varepsilon_i \geq \frac{\sigma^2}{N}$, and that it is possible to have $\varepsilon_i = \frac{\sigma^2}{N}$ for i=1,... N if and only if a Hadamard Matrix H_N of the order N exists (by taking $W=H_N$). This leads to the discussion of the Hadamard Matrix.

(C) Hadamard Matrix

A Hadamard matrix of order N is an NxN matrix H_N of +1's and -1's which satisfies:

$$\underline{H}_N \underline{H}_N^T = \underline{HI}_N \qquad (2\text{-}10)$$

where I_N is an NxN unit matrix.

A Hadamard matrix has following properties: (Golomb(1964))

(1) Its row vectors (or equivalently, its column vectors) are mutually orthogonal.

(2) The Hadamard properties will not be disturbed by:

a. Interchanging rows,

b. Interchanging columns,

c. Changing the sign of every element in a row, or

d. Changing the sign of every element in column.

These properties enable the first row and column of every Hadamard matrix to be normalized to contain only +1's. If $\underline{G}$ represents the remaining M x M matrix (M= N-1), then $\underline{H}$ can be partitioned into

$$\underline{H} = \begin{bmatrix} 1 & 1 & 1 & 1 & \cdots & 1 \\ 1 & & & & & \\ 1 & & \underline{G} & & & \\ \cdot & & & & & \\ \cdot & & & & & \\ \cdot & & & & & \\ 1 & & & & & \end{bmatrix} \qquad (M= N-1)$$

It is conjectured that Hadamard matrices exist for all multiples of four. Further, if one of the following conditions is also satisfied,

(1) $N = P + 1$ P prime

(2) $N = P(P + 2) + 1$ P and P + 2 prime

(3) $n = 2^m$ m an integer

then $\underline{G}$ can be made cyclic. That is, the $(j + 1)^{th}$ row can be generated by shifting the j^{th} row one position to the left. For example, when N=8, we have matrices of the form shown in Fig. 1-1. Note that $\underline{H}$ and $\underline{G}$ are symmetrix.

Another choice for $\underline{W}$ is the matrix $\underline{S}$ obtained from $\underline{G}$ by replacing +1's by 0's and -1's by +1's.

The properties of the $\underline{H}$, $\underline{G}$ and $\underline{S}$ are discussed by Sloane *et al*. If rows i and j are any two rows of $\underline{H}$, $\underline{G}$ or $\underline{S}$, it can be shown that their dot product is:

$$\text{In } H_N : \text{row } i \cdot \text{row } j = \begin{matrix} 0 & i \neq j \\ N & i = j \end{matrix}$$

$$\text{In } G_M : \text{row } i \cdot \text{row } j = \begin{matrix} -1 & i \neq j \\ M & i = j \end{matrix}$$

$$\text{In } S_M : \text{row } i \cdot \text{row } j = \begin{matrix} M/4 & i \neq j \\ M/2 & i = j \end{matrix}$$

The inverse of each matrix is:

$$\underline{H}_N^{-1} = \frac{1}{N} \underline{H}_N \ ; \ \underline{G}_M^{-1} = \frac{1}{M+1}(\underline{G}_M - \underline{J}_M) \ ; \ \underline{S}_M^{-1} = \frac{2}{M+1}(2\underline{S}_M \ \underline{J}_M)$$

where $\underline{J}$ is a M x M matrix consisting entirely of -1's and N= M+1.

Table 2-1 gives the value of Δ for different matrices. The matrix $\underline{I}$ represents the weighing scheme weighing each object separately. This corresponds to a conventional single slit spectrometer or to a wedge filter monochromator.

Table 2-1

MATRIX A	ELEMENTS OF A	Δ^{-1}	(FOR LARGE N)
$\underline{I}$	1,-0	1	1
$\underline{H}$	1,-1	$\sqrt{N}$	$\sqrt{N}$
$\underline{G}$	1,-1	$\sqrt{N}(2-\frac{2}{N})^{-\frac{1}{2}}$	$\sqrt{\frac{N}{2}}$
$\underline{S}$	1, 0	$\sqrt{N}(2-\frac{2}{N})^{-1}$	$\frac{\sqrt{N}}{2}$
*$\underline{F}$	cosine squared functions	$\frac{N}{4} \frac{2}{N+1}$	$\sqrt{\frac{N}{8}}$

* F is the Fourier Transform case which will be disscussed in Chapter IV.

If the number of measurements N is a multiple of 4, and the matrix coefficients are +1, the best weighing scheme is the Hadamard matrix H. ε will be reduced by a factor $\frac{1}{\sqrt{N}}$ compared to weighing the unknown separately. This is the maximum advantage a weighing scheme can obtain with weighing coefficient $|W_{ij}| \leq 1$. If N is not a multiple of 4, or if the weighing coefficients are 0's and 1's, it is not possible to simultaneously minimize $\varepsilon_1 \ldots \varepsilon_n$ and some other criterion must be used (Sloane et al, 1976). Also the errors are uniformly larger than for the H-matrix, as shown for the G and S matrices in Table 2-1 above.

It is interesting to see that a spectrometer using the Fourier Transform, such as a Michelson interferometer, has a multiplex advantage a factor of $\sqrt{8}$ lower than the H-matrix and a factor of $\sqrt{2}$ lower than the S-matrix encoding instrument.

Following are some computer simulations for S-matrix transformations with various inputs (See Fig. 2-1(a) to (c)).

	INPUT	OUTPUT
1.	Constant	Constant
2.	Hadamard code: representing single line emission	Single line
3.	Single line: 1 at the 1st element and 0 for the rest. This represents an unknown impulse coming in during the	Hadamard code. Note, unlike the monochromater, the error propagates to other

INPUT	OUTPUT
observation.	elements.
4. Sine wave.	sine wave with different phase.
5. Square wave. The input is not a perfect wave because we have an odd number of elements. The input values have amplitudes 0 or 1 for each element.	Not a perfect square wave.
6. Straight line at a slope 1/255. This may represent a shift in baseline.	Refer to figure (2-1C).

(D) Optical Realization of Hadamard Encoding

We have made use of (modified Hadamard) S-matrices in two optical instruments: One is a Hadamard transform spectrometer having an encoding mask at the exit aperture. The other is a doubly encoded HTS which has encoding masks at both the entrance and exit apertures.

S codes can be used for both the entrance and exit masks for the HTS, with +1 standing for an open slot through which radiation is transmitted, and with 0 standing for a closed slot where radiation is blocked.

The cyclic property of the S-matrix is very desirable, for then only a single mask 2N-1 slots wide need be constructed. Successive encoding positions are generated by stepping the mask one slot width along its length. This avoids the consturction of N masks with N^2 slots.

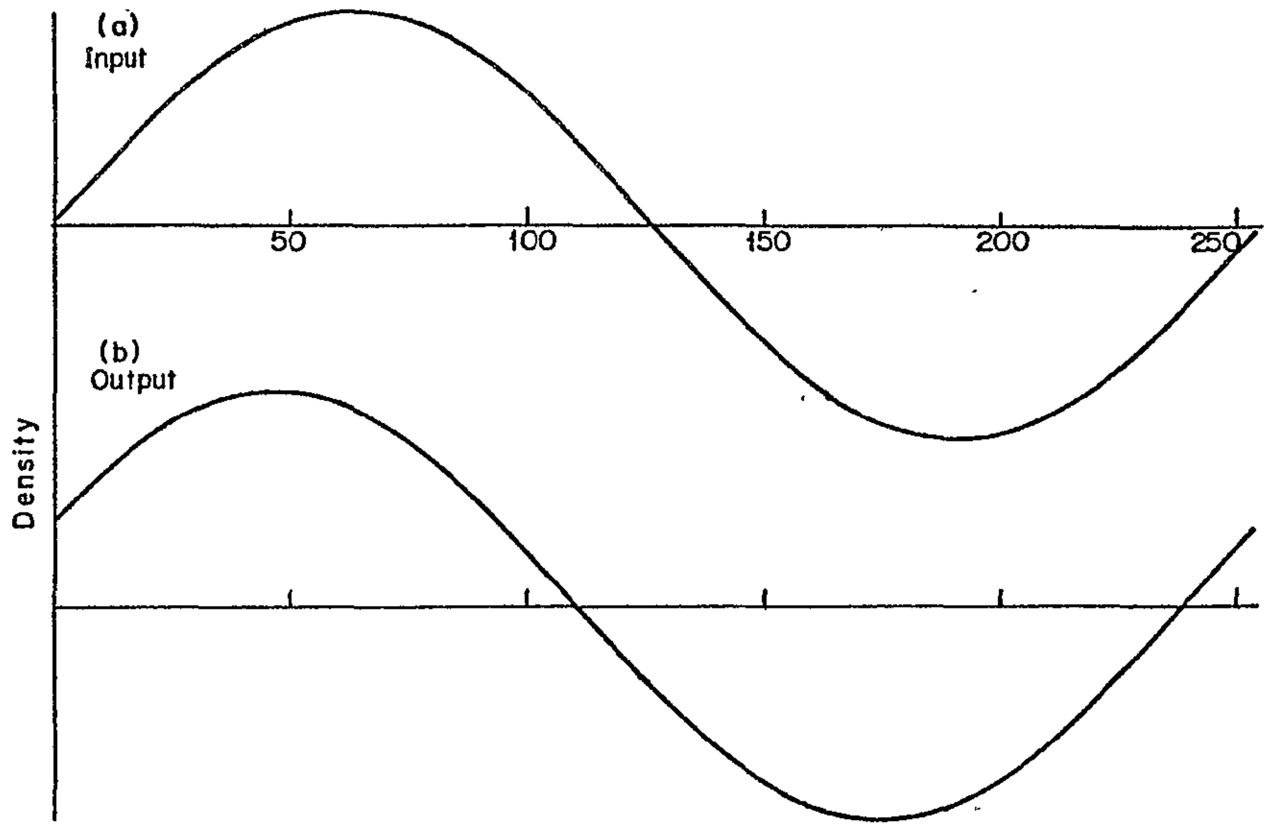

Figure 2-1a. Hadamard transformation of a Sine wave input.

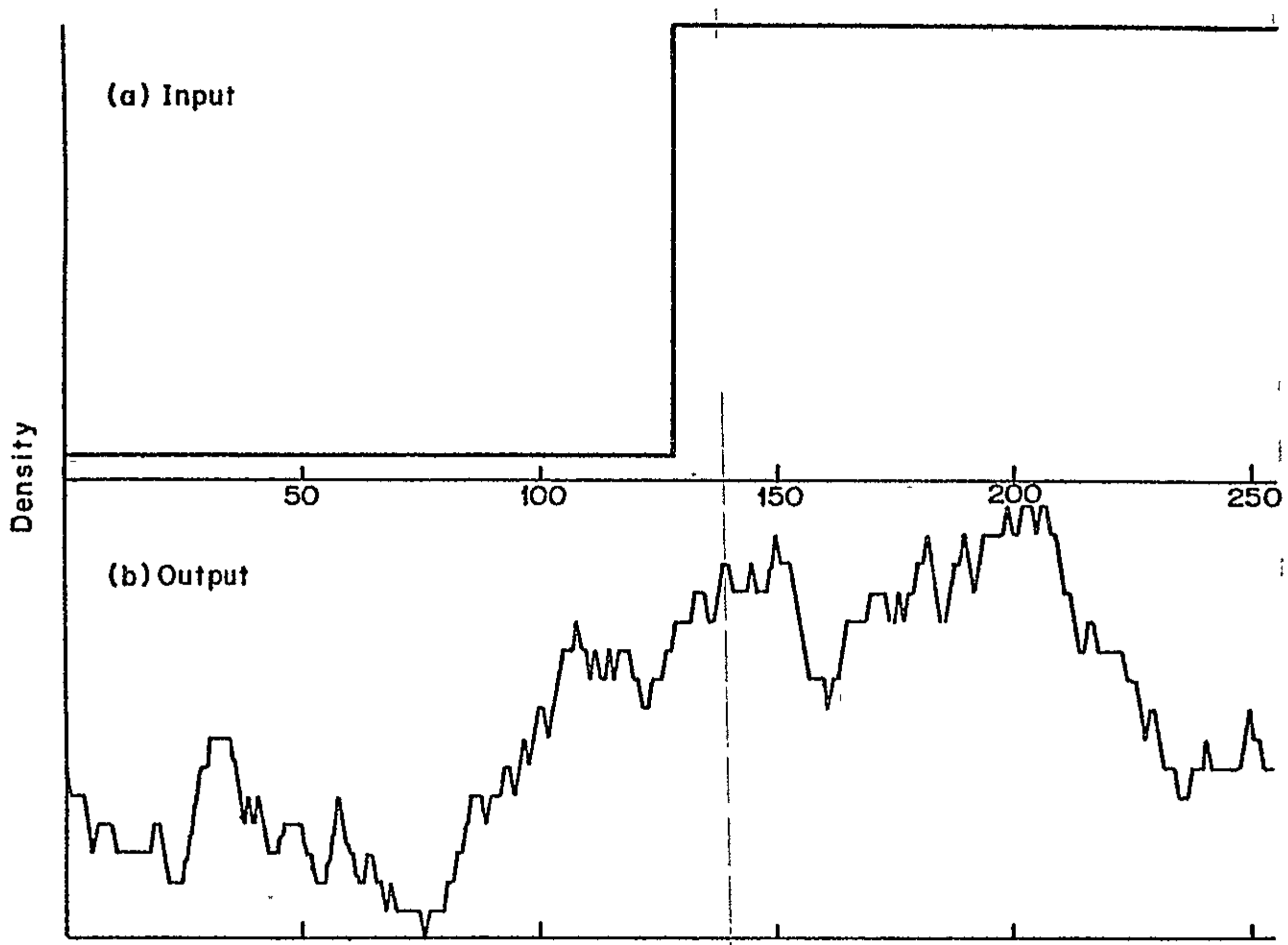

Figure 2-1b. Hadamard transformation of a square wave input

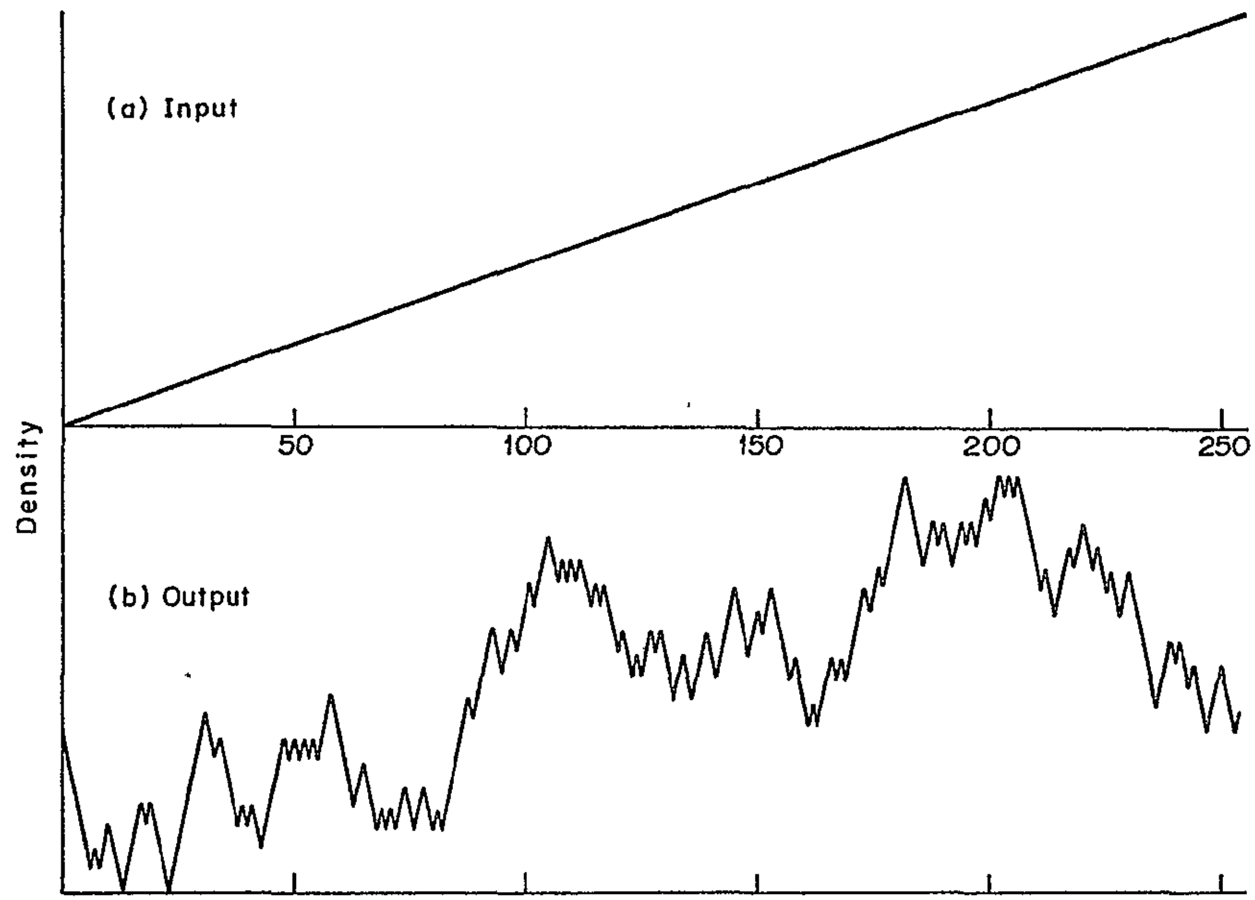

<u>Figure 2-1c</u>. Hadamard transformation of a straight line input.

Although H and G matrices have better coding efficiency than the S matrix, they introduce technical difficulties when used for spectrometer coding schemes. To utilize H and G matrices, one must measure the reflected as well as the transmitted radiation. In this case +1's represent reflecting slots and -1's represent transmitting slots. Therefore a minimum of two detectors must then be used, one in a subtracting mode, the other in the normal mode. The use of two detectors, however, increases the noise. Furthermore, the H matrix, with all elements +1 in the first row, makes the dynamic range of the detector system change by about a factor of two. Also its lack of the cyclic property does not allow one to generate the rest of the masks by the simple stepping technique mentioned above.

1. Hadamard Transform Spectrometer (HTS)

For the singly encoded HTS, we use the following optical arrangement (figure 2-2). Radiation passing through the single entrance slot is rendered parallel and directed to the dispersing element. The dispersed radiation is then de-collimated and focused upon the multi-slot mask at the exit aperture. The spectral elements transmitted by the mask pass through suitable post-optics and are collected onto a detector. One then makes N (in our case N=255) measurements by sequentially stepping the mask N times. The inversion procedure $\underline{\hat{\psi}}=\underline{S}^{-1}\underline{n}$ recovers the spectrum. Figure (2-3) gives a 255 cyclic S-matrix code for the exit mask.

Theoretically, the mean square error in the spectrum

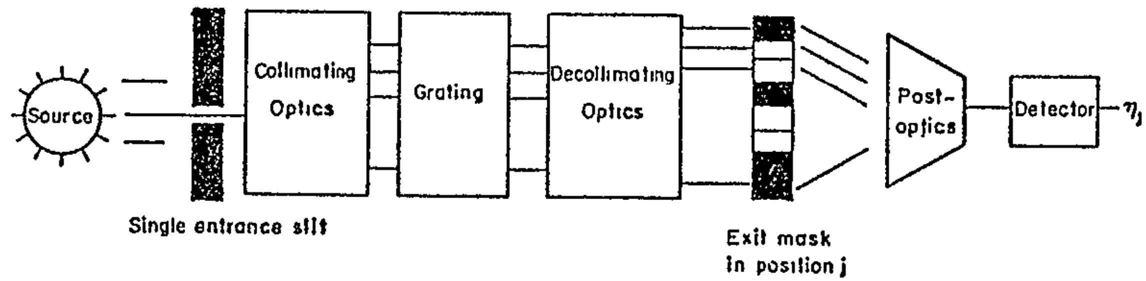

Figure 2-2. Schematic representation of HTS using the S code.

00000	00101	10001	11101	00001	11111	11001	00001
01001	11110	10101	01110	00001	10001	01011	00110
01011	11110	11110	01101	11011	10010	10100	10100
01001	01101	00011	00111	00111	10001	10110	00010
00101	11010	11110	11011	11100	00110	10011	01011
01101	01000	00100	11101	10010	01001	10000	00111
01001	00011	10001					

Figure 2-3. The 509 exit slit mask and the 255-element S code.

given by a monochromator is σ^2. For an HTS using the S code, this error is $\frac{1}{N}(2-\frac{2}{N})^2\sigma^2$ (Sloane et al, 1969). Hence the rms gain in S/N for the HTS is $G= \frac{N\sigma^2}{(2-\frac{2}{N})^2\sigma^2} = \frac{\sqrt{N}}{2-\frac{2}{N}}$. For N=255, $G\sim 8.0$ (figure 2-4 gives Decker's results. The experimental gain was measured as 8.0±0.3). Note that the scale in figure (2-4) are in arbitrary units, and the zero point appears to be shifted between parts (a) and (b).

2. Doubly Encoded Hadamard Transform Spectrometer (DHTS)

Figure (2-5) is a schematic representation of an optical system which has a number of entrance as well as exit slits. Instead of passing radiation through only one entrance slit, a mask M slits wide is placed at the entrance aperture. Radiation passed into the spectrometer through different combinations of open and closed slits. The dispersed radiation at the exit plane is analyzed in the same fashion as in the HTS. Encoding is accomplished by sequentially stepping one of the masks through its N different positions for each position of the other mask.

In a DHTS the entrance aperture is modulated by a P x P S matrix.

Let $\varepsilon=\varepsilon_{ir}$ be the P x P matrix whose rows represent P different entrance masks. $\varepsilon_{ir}=1$ for open slots and 0 for closed slots ($1\le i\le P$, $1\le r\le P$). Similarly let $\chi=\chi_{ij}$ represent the exit mask. When the entrance mask is in position i and the exit mask is in position j, the detector measurement η_{ij} is

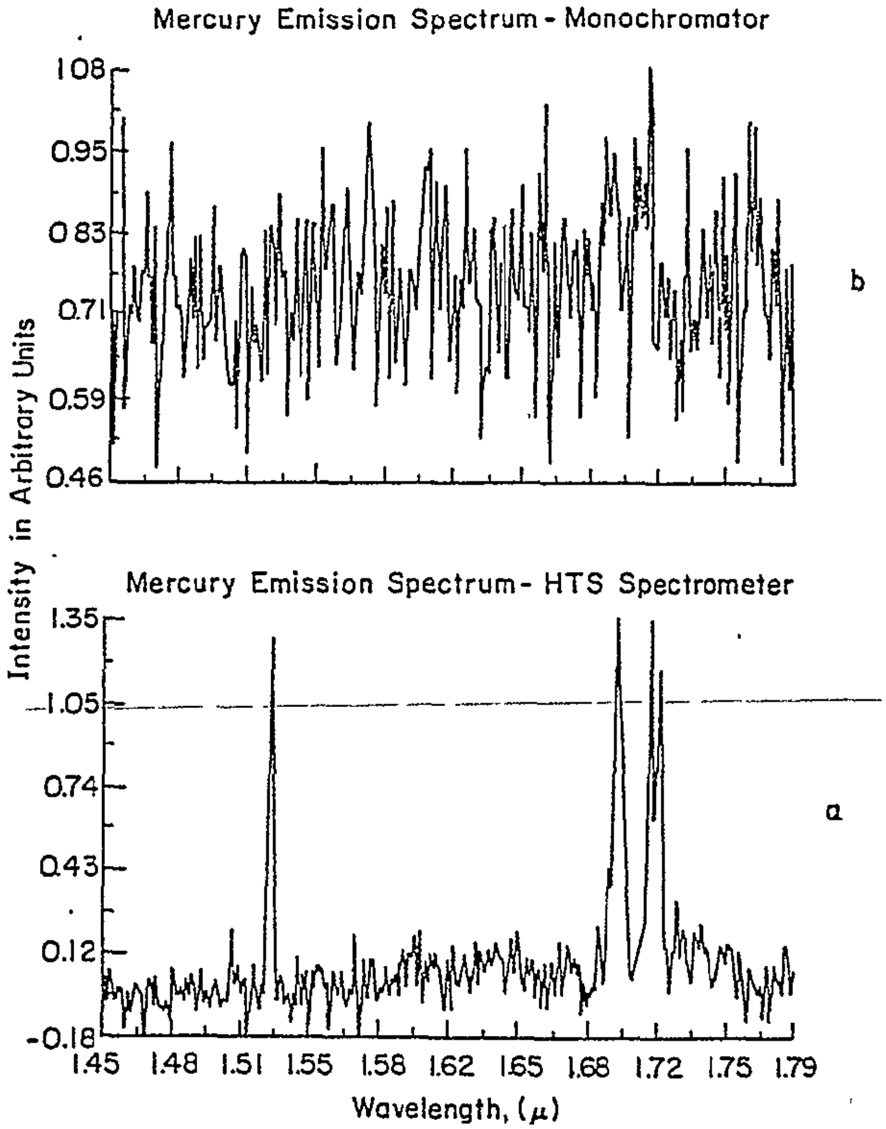

Figure 2-4. Comparison spectrum of the mercury emission lines in the 1.4-1.8μm region: (a, bottom) as obtained in the Hadamard-transform mode, (b, top) as obtained under identical conditions using the same optical system as a conventional monochromator. This figure is taken from Decker, 1971b.

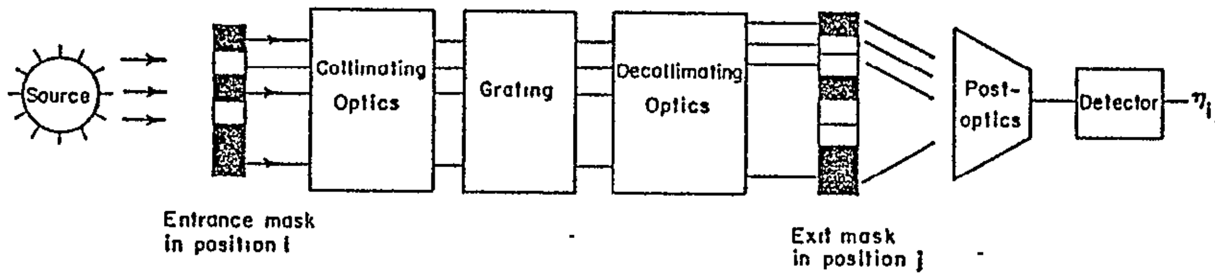

Figure 2-5. Schematic representation of DHTS.

$$\eta_{ij} = \sum_{r=1}^{P} \sum_{s=1}^{N} \varepsilon_{ir} \psi_{rs} \chi_{sj} + \nu_{ij} \qquad (2\text{-}11)$$

where ψ_{rs} is the spectral element produced by radiation passing through the r^{th} entrance slot and the s^{th} exit slot, ν_{ij} is the noise in the $(i,j)^{th}$ measurement; it has the following properties:

$$\langle \nu_{ij} \rangle = 0 \qquad \langle \nu_{ij}, \nu_{k\ell} \rangle = \sigma^2 \delta_{ik} \delta_{j\ell}$$

If the instrument has no optical magnification, the spectrum of radiation that passes solely through the r^{th} entrance slot to first order is shifted by r spectral channels from the spectrum passing solely through the first entrance slot. Hence, only P+N-1 distinct spectral elements exist:

$$\psi_{-(P-1)}, \ldots \; \psi_{-1}, \; \psi_0, \; \psi_1, \ldots \; \psi_{N-1}$$

where

$$\psi_{rs} \equiv \psi_{r-s} \equiv \psi_t \qquad (t=r-s)$$

In matrix notation one may write

$$\underline{\eta} = \underline{\varepsilon} \; \underline{\psi} \; \underline{\chi}^T + \underline{\nu} \quad . \qquad (2\text{-}12)$$

Employing the same analysis as one does for the HTS, i.e. using the unbiased condition $\langle \hat{\underline{\psi}} \rangle = \underline{\psi}$ and the properties of $\underline{\nu}$, one obtains

$$\hat{\underline{\psi}} = \underline{\varepsilon}^{-1} \underline{\eta} (\underline{\chi}^{T})^{-1}$$

where

$$\hat{\underline{\psi}} = \begin{matrix} \hat{\psi}_0 & \cdots\cdots\cdots & \hat{\psi}_{-N+1} \\ \hat{\psi}_1 & \cdots\cdots\cdots & \hat{\psi}_{-N} \\ \vdots & & \vdots \\ \hat{\psi}_{P-1} \; \hat{\psi}_{P-2} & \cdots\cdots & \hat{\psi}_{-N-P+2} \end{matrix}$$

Each row i of $\hat{\underline{\psi}}$ represents a spectrum at the exit mask for radiation that enters the instrument through the i^{th} entrance position. Hence the j^{th} diagonal gives a one-dimensional spatial picture across the entrance aperture for the spectral element j.

One may obtain an average spectrum $\hat{\underline{\psi}}_i$ by averaging all the elements in each diagonal.

$$\hat{\psi}_i = \frac{1}{N-|t|} \sum_{r=1}^{P} \psi_{r,r-t} \qquad t \geq 0$$

$$= \frac{1}{N-|t|} \sum_{r=1}^{P} \psi_{r,r-t} \qquad t < 0$$

Harwit et al (1970) showed that if both the entrance and exit masks are S matrices and we define

$$\sigma_t^2 = \langle (\underline{\psi}_t - \hat{\underline{\psi}}_t)^2 \rangle$$

Then

$$\sigma_t^2 = \frac{16}{(N+1)} \frac{N^2-1}{N-|t|} \sigma^2$$

$$\sim \frac{16\sigma^2}{(N-|t|)N^2} \qquad \text{for N large} \qquad (2\text{-}13)$$

where

$$t = -(N-1),\ldots\ldots (N-1)$$

If the total mean square error for the unknown is

$$\varepsilon = \sum_{t=\frac{-N-1}{2}}^{t=\frac{N-1}{2}} \sigma_t^2$$

where one sums only the central element, then for the S-code

$$\varepsilon = \sigma^2 \left[\frac{22.18}{N} + O\left(\frac{1}{N^2}\right)\right] \qquad \text{N large}$$

where σ^2 = constant $\frac{N}{T}$.

There are two points that should be made about the DHTS. (1) It has not been shown that Hadamard codes are the best codes for such an instrument. In fact some evidence suggests that Hadamard codes are not precisely optimum for this "two-ended" operation (Harwit et al,1974b). (2) For PxN data points the spectrum yields only P+N-1 spectral elements, plus a one-dimensional image. It is also possible to reconstruct the (P+N-1) elements with (P+N-1) data points only (Harwit et al, 1974b). Fig. (2-6) gives a 15 element cyclic S-matrix code for the entrance mask.

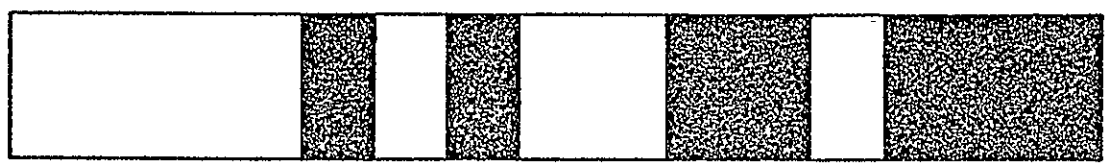

1 1 1 1 0 1 0 1 1 0 0 1 0 0 0

Figure 2-6. The 29 entrance slit mask and the 15-element S code.

Table 2-2 compares three different grating spectrometers. The first column represents the conventional single entrance and exit slot instrument. N measurements are made in time T, with a mean square error σ^2 in each. The second column is for a singly multiplexed instrument with an exit mask S, and is taken from Sloane et al (1969). The last column is for the doubly multiplexed system, using Equation (2-13) for σ_t^2, and has been multiplied by a factor of N to allow for having to make N^2 measurements in time T.

Table 2-2

	NO MASK	SHT	DHT
Δ^{-1}	1	$\frac{\sqrt{N}}{2}$	$\frac{N}{\sqrt{22.2}}$

(E) Errors in Hadamard Spectroscopy

During the manufacture of the masks, whether by deposition of metal or by removal of metal through an etching process, it is possible to obtain a systematic error that leaves each of the opaque portions of the mask either too wide or too narrow by a fixed amount. This will cause a systematic variation in signal passing through the slit. For example if the open slit is too narrow by a fixed amount ε, the light passing through an open slit position will be

I_o when the open slit is bounded by two open slits.

$I_o(1-\varepsilon)$ when the open slit is bounded by one open slit and one closed slit.

$I_o(1-2\varepsilon)$ when the open slit is bounded by two closed slits.

A similar analysis holds for open slits that are too wide, except that the minus sign in these expressions is replaced by a plus sign.

The spectrum of a single (spectral line resulting from such imperfect masks) is remarkably simple (Tai et al, 1975 b). Independent of the particular S-matrix mask to be used, there are always precisely four false blips present in the final spectrum. The amplitude of these blips is always the same for a fixed narrowing or widening of the transmitting slits. Two of the blips always surround the main spectral line, and a pair of adjacent blips always are some distance removed from that line. For the 255 element S-matrix, these two are located 24 and 25 elements away to the left of the parent line. The amplitude of the displaced blips is positive when the transparent slits are too wide and is negative when the slits are too narrow. In contrast, the two blips surrounding the parent line always are positive. Figure (2-7) shows the negative features accompanying the 1.7 μm mercury vapor doublet and the computer simulation of a pure spectral line input and its distorted spectrum. For the general case the reader may refer to Tai et al (1975 b).

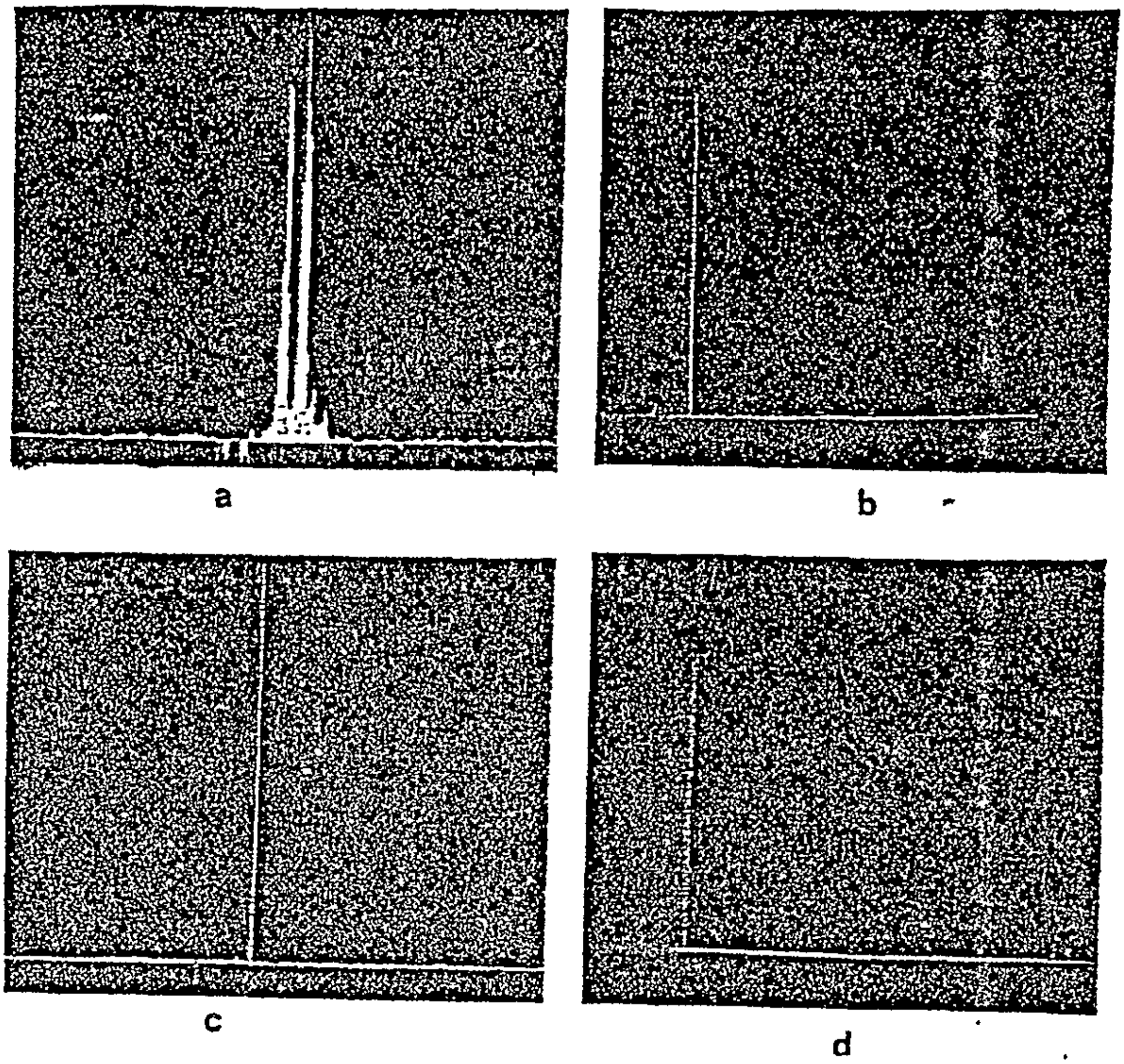

Figure 2-7. (a) Spectrum of the 1.7μm mercury vapor doublet showing negative peaks to the left at the emission peaks; (b) Shows the response we would obtain to a single spectral line with a perfect mask; (c) Shows the response for a single line with the radiation simulated as passing through a mask with slits too narrow because each opaque mask element protrudes into the adjacent transparent slot by a tenth of a slot width; (d) Shows the effect of simulating slits that are systematically too wide. Note that the main spectral line has been placed in different positions for the synthetic runs (b),(c), and (d).

CHAPTER III

INSTRUMENTATION

(A) Multislit Spectrometer

A conventional spectrometer has four essential elements, an entrance slit, a dispersive device such as a grating or prism, a set of imaging optics, and an exit slit.

Such a spectrometer has two important parameters. The first is the "resolution" R, which is a measure of how well the spectrometer can separate two neighboring lines. The second parameter is the "throughput" E. This is a measure of the light gathering capability of the system. The two parameters, R and E, are lumped together into what is called "luminosity" L, defined as (Vanasse, 1974).

$$L = E \cdot R$$

For a conventional grating spectrometer having a grating of area A_g given by WH, where W and H are the width and height respectively of the grating, the throughput is determined by the product of A_g with the solid angle Ω subtended by the slit at the collimating mirror (or lens). The solid angle is given by

$$\Omega = \frac{w \cdot l}{F^2}$$

where w and l are the width and height respectively of the slit and F is the focal length of the collimating mirror

$$E \sim W \cdot H \cdot \frac{w \cdot h}{F^2} \qquad (3\text{-}1)$$

The resolution of this instrument is

$$R = \frac{\lambda}{\Delta\lambda}$$

$$= nN$$

$$= n \cdot \frac{W}{d} \qquad (3\text{-}2)$$

where λ is the wavelength, $\Delta\lambda$ the closest wavelength that can be separated, n the order, N the total number of lines on the grating, W the width of the grating and d the spacing between rulings.

Since $d \sin\alpha = n\lambda$ (3-3)

substitute (3-2) into (3-3)

$$\frac{W}{R} \sin\alpha = n\lambda \qquad (3\text{-}4)$$

if the slit width is limited by diffraction, which is the minimum slit width, then

$$w \sim \frac{F\lambda}{W \cos\alpha} \qquad (3\text{-}5)$$

substituting (3-5) into (3-4) one gets

$$R \sim \frac{F}{w} \tan \alpha \qquad (3\text{-}6)$$

Comparing equation (3-1) and (3-6) one sees immediately that, for a fixed grating area W·H, and fixed optical system, E is proportional to the slit width w and R is inversely proportional to the slit width w. This means that an increase in luminosity of the system by increasing the slit width is made at the sacrifice of resolution, and vice versa.

From (3-1) and (3-6) one obtains

$$\begin{aligned} L &\sim E \cdot R \\ &\sim W \cdot H \cdot \frac{1}{F} \end{aligned}$$

Another feature of a conventional spectrometer is that it transmits only one narrow spectral range of light to the detector, and all other spectral elements are wasted. As a result, the instrument is inefficient.

Within the past two decades there has been much research done in an effort to design new spectrometric systems with a view to maximizing the luminosity L, and to observe a number of spectral elements simultaneously. This can provide a multiplex advantage, or a wide aperture advantage. Two quite distinct modulation techniques have been employed in the past. The first depends on the wave nature of radiation, and makes use of interferometry. The Fabry-Perot interferometer, Michelson interferometer, and Mach-Zehnder interferometer (Jacquinot, 1954, 1960; Vanasse and Sakai, 1967) are instruments of this type. The other technique employs dispersing spectrometers in which entrance and exit slits are replaced by opaque or transmitting masks. Golay's multislit spectrometer, Girard's Grill spectrometer and Hadamard spectrometers (Harwit *et al*,1974a) are representative of these instruments.

A spectrometer, whether interferometric os mask-multiplexed, yields a multiplex advantage mainly for detector noise or amplifier noise limited applications. In these cases it can be shown that for N spectral elements, one can achieve of the order $N^{\frac{1}{2}}$ improvement in the overall spectral signal-to-noise ratio, S/N, over a conventional spectrometer (Chapter II).

For photon noise limited applications, the multiplexing advantage is cancelled by the N-fold increase in the photon noise attributed to the N-fold increase in the energy falling onto the detector. Nevertheless, for photon noise limitations. the throughput advantage can still be realized. The large throughput will become a disadvantage when the noise is background noise which increases faster than the noise due to the source (Harwit *et al*, 1974a).

In this chapter we will describe the experimental study of a Hadamard transform spectrometer (HTS) and calibration in the laboratory. Figure (3-1) is the flow chart of the whole process, starting with radiation from the telescope and ending with the output of the computer. Each component will be described.

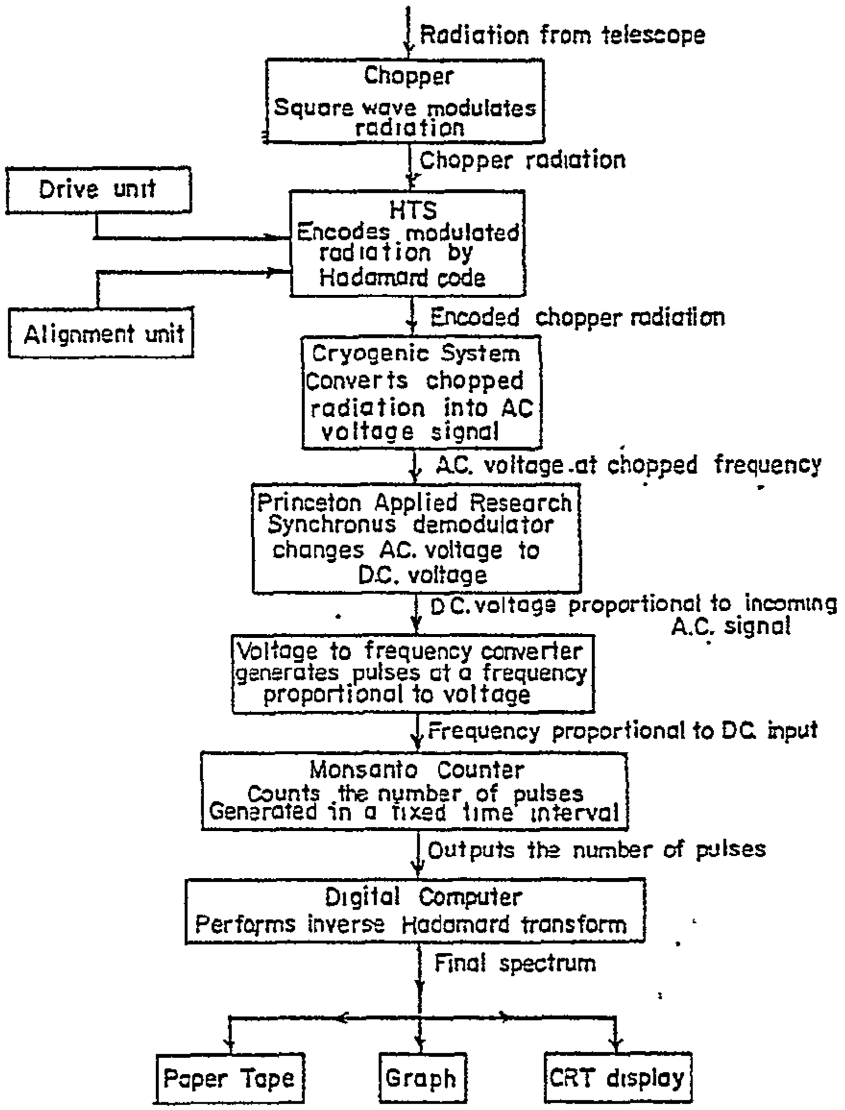

Figure 3-1. The flow chart of the data taking process, starting with radiation from the telescope and ending with the output of the computer.

(B) The Optics

1. Spectrometer

Fig. (3-2) shows the basic spatial design of the spectrometer. It works in the Ebert-Fastie mode. Radiation passing through the entrance aperture S falls upon the spherical mirror M which, in turn, renders it parallel and directs it to the grating G. The dispersed radiation is collimated by the other half of the spheroid and focused upon the exit aperture S'. A 255-slot encoding mask is located at this position. The exit focal plane is positioned in such a way that it bisects a 90° corner reflection. The corner reflector returns the radiation through the spectrometer again and displaces the beam from the center of the principal plane to one side. This reverse process dedisperses the beam and allows it to be brought to a focus at the entrance plane. The dimensions of the focused image are roughly the same as the dimensions of the entrance aperture (Decker 1971). These procedures allow one to use a smaller detector.

A diagonal mirror at the entrance directs the dedispersed radiation to the liquid helium cooled post optics.

The entrance mask can be a single entrance slit with any width between zero to 1.5 mm for the 1x255 program, or it can be a fifteen S-matrix code with each slit having width 0.1 mm for the 15x255 element program. In normal use the height of of entrance slit is 3.5 mm. It can be increased up to 10 mm.

M_1 is a spherical mirror with a 49.5 cm focal length. On its back it is held in place with three teflon-tippled

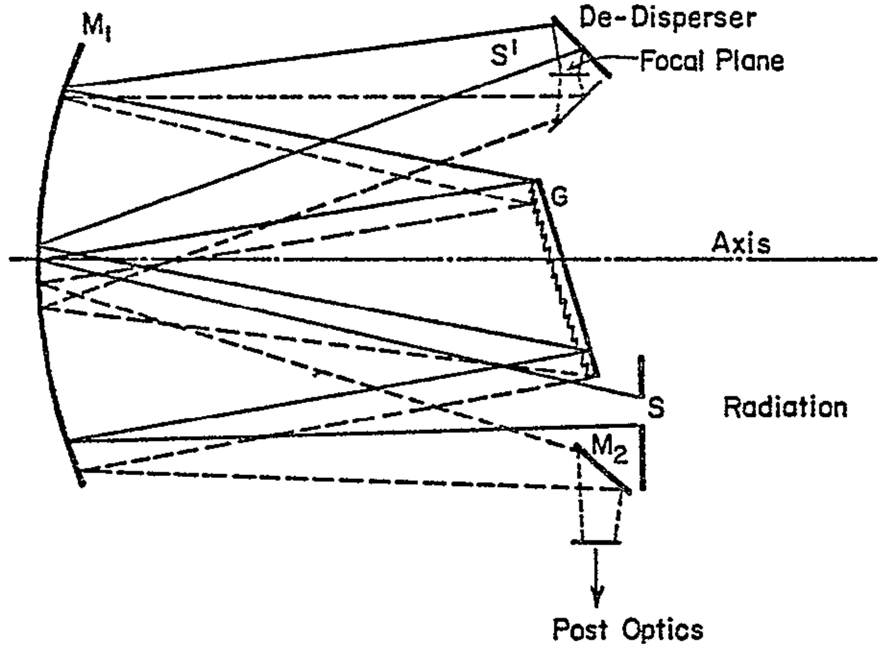

Figure 3-2. Optical path through the spectrometer. The dedisperser and exit mask are shown rotated by 90°.

screws. Three teflon-tippled springs bear on the front edges of the mirror. This design allows one to make slight adjustments in the position of M when aligning the instrument. The central part of the mirror is blocked off to reduce stray radiation.

G is a 75 mm x 75 mm grating with 20 lines/mm and blaze angle 5°11'. The corresponding blaze wavelength at first order is 9.03μ. Figure (3-3) is the calculated grating efficiency as a function of slit position, at two wavelengths. At 8μ the energy imaged within one slit width is 80% of the total. For 14μ the energy within one slit is 52%. The grating is mounted on a yoke which allows it to be adjusted in three mutually perpendicular directions. It is located at 0.82 focal length from the primary mirror M.

All mirrors inside the spectrometer are silver coated with a protective coating of SiO_2. The reflectivity of silver coating at 10μ is better than 97%.

For a multiplexing spectrometer which has N entrance and N exit slits, one wishes to image entrance slits S_1, S_2,....., S_n onto exit slits S_1', S_2',....., S_n' such that S_1 is imaged onto S_1' ,....., S_n onto S_n' at a particular wavelength λ. Let δ be the angle subtanded by S. Where δ and δ' are measured from the center of M. The grating equation for imaging S onto S' is

$$\sin \alpha + \sin \beta = \frac{m\lambda}{a} \qquad (3\text{-}7)$$

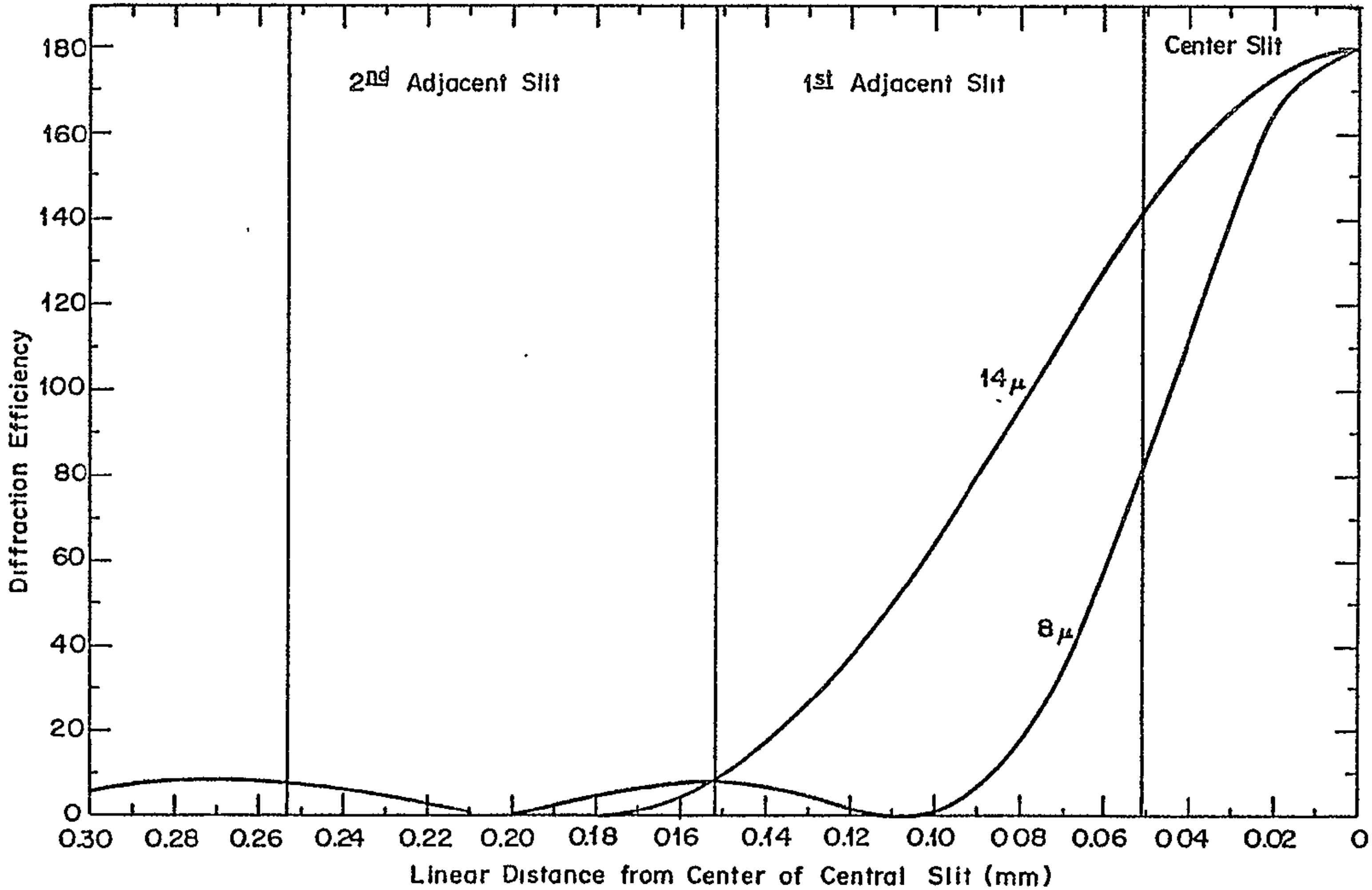

Figure 3-3. Grating diffraction efficiency as a function of slit position at 8 and 14μm.

Differentiating (3-7) with respect to α gives

$$\frac{d\beta}{d\alpha} = -\frac{\cos\alpha}{\cos\beta} \qquad (3\text{-}8)$$

The minus sign indicates that α and β change in opposite directions. $d\alpha$ is the width of the entrance slit and $d\beta$ is the width of exit slit, so $\delta \neq \delta'$ unless $\alpha=\beta$.

In our spectrometer, the exit slit width is 0.1024 mm, 2.4% larger than the entrance slit width. This is the effect of anamorphic dispersion- a magnification produced by the grating (3-8), when the lower limit on the slit width is set by diffraction. The total number of spectral elements that can be observed simultaneously is limited by the optical aberrations of any particular optical system, which set a limit on the total useful width over which the spectrum can be displayed.

2. Post Optics

The post optics consist of a liquid helium cooled Arsenic-doped silicon (As:Si) detector, with appropriate optics for focusing the radiation onto the detector (Fig. 3-4). Radiation enters the evacuated dewar through a barium fluoride window, passing through a filter with pre-selected band-width. The filtered radiation then passes through a cooled barium-fluoride filter and is focused onto the detector inside the housing by a gold coated mirror. A light baffle is partitioned in front of the detector housing.

Below is a brief discussion of each of the cryogenic components

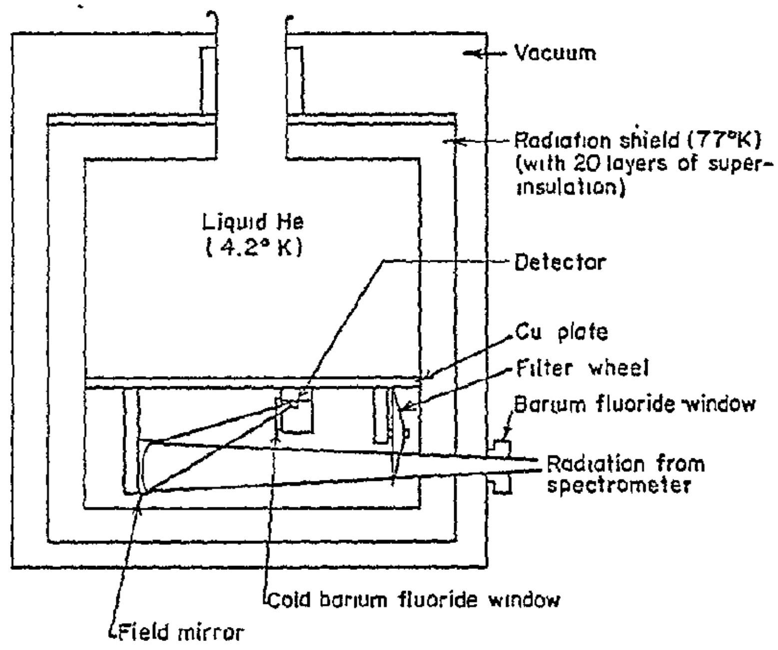

Figure 3-4. Liquid helium cooled post optics.

(a) Barium Fluoride Window

The barium fluoride window is 2 mm thick and 0.75" in diameter. It is used to cut off wavelengths longer than 14μ. It has a transmission efficiency of around 90% out to 11μ before it starts to cut off. At 14.29μ (700 cm^{-1}), its transmission efficiency is 50%.

(b) Filters

A liquid helium cooled filter wheel with 8 filter positions is housed inside the dewar. Table 3-1 gives a brief description of each filter.

Table 3-1

Filter position	Range	Band-width	Peak transmission efficiency
1	no filter		
2	closed (blocked by aluminum foil)		
3	8μ - 9.9μ	1.9μ	71%
4	8.7μ - 11.1μ	2.4μ	83%
5	11μ - 12.4μ	1.4μ	82%
6	11.1μ - 13.8μ	2.7μ	86%
7	8.4μ - 15μ	6.0μ	85%
8	glass	shorter than 2μ	

Filter positions 1 and 2 are for testing purposes.

The filter wheel is held in place by a spring-loaded screw.

The wheel was originally connected to the outside world through a stainless steel rod and could be changed to different positions by turning the rod. It was found that the stainless steel rod conducts too much heat from the outside into the helium containing can. When the stainless steel is replaced by a G-10 Glass Epoxy Lamitex rod, the holding time for the liquid helium of the dewar increases from 9 hours to 15 hours.

(c) Field Mirror

A gold coated mirror with focal length 7 mm and f/0.41 is used as a field mirror to focus the radiation onto the detector. The reflection efficiency for gold mirrors at 10μ is over 99%. The mirror has 3 degrees of freedom of adjustment, one translational and two rotational adjustments.

(d) Liquid Helium Cooled Barium Fluoride Filter

This barium fluoride window is also used to cut off the radiation longer than 14μ . Although the filter barium fluoride window cuts off radiation longer than 14μ from the outside world, it will emit radiation of its own because it is at room temperature. Since all the interference filters have a long wavelength leak between 20μ to 26μ, and since the detector will cut off radiation longer than 24μ only, there is still radiation from 20μ to 24μ that gets into the detector as background radiation. The insertion of the liquid helium cooled barium fluoride filter eliminates this peak. It was found to cut down the background radiation by a factor of four.

(e) Detector

An arsenic doped silicon detector with dimension 1.2 mm x

3.2 mm is positioned inside a housing, which has a baffle at its entrance.

Arsenic doped silicon is a N-type extrinsic semiconductor. When the detector absorbs radiation, free carriers are provided for the conduction band, thus changing the resistence of the detector. The following discussion follows the work of Putley. For further details, one can refer to Putley (1964) and Kittel (1966).

Let σ be the conductivity of the detector

e be the electric charge of the carrier

τ be the life time of free carriers

N be the density of free carriers, and

μ be the mobility of free carriers

Then,

$$\sigma_D = NeP\mu \qquad (3\text{-}9)$$

and

$$\Delta\sigma_D = \Delta J e\tau\mu\eta$$

$$= \frac{\Delta P}{h\nu} e\tau\mu\eta \qquad (3\text{-}10)$$

where

$\Delta\sigma_D$ is the change in conductivity of the detector

ΔJ is the number of photons incident in unit time

ΔP is the radiation power incident

ν is the frequency of the incoming photons, and

η is the quantum efficiency, i.e. nmuber of electrons freed per photon.

Since

$$R_D = \frac{1}{\sigma_D} \frac{\ell}{A} \qquad (3\text{-}11)$$

where R_D is the resistance of the detector

ℓ is the length of the detector, and

A is the area of the detector

Then

$$\Delta R_D = -\frac{\ell}{A} \frac{\Delta\sigma_D}{\sigma_D^2}$$

$$= -\frac{\ell}{A} \frac{\Delta P}{h\nu} \frac{\eta}{N^2 e\mu\tau} \qquad (3\text{-}12)$$

Let

$$I_D = \frac{V_B}{R_D} \qquad (3\text{-}13)$$

where I_D is the detector current, and

V_B is the bias voltage across the detector

Then

$$\Delta I_D = -\frac{V_B}{R_D} \Delta R_D$$

$$= \frac{V_B}{R_D} \frac{\ell}{A} \frac{\Delta P}{h\nu} \frac{\eta}{N^2 e\mu\tau} \qquad (3\text{-}14)$$

Let

$$V_o = I_D R_L$$

$$= \frac{R_L}{R_D} V_B \qquad (3\text{-}15)$$

where V_o is the voltage across the load resistor

R_L is the load resistance

Then

$$\Delta V_o = \Delta I_D R_L$$

$$= R_L V_B \frac{\Delta P}{h\nu} \frac{A}{\ell} \eta \dot{e} \mu \tau \qquad (3\text{-}16)$$

From equation (3-16) one can calculate ΔP from ΔV_o.

(f) Procedures for Alignment of the Optics

i) Place all components in their respective positions and line them up visually. Be sure there is no mechanical binding in the mask and in the driving mechanism.

ii) Using a laser, put the spot from the entrance slot on the middle of the grating. It is suggested that only one entrance slot be used.

iii) Adjust the grating tilt until the line of dispersed dots exits at the proper position at exit. As the grating is rotated, this line of spots should remain level, not displaced normal to itself.

iv) Put one half of the dedispersing mirror combination in place. Use a T square to line it up roughly. At this point, use a mercury emission lamp with proper f-number to simulate the beam coming from the telescope. A number of colored image of the single entrance slot will be seen at the exit.

v) Adjust the spherical mirror for coarse adjustment and the position of the dedispersing mirror as a fine adjustment to bring the image to a focus on the exit plane.

vi) Adjust the grating position in its yoke until the color image from the mercury lamp is parallel to the exit slit length.

vii) Adjust the angle of the dedisperser so that the color image reflected by it is perpendicular to the exit mask.

viii) Put in the other half of the dedisperser and line it up at an angle so the radiation falls back upon the grating. Adjust with fine adjustment screws so the grating is fully illuminated. The image of the grating will appear on itself when viewed from the diagonal, 45°, mirror which diverts the radiation to the dewar.

ix) Place the dewar on the spectrometer using ¼" spacers to represent the thickness of the dewar bottom cover. Adjust the 45° mirror so that the dedispersed image (with color) falls on the center of the filter on the filter wheel.

x) Turn the filter wheel to position one (no filter), so that radiation can fall on the field mirror. Adjust the field mirror until the dedispersed radiation impinges upon the detector. Be sure that all the light falls onto the detector. Be sure that the mirrors accept all the radiation.

xi) Insert the housing. Be sure that the incoming radiation is clear of the housing.

xii) Put in the liquid helium shield, and the radiation shield. Put on the nose. Use GE varnish and aluminum foil to reduce openings in the baffles so that they will transmit only the bright white fringes.

xiii) When the spectrometer is on the telescope, maximize the signal by tilting and rotating the dewar.

(C) The Electronics

The data-taking process is controlled electronically to ensure a smooth process. The operator only needs to turn the switch on. The spectrometer will then automatically take date in, process it, and stop at the end of the transform indicated by the operator. All the operator has to do in the whole observation is to keep the astronomical object in the beam. Figure 3-5 shows the block diagram of electronic and computer set up. The following are brief descriptions of the electronic parts incorporated in the system.

1. Alignment Sensor

The alignment sensor (figure 3-6) is used to synchronize a Monsanto electronic counter, and the computer with the spectrometer. The circuit is shown in figure (3-6). The exit mask is continuously moving. When the exit mask is at its starting position, i.e. the first 255 slots are at the exit aperture, a light pulse goes through an alignment slot on the exit mask and is detected by a photo-cell on the other side of the exit mask. Two transistors amplify the output light curve and two IC chips change the light curve into an alignment pulse. This alignment pulse, through the drive unit, readies the counter for counting, readies the computer to accept data, and to turn on an indicator light showing that the system is taking data. One can adjust the starting position of the exit mask by adjusting the intensity of the light. After 255 data points have been obtained, the exit mask is at its other end, and another alignment pulse turns off the counter and the indicator light.

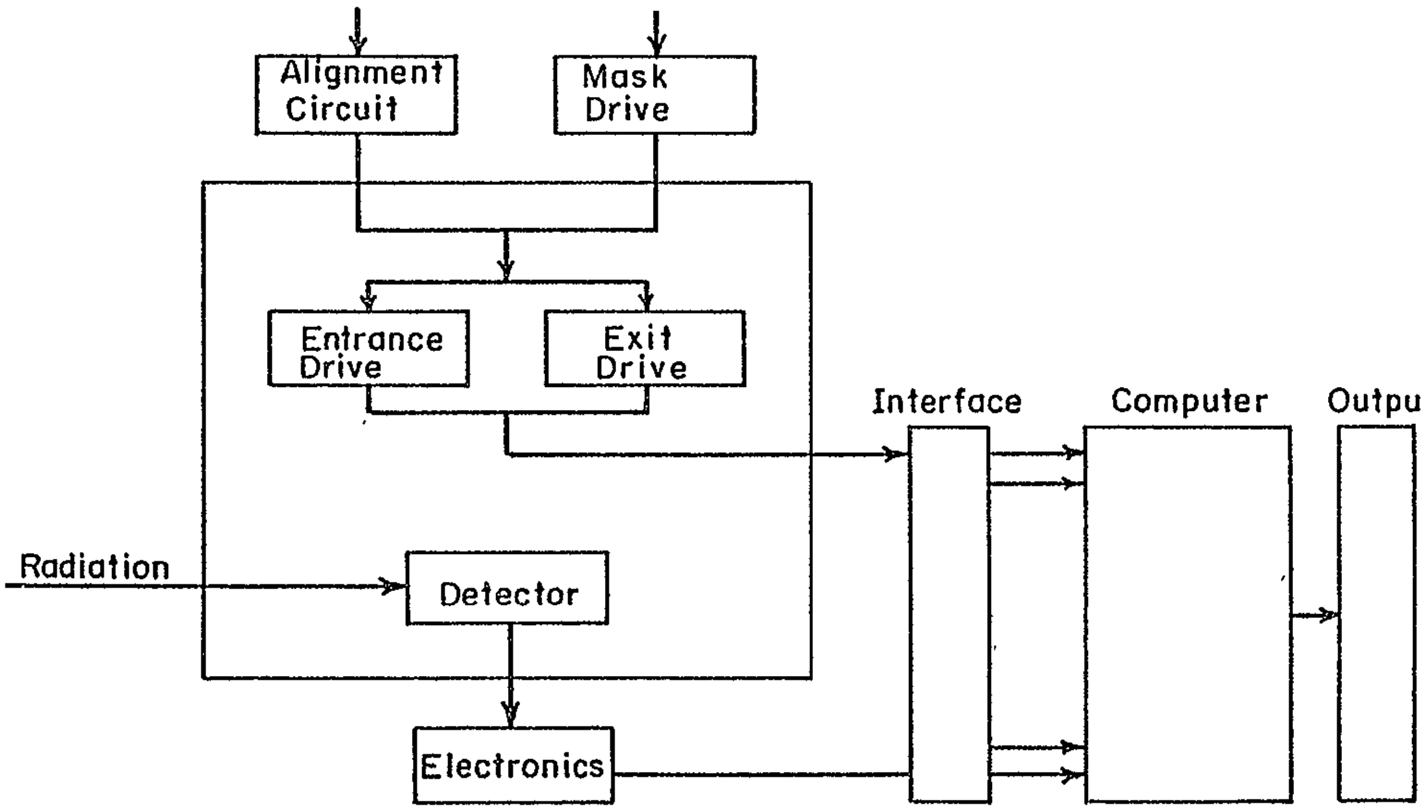

Figure 3-5. HTS drive unit block diagram.

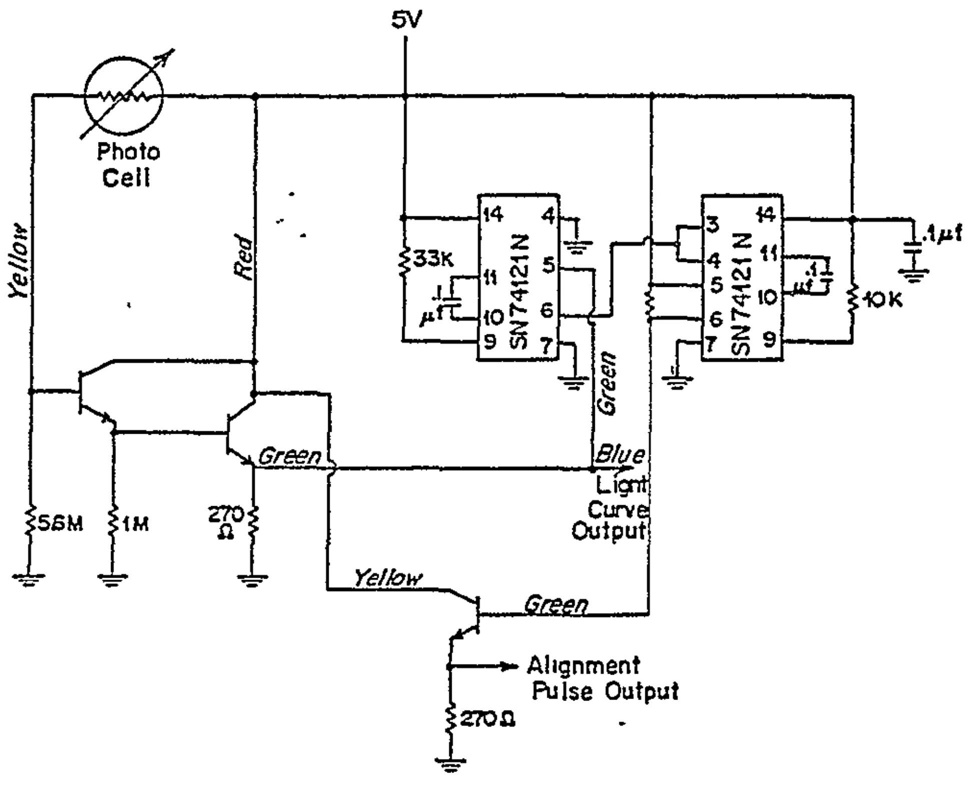

Figure 3-6. HTS alignment circuit.

The computer after taking 255 readings checks that the indicator light is off. This step ensures the synchronization of computer and spectrometer.

2. Drive Unit

A drive unit (Fig. 3-7) is used to drive the entrance and exit masks of the spectrometer. It can be set to be adjusted by pulse streams at 100 Hz, 200 Hz, or 400 Hz. The unit performs the following functions:

(a) It receives an alignment pulse from the sensor circuit(18) and generates a pulse to reset the counter for counting(17). The pulse will also ready the computer for taking the data.

(b) It drives the exit mask in a continuous mode at a displacement rate of one slot for every 41 pulses(18).

(c) After each set of 41 pulses the unit instructs the the mini-computer to read the integrated signal off the counter and then reset the counter for the next data integration.

(d) After 255 reset pulse the unit advances the entrances mask by one slot by sending the entrance mask advance motor 40 pulses (11).

3. Preamplifier

The circuit (Fig. 3-8) shows a transimpedance amplifier implemented with a Burr Brown operational amplifier. The circuit has the advantage of high speed, low susceptibility to microphonics, and detector operation at constant voltage with a high resistance load resistor.

Neglecting the voltage noise and current noise in the

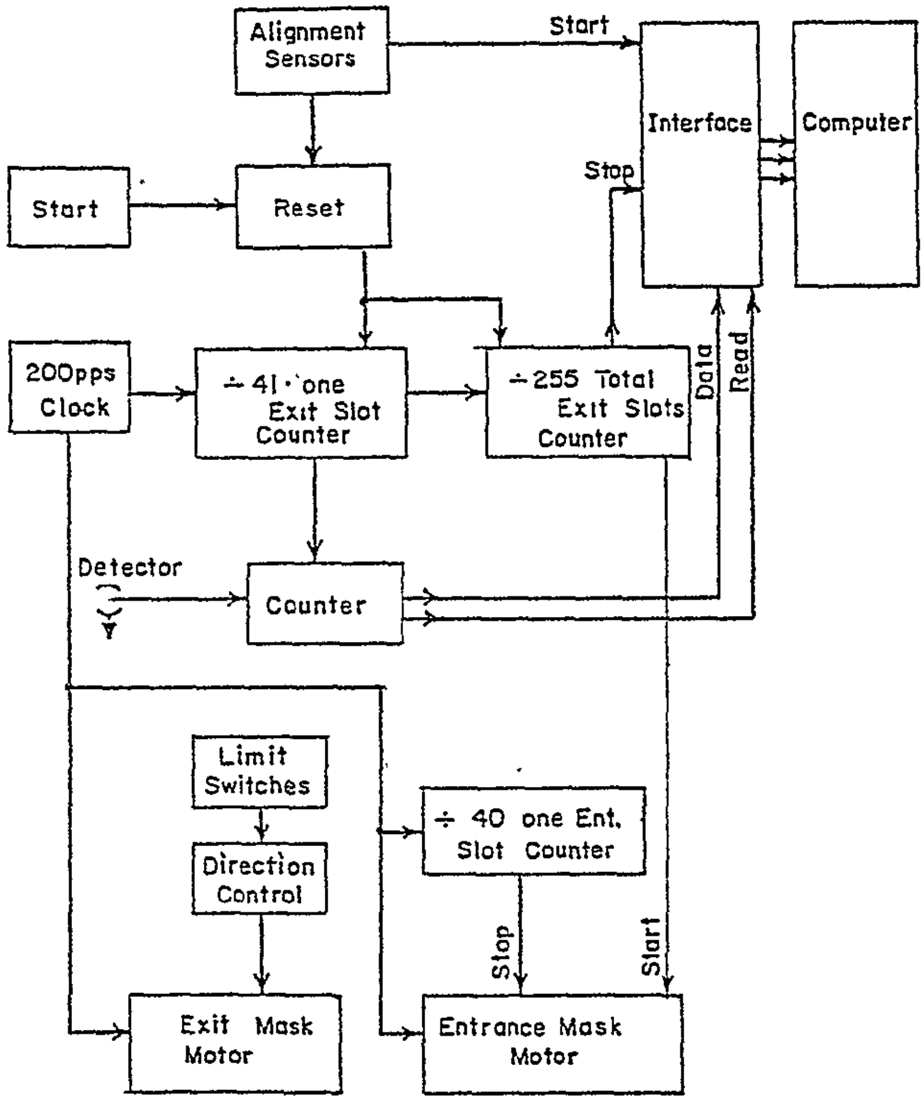

Figure 3-7. Logic diagram for mask motion and data processing.

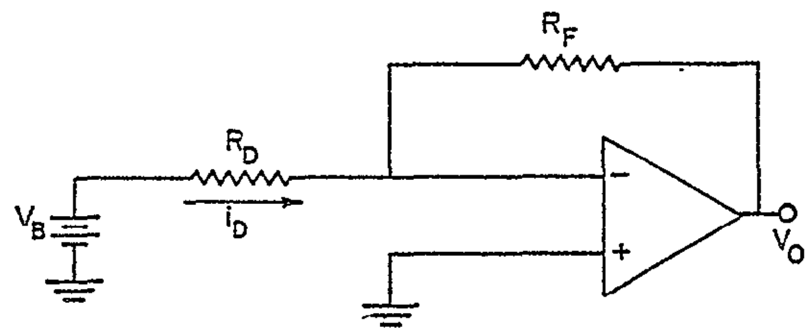

Figure 3-8. Basic detector bias and preamplifier circuit.

first order approximation, the current through the detector, I_D, also goes through the load resistor R_F because the input impedance of the operational amplifier can be taken to be very large, so

$$V_o = I_D R_F$$

$$= V_B \frac{R_F}{R_D}$$

where V_o is the output voltage,

V_B is the constant bias voltage, and

R is the load resistance

(D) Laboratory Calibration

1. Calibration of Post Optics

Liquid nitrogen is used to calibrate the efficiency and sensitivity of the post optics. Liquid nitrogen is in a dewar with black paper along the wall to simulate a blackbody. Through a chopping device, the post optics will alternately see radiation from the liquid nitrogen and from the room. The difference between these two radiations gives the A.C. signal. D.C. measurements are obtained by putting liquid nitrogen directly in front of the dewar window. The following are the results of the calibration:

Dewar profile:	$f_H = 7.6$
	$f_V = 10.3$
Wavelength region:	$8.7\mu - 11.1\mu$

Band-width:	2.4μ
Bias voltage:	15μ
Load resistor at LH_2 temperature:	1.2 MΩ
A.C. power:	$9x10^{-10}$ watt.
A.C. signal:	272.7 mv
A.C. noise:	4.4μv
(NEP) A.C. detector:	$5.2x10^{-13}$ $H_z^{1/2}$
(NEP) A.C. system:	$1.25x10^{-12}$ $H_z^{1/2}$
A.C. responsivity:	1.2 amp/watt.
D.C. power:	$3.05x10^{-6}$ watt.
D.C. signal:	11.32V
D.C. noise:	4μv
(NEP) D.C. system:	$1.47x10^{-12}$ $H_z^{1/2}$
D.C. responsivity:	2.58 amp/watt.
Background noise:	$NEP_{Blip} = \sqrt{2\ P_{BG} h\nu}$ $=3.5x10^{-13}$

where P_{BG} is the D.C. power

ν is the frequency that is assumed to be $10H_z$.

The system is a factor of 3.57 away from background limited.

2. Test of the Spectrometer

A mercury vapor lamp with emission at 1.7μ is used with the spectrometer to test the computer program. A PbS detector and an appropriate blocking filter isolates the 1.7μ doublet of mercury. The slit width and length for each mask is 0.15 mm and 3.5 mm. Fig. (3-9) is the mercury vapor spectrum at 1.7μ for the 1 x 255 mode. Fig. (3-10) is the mercury vapor spectrum

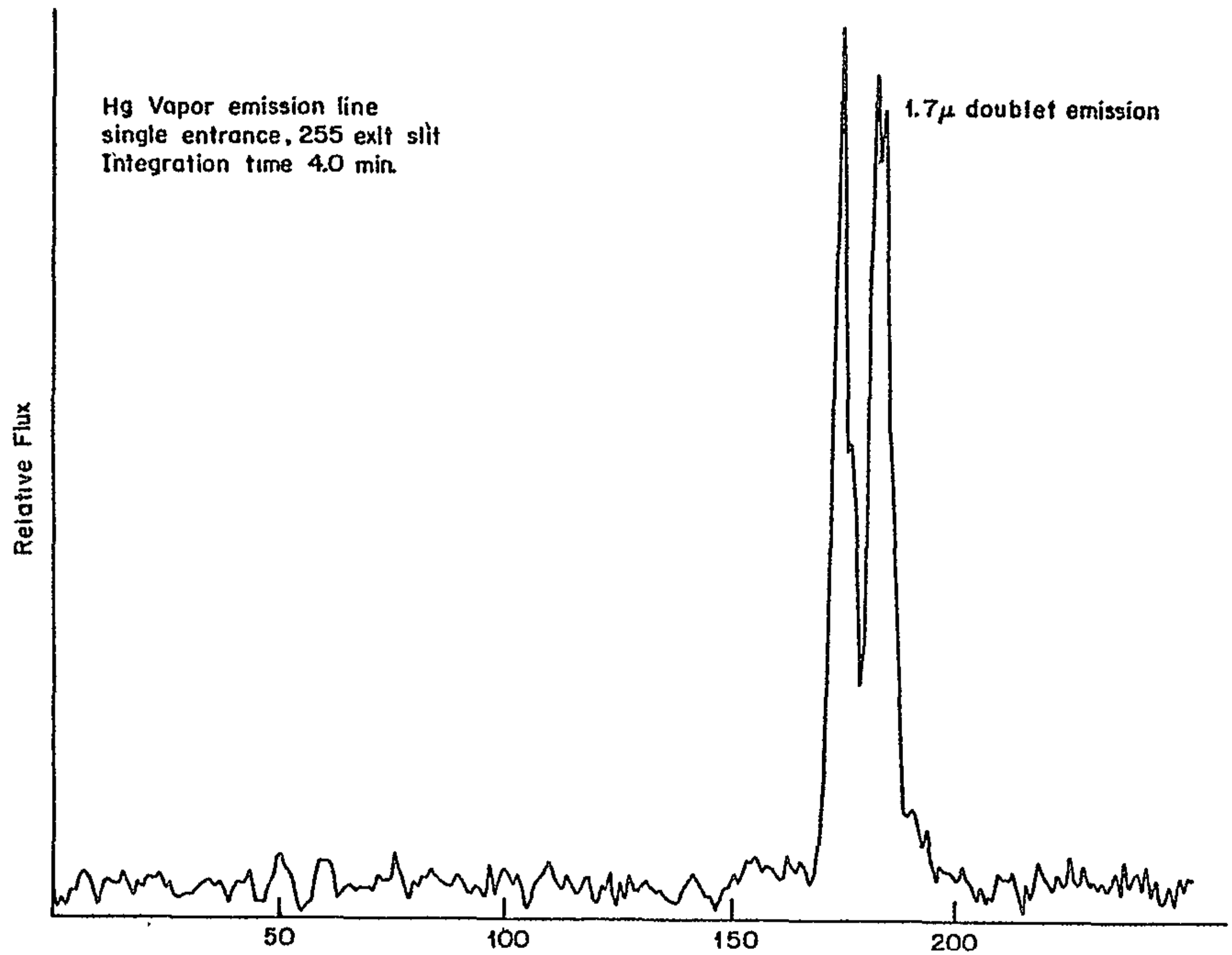

Figure 3-9. Spectrum of the mercury vapor 1.7μm line using the 1x255 mode.

for 15 x 255 mode. Figure (3-10a) shows the eighth of a series of fifteen individual spectra. Figure (3-10b) shows an average of all fifteen spectra, and (3-10c) shows all 15 spectra, each spectrum being displaced vertically from the next. The diagonal pattern near the right-hand edge represents a displacement of the peak between successive spectra. This represents the actual shift in spectral range between adjacent spatial elements.

Once it was clear that the instrument with the computer program worked properly in the 1.7μ region, the spectrometer was tested with the cryogenically cooled, arsenic-doped silicon detector. The transmission spectrum of polystyrene with a soldering iron as the source was obtained. The shap e of the filter profile and the transmission spectrum of polystyrene showed that the instrument worked in the 10μ region.

The wavelength calibration of the spectrometer is obtained by comparing the polystyrene transmission spectrum obtained by the spectrometer and the spectrum obtained by a Perkin-Elmen monochromator. The wavelength calibration is then checked against the moon spectra at 9.5μ where the atmosphere has strong absorption features.

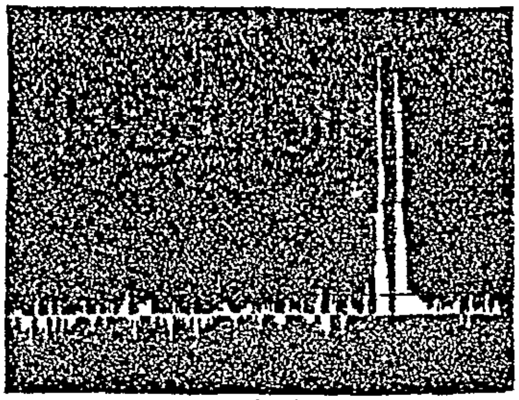

(a)

Figure 3-10.
Calibration spectra obtained for the mercury vapor emission lines at 1.69μm and 1.71μm: (a) The eighth of a series of fifteen individual spectra obtained;

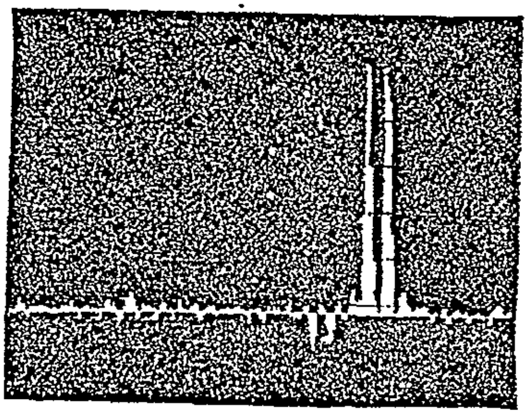

(b)

(b) An average of all fifteen spectra;

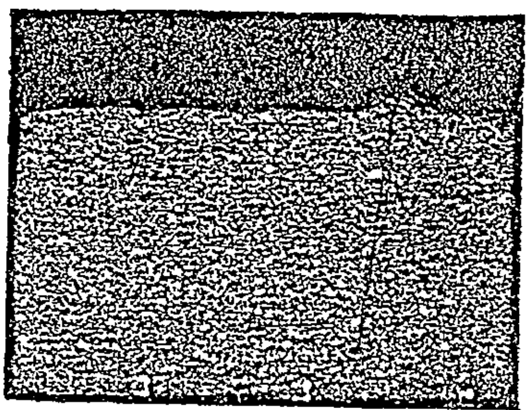

(c)

(c) A display of the fifteen spectra, each spectrum being displaced vertically from the next. The diagonal pattern near the right-hand edge represents a displacement of the peak between successive spectra. This represents the actual shift in spectral range between adjacent spatial elements.

CHAPTER IV

COMPARISONS BETWEEN FOURIER TRANSFORM AND HADAMARD TRANSFORM SPECTROSCOPY

Since the Michelson interferometer spectrometer (MIS) and Hadamard transform spectrometer (HTS) both have the multiplex advantage and the advantage of large through-put, there are a number of comparisons between them in the literature. In this chapter the comparisons are carried out in four different aspects: mathematically, computationally, optically and mechanically.

(A) Mathematically

Fourier transforms and Hadamard transforms can be viewed as using two different weighing schemes. Appendix A gives the mathematical analysis of the coding error for Fourier transform.

Let ξ be the path difference in a two beam interferometer. $P(\nu)$ is the power at wave number ν (i.e. the spectral density function). ν here is taken to be the inverse of wavelength, then $S(\xi)$, the power received for path difference ξ, is:

$$S(\xi) = \int_0^\infty P(\nu)\cos^2(2\pi\xi\nu)d\nu \quad . \qquad \text{A-1}$$

$$= 1/2P_o + 1/2\int_0^\infty P(\nu)\cos(4\pi\xi\nu)d\nu \qquad \text{A-2}$$

In the Fourier transform each spectral element can be viewed as having a phase modulation by a cosine squared term. Its argument depends on the stepped distance and the particular wavelength. In the Hadamard transform each spectral element is modulated by a step function of 1 and 0 for a S-matrix coding.

One can ask oneself whether these modulating or encoding schemes are equally efficient?

In table 2-1 we stated that for large N the multiplex advantage, or the efficiency, of the H-matrix coding of elements 1 and -1 is $\sqrt{N}$, the S matrix coding of element 1 and 0 is $\frac{\sqrt{N}}{2}$, and for a single detector MIS the Fourier coding is $\sqrt{N/8}$. This last figure is based on calculations shown in Appendix A. The other two values were described by Sloane et al (1968). The H-matrix is an orthornormal matrix. The element -1 means "subtract" the radiation, while the +1 element means "add" the radiation. No radiation is wasted and thus the coding scheme has the highest efficiency. For S-matrix coding half the slits are open, 1, letting light pass through; and half the slits are 0, blocking the light. Half the radiation is therefore wasted each time and one can intuitively see why the efficiency of the S-matrix is only half that of the H-matrix.

Although the S-matrix is less efficient, it has the important advantage that it is cyclic; that is, the $(i+1)^{th}$ column of the S-matrix is obtained by shifting the i^{th} column cyclically one place downwards. Instead of constructing a mask of N^2 slits for N spectral elements, one constructs only one mask with 2N-1 slits. Such a mask has two advantages. First, the cost of mask construction is reduced by $\sim N/2$ and the design of the advance mechanism is considerably simplified, since the total weight of the mask also decreases as $\sim N/2$. Secondly, it can be self-supporting and therefore permits the construction of a spectrometer which requires no transmission materials. In operation the mask is stepped one slit width - along the length of the mask- for each successive encoding position.

In the Fourier case, equation (A-2) of Appendix A

$$S(\xi) \quad = \quad 1/2P_o + 1/2\int_0^{\infty} P(\nu)\cos(4\pi\xi\nu)d\nu \qquad \text{(A-2)}$$

shows that half the power goes into $1/2P_o$, the first term on the right hand side, which is not modulated at all. This reduces the efficiency by a factor of two as in the S-matrix case. The other half of the power is modulated by a cosine term. Cosine modulation gives a factor $1/\sqrt{2}$ because cosines functions do not form an orthronormal set themselves. The total Fourier modulation efficiency is therefore $1/2(\sqrt{N}/2)$. Mathematically, the S-matrix is a factor of $\sqrt{2}$ better in SNR than the Fourier transform. The true Hadamard code, which cannot be realized experimentally, as yet, is a factor of $\sqrt{8}$ better that the Fourier code.

(B) Computer Requirements

Both MIS and HTS require a digital computer to decode the data. However, in the HTS case this reduces to nothing more than a series of additions and subtractions. Hence, as much as an order of magnitude in computer time can be gained over the Fourier decoding procedure required by MIS (Decker, 1971). In addition, HTS do not have the large zero path-length spike which is characteristic of MIS, and hence can be operated with a substantially lower dynamic range.

(C) Optics

HTS attempts to "liberate" the grating instrument from its inferior position and offers a possibility to convert a conventional scanning spectrometer into a multiplex instrument at a moderate cost. However, it is also the grating and optics that limit the capabilities of HTS.

1. Resolution

The resolution of a grating instrument is

$$R = \frac{\lambda}{\Delta\lambda}$$

$$= mN \qquad (4\text{-}1)$$

$$= m\frac{W}{d} \qquad (4\text{-}2)$$

where m is the order of diffraction. N is the total number of rulings in the grating. W is the width of the grating. d is the separation of lines.

The MIS introduces variable path differences between two interfering beams. The resolution is determined by the maximum permissible path difference in the interferogram.

$$\Delta\nu = \frac{1}{2x} \qquad (4\text{-}3)$$

$$= \frac{1}{4\xi} \qquad (4\text{-}4)$$

where x is the maximum path difference between interfering beams.

ξ is the displacement of one of the two mirrors from the white light fringe position, and

$\Delta\nu$ is the increment in wavenumber.

Since

$$R = \frac{\lambda}{\Delta\lambda}$$

$$= \frac{1}{\lambda\Delta\nu} \qquad \text{(Mertz a, P.5)}$$

$$\doteq \frac{2x}{\lambda} \qquad (4\text{-}5)$$

A MIS can have a resolutuion as high as $\sim 10^6$.

2. <u>Slit Width</u>

In the HTS, the minimum usable slit width is determined by the diffraction pattern

$$w \sim \frac{\lambda}{W} F \qquad (4\text{-}6)$$

where F is the focal length of the imaging mirror.

It has been argued that a boxcar profile is a poor match to a sine diffraction pattern(Hirschfeld, <u>et al</u>, 1973, Mertz, 1976 b). In the presence of diffraction, the transmission at each point of the mask will be a complex function of the spectral distribution, the mask position, and the relative width of the nearby transparent and opaque slits.

One way to correct this is to make the slits, wider than the diffraction limit, allowing the mask's transmission to approach the geometric optical limit. This way, however, not only the resolution of the instrument is reduced, but the total number N of spectral elements that can be observed simultaneously, also decreases.

There is another way to look at the same problem. The grating is an operator that changes the frequency domain into the spatial domain, so that intensity as a function of frequency, after passage by the grating, becomes a function of position. With diffraction effects included, the intensity has a new functional dependence on distance. The Hadamard mask code and the subsequent decoding process just translate this spatial distribution function back into its spectral domain. Therefore, an intensity pattern which is complicated by the diffraction pattern, after the Hadamard coding and decoding, should still show up the same intensity pattern. Since one knows the diffraction pattern for a given optical system, the diffraction effect on the spectral intensity distribution can be computed and corrected, so that the $sine^2$ diffraction effect would not make the slit width any larger than the diffraction limit. One point, however, should still be noted. The correction that would have to be applied is wavelength dependent because diffraction is wavelength dependent.

A similar problem exists in MIS (Stewart P.296) because the moveable mirror must be stopped when its maximum displacement is reached.

The sidelobes in the interferometric case is of the form

$$S(\omega') = \frac{\sin\ (\omega-\omega')T}{\omega-\omega'} \quad , \quad \omega \simeq \omega' \tag{4-7}$$

(Stewart P.295)

which has considerably stronger side lobes than the diffraction pattern. Here, T is the time for the mirror to travel from one end to the other, and ω is the central frequency. Various schemes of apodization have been introduced to compensate for the side lobes in the interferometric case.

3. Multiplex Number

The total number of elements N that can be observed simultaneously yields the multiplex advantages. In HTS, the total aperture size is limited by aberrations largely due to off axis radiations. The aperture width is (Hirschfeld, 1973)

$$w = F \cdot S_W \tag{4-8}$$

where F is the instrument focal length and $S_W/2$ is a factor of the order of $0.05 \sim 0.1$, that describes how far off axis one can go before the aberration pushes the individual slit width up to the point where no further gain in N is possible. Since the minimum slit width, determined by diffraction effects, is $\sim 1.22\lambda f$, the total number N is

$$N = \frac{FS_W}{1.22\lambda f} \tag{4-9}$$

and is of the order of 10^3.

For our HTS at Cornell, we have

$$F = 49.5$$

$S_w \sim 0.08$ (assume ~ medium value)

$\lambda = 10.0 \mu m$

$f = 7.5$

$N \sim 250$

Actually, however, Mertz and Flamand (1976) suggested that S_w values >>0.1 may be realized in practice.

The MIS has a very large effective value of N. This is its main gain. The total wave number range observed in MIS is

$$\nu_{max} - \nu_{min} = \frac{1}{4\Delta}$$

$$= \frac{1}{4\Delta\delta}$$

where Δ is the step size of the mirror, σ is the resolution in wave number. N for the MIS can be 10^6.

4. Spectral Range

The MIS also has a broad free spectral range. Its range is limited by the beam splitter efficiency which usually varies approximately as the cosine of the wavelength. HTS free spectral range is usually about one grating order. Its free spectral range can be increased by using order sorting, but this increases the technical difficulty. Although the HTS has a smaller spectral free range, it can be set to recover only those spectral bands of particular interest throughout any spectral regions (Decker, 1971). This is impractical with a MIS.

5. Throughput

The throughput is defined in section 1-A as the product of aperture A and angular acceptance Ω

$$E = A\Omega$$

For a MIS it can be shown that $\Omega R = 2\pi$ and

$$E_{MIS} = A_m \cdot \frac{2\pi}{R}$$

where R is the resolution of the instrument. A_m is the area of the interferometer mirror. Typically, $A \sim 1\ cm^2$, and for $R \sim 10^3$, $E_{MIS} \sim 6 \times 10^{-3}$.

For the HTS, from equation (3-1) one obtains

$$E_{HTS} = A_g \left(\frac{w \cdot h}{F^2}\right)$$

where h and w are slit height and width and F is the focal length. For a double multiplexed spectrometer, the throughput of MIS and DHTS are about the same, of the order $10^{-2}\ cm^2$. For the same throughput, the HTS may have a worse system transmission because the HTS requires a dedispersing process.

DHTS has the additional advantage that one can construct a one dimensional picture of the source.

(D) Mechanical Requirements

The HTS mask can be made self-supporting hence no beam-splitters or transmission optics, are required. Furthermore, in the MIS, construction tolerances usually involve dimensions and motions that have to be maintained to within fractions of wavelengths. For a HTS, the corresponding tolerances are fractions of a slit width, and these tolerances are normally two orders of magnitude more relaxed, so that this instrument will be more suitable for rugged applications and less costly.

It is clear from the above comparison that the MIS has the advantages of highest resolution, very large multiplex number and free spectral range. The HTS has the mechanical advantages and computational advantages for large N. The HTS can have on the order of 10^3 spectral elements and a resolution sufficient to resolve the rotational lines of many molecules. For most IR astronomical observations this will be sufficient. Furthermore, its potential for modifying the existing sacnning spectrometer at a moderate cost make this a very worthwhile field for further study.

CHAPTER V

PROGRAMMING FOR HADAMARD TRANSFORM SPECTRAL DATA REDUCTION

An 8K Computer Automation minicomputer model L.S.I. or model Alpha-16 can be used to interface with the output of a Monsanto scalar counter which digitized the output of the detector used with the Hadamard transform spectrometer. The computer processes each data point as soon as it receives it and when the data gathering run is completed, the computed spectrum is also ready within a fraction of a second. The final spectrum can be displayed on a cathode ray tube for quick visualization, or printed on paper by a teletype machine for more detailed analysis. Also, it can be stored on paper tape for future use.

There are two inverse transformation programs: 1 x 255 for the single entrance slit and 255 exit slit Hadamard transform spectrometer, HTS, and 15 x 255 for the 15 entrance slit and 255 exit slit instrument, DHTS.

(A) HTS Program

The inverse HTS program processes the raw data obtained by the combination of a single entrance slit and 255 exit slit. This program is in double precision format. Two areas in the memory are reserved by the program to store the final spectrum. The final spectrum can be stored in either the plus beam or the minus beam area. The plus and minus beams are arbitrarily named.

Data can come in at a rate of 10 data points per sec., 5 data points per sec., or 2.5 data points per sec., depending on how the clock driving the spectrometer is set. Since a complete pass has 255 points, each pass takes 25.5 sec., 51 sec., or 102 sec., depending on the data rate. Each pass yields one spectrum. One can take as many passes as one wants until one is satisfied with the SNR of the spectrum.

The whole program (Appendix B) is linked by the following subprograms: COMMAND, TRANSFORM, INPUT/OUTPUT, READ, CLEAR, PUNCH, GRAPH, DISPLAY, MATHMATICAL PACKAGE and MASK. The function of each subprogram is described briefly in the following sections.

1. <u>COMMAND:</u> This subprogram performs two functions.
(a) It commands the computer to do one of the following functions: TRANSFORMATION, CLEAR, READ, PUNCH, GRAPH or DISPLAY.
(b) If two distinct spectra are stored in two different beam areas, the COMMAND program can take the difference and ratio of the two spectra.

2. <u>INVERSE TRANSFORM:</u> This is the most important subprogram in the whole program. It will take data points from the counter, transform them and enter them into either the plus or minus beam areas, or it will read the data points from the paper tape into one beam area, transform them and enter them into the other beam area. This program is called the inverse transform, since it inverts the transformation performed by the coding mask, and

yields a spectrum. The program also performs the Hadamard transform, i.e. transforms the spectrum back to raw data, from either input.

The algorithm is based on the following idea: Let ψ_j be the j^{th} spectral element and w_{ij} be the weight of the j^{th} element of the i^{th} mask. w_{ij} equals 1 for transmitted radiation and 0 for blocked radiation. Each measurement then has a value

$$\eta_i = \sum_{i=1}^{255} S_{ij}\psi_j + \nu_i$$

where ν_i is the random detector noise satisfying the properties mentioned in Section II-B. $\underline{S}$ is the 255 x 255 matrix. η_i is the i^{th} data point entered into the computer. The computer's job is to decode η_i to reconstruct the original spectral values ψ_j. Therefore

$$\hat{\psi}_j = \sum_{i=1}^{255} S_{ji}^{-1} \eta_i$$

where $\hat{\psi}_j$ is the unbiased estimate of ψ_j and $\underline{S}^{-1}$ is the inverse of the S matrix.

According to the relation

$$\underline{S}^{-1} = \frac{2}{N}(2\underline{S} - \underline{J})$$

one obtains $\underline{S}^{-1}$ by keeping all +1's in the S-matrix and replacing all 0's by -1. The matrix obtained in this way is the inverse matrix of $\underline{S}$ except for a constant factor $\frac{2}{255}$, which only gives a different normalization.

To reconstruct the spectral values ψ_j one needs to add or subtract each measured value to n_i different bins, according to whether $\underline{S}^{-1}$ is plus or minus. Fig. (5-1) is a flow chart for the 1 x 255 transform program.

By a Hadamard transform we mean a program that transforms the spectrum back to its raw data*. This procedure is useful because by inspecting the raw data display which usually appears quite smooth, any bad data point can be easily identified, and for example, replaced by the average of its two adjacent data points. This procedure will improve the final spectrum.

The Hadamard transform turns out to be extremely easy. All one has to do is to change one statement in the inverse transform program. When S^{-1}_{ij} is -1, instead of negating the data, one just sets it to zero.

Data points are taken both with the exit mask moving in a forward and in a reverse direction. The inverse transform program takes care that when the exit mask moves in the forward direction, the spectrum is transformed into the plus beam area. When the exit mask moves in the reverse direction, the final spectrum is stored in the minus area. Not adding the

---

* The notation here may be a bit confusing. We use the $\underline{S}^{-1}$ to transform the raw data into an intensity spectrum. The inverse transform uses $\underline{S}$ to transform the intensity spectrum back into raw data.

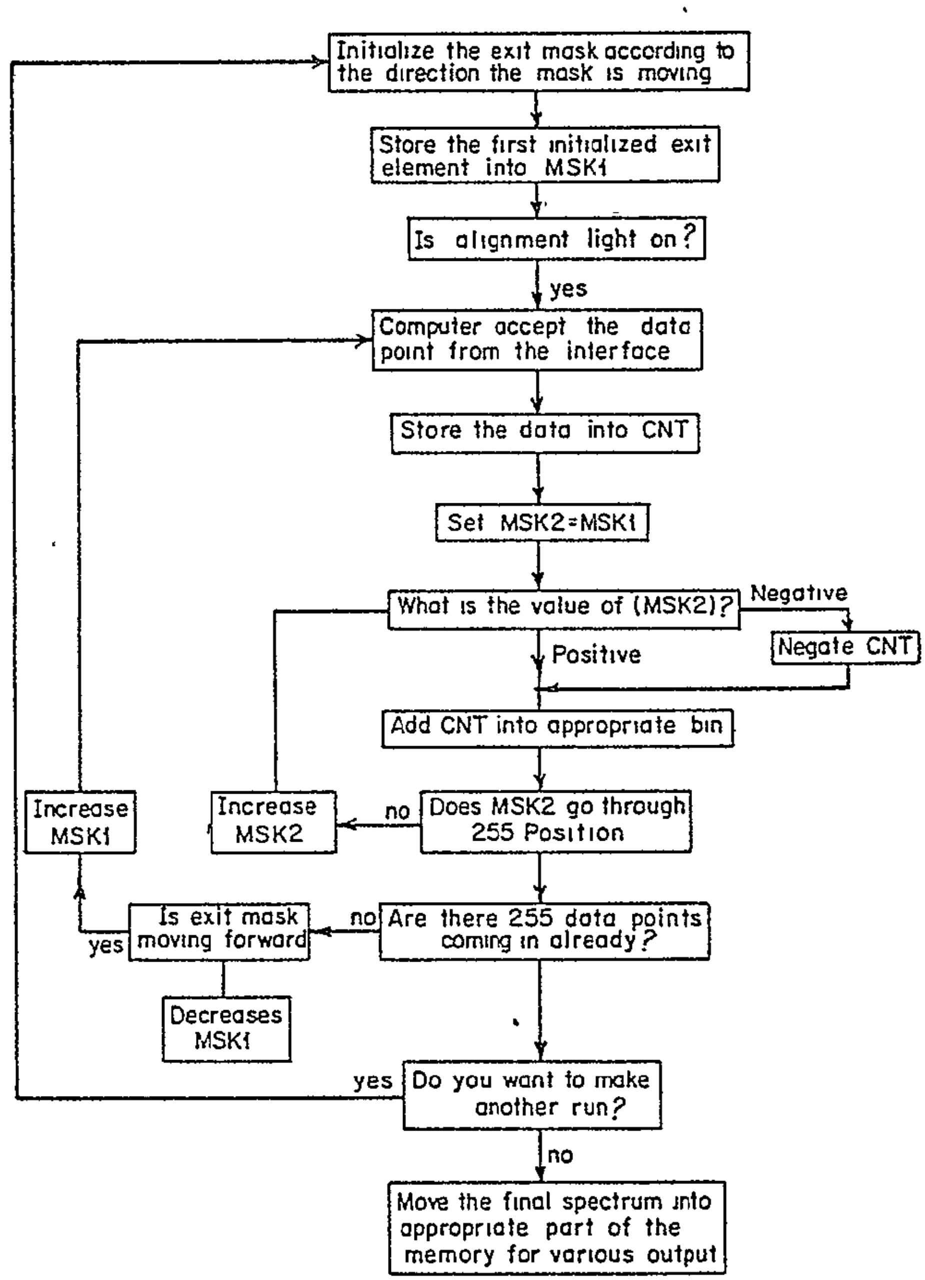

Figure 5-1. The flow chart of the 1x255 inverse transform program.

forward and backward spectrum eliminates a degradation of the final spectrum due to any asymmetry between the data taking for different directions of motion of the mask.

3. INPUT/OUTPUT: This program links up the computer, the teletype and high speed reader. It consists of the following functions: Keyboard Input, Paper Tape Input, Output to Teletype, Output Text from Buffer, Output Floating Point Number, Wait for Execute Signal, Command Error Exit, Carriage Return-Line Feed.

4. READ, CLEAR, PUNCH: This program reads the spectrum from the paper tape into either plus or minus beam areas for further maniption, or punches the spectrum out from the beam area; it also can clear the beam area. The speed of teletype for reading is 100 words per sec. Hence it takes about 12 min. to read the spectrum. Punching has the same rate.

5. GRAPH: This program plots the graph on teletype paper, with its numerical value in floating point format. This procedure offers one the chance to inspect the spectrum in detail if it is needed. It takes about fifteen to twenty minutes to finish a spectrum, depending on the complexity of the spectrum.

6. CRT: A cathode ray display is interfaced with the output of the computer. It takes about 2 sec. to display the spectrum, with a factor of 5 higher resolution than the graph printed by the teletype on paper. One can display the spectrum at the end of any pass to see how good it is.

7. MATHMATICAL PACKAGE: This package is supplied by the Computer Automation library tape, with a little modification

from our own on its double precision part.

8. MASK: This part contains the $\underline{S}^{-1}$ matrix, the 255 elements exhibited in the first mask position plus an additional 254 elements representing the further cycling of this mask.

(B) DHTS

The doubly encoded Hadamard transform program processes the data obtained by the various combinations of fifteen entrance slots and 255 exit slots. It is a single precision program. It can accept data at a rate of 5 data points per sec. and 2.5 data points per sec. only, because it takes a longer time to process each data point. The whole transform takes about 14 minutes. The final spectrum consists of 15 separate spectra, representing a one-dimensional color picture across the spectrometer entrance aperture. Each separate spectrum contains 255 spectral elements. The program can co-add all fifteen separate spectra yielding a sum spectrum with improved SNR.

The program consists of the following subprograms: COMMAND, TRANSFORM, DATA, INPUT/OUTPUT, READ, CLEAR, PUNCH, GRAPH, DISPLAY, ENTRANCE MASK, EXIT MASK. (Appendix C). Since most of the subprograms are preforming the same function as their counterpart in the 1 x 255 case, except written in single precision format, their description will not be repeated here. Only the TRANSFORM, DATA, and DISPLAY programs will be discussed because they are different from those in the 1 x 255 scheme.

1. INVERSE TRANSFORM: The program can accept data eigher from the counter or from paper tape. In order to eliminate any asymmetry due to the different directions of motion of the exit mask, the computer will accept data only when the mask is moving in a given direction, either forward or backward, depending on the operator. If one wants to save time, one can still choose the mode in which the computer will accept data in both directions of mask motion. Hence, the program provides six modes for operation: accepting data from the counter, in the forward, backward, or both directions, and accepting data stored on the paper tape, in the forward, backward and both directions. Figure (5-2) shows the flow chart for 15 x 255 program.

Let both the entrance and the exit masks be linear arrays encoded by Reed-Muller codes. Then the matrix of spatial-spectral elements ψ is related to the matrix of measurements η by

$$\underline{s}\ \underline{\psi}\ \underline{S} = \underline{\eta}$$

To obtain the spatial-spectral information about the viewed scenc we solve this equation by premultiplying the data matrix by $\underline{s}^{-1}$ and postmultiplying by $\underline{S}^{-1}$

$$\underline{\psi} = \underline{s}^{-1}\underline{\eta}\ \underline{S}^{-1}$$

Now consider the element η_{11}. It is multiplied only by elements of the first column of $\underline{s}^{-1}$; and in turn it multiplies only the elements of the first row of $\underline{S}^{-1}$. To a given spectral-

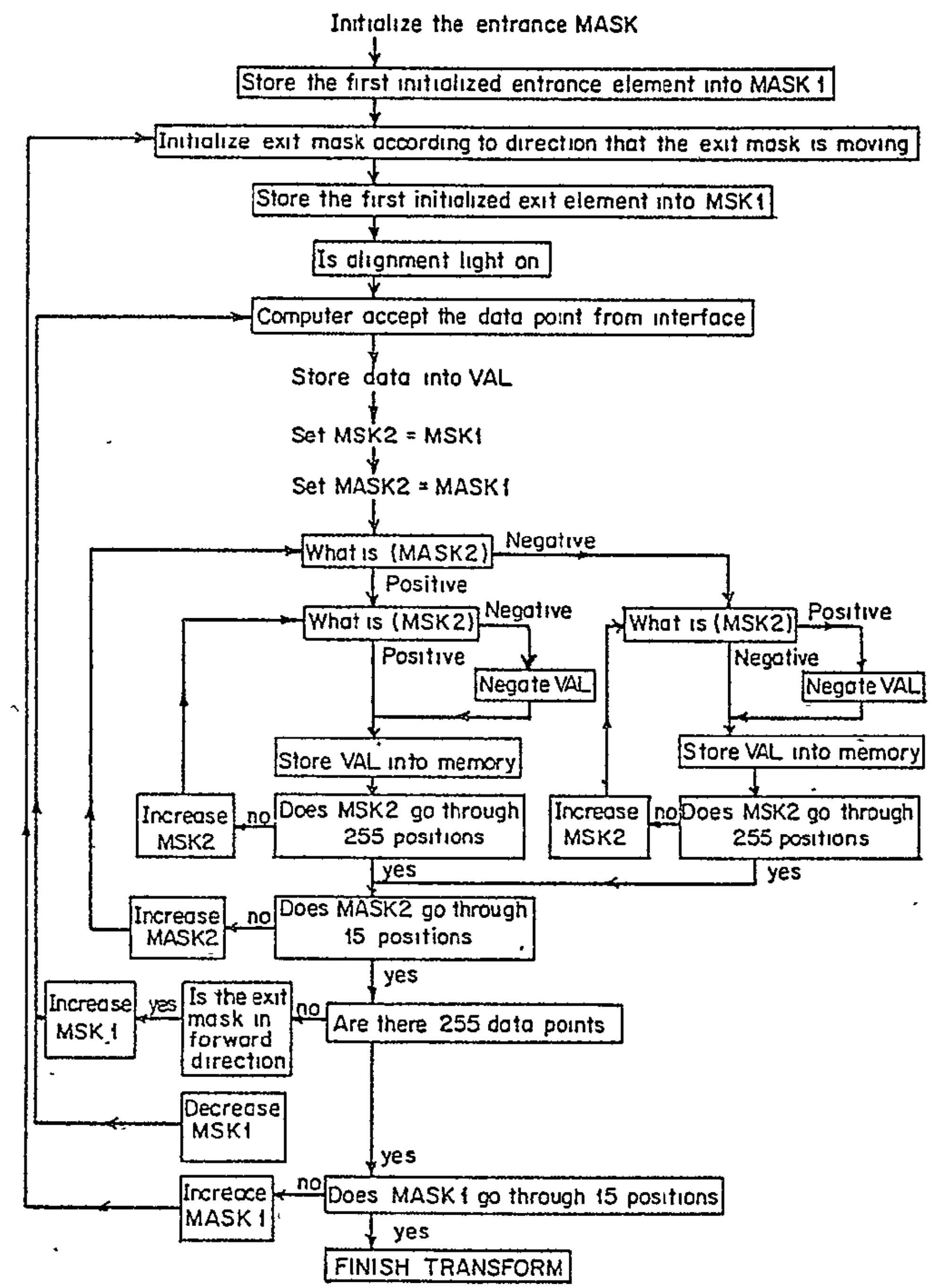

Figure 5-2. The flow chart of the 15x255 inverse transform program.

spatial element ψ_{ij}, it therefore contributes an amount $s_{i1}\eta_{11}S_{1j}$. But the elements s_{i1}^{-1} and S_{ij}^{-1} all have values, either +1 or -1, and the result is that each element ψ_{ij} of the matrix ψ receives a contribution $+\eta_{11}$, or $-\eta_{11}$ from the reading, η_{11}.

This procedure is generally valid. Any reading $\eta_{k\ell}$ will make additive contributions that can only have values $+\eta_{k\ell}$ or $-\eta_{k\ell}$ to each element ψ_{ij} of the ψ matrix.

For real time decoding we therefore need the following:

(a) A memory that consists of bins containing the contributions to the elements ψ_{ij} accumulated up to any given time t in the cycle of measurements. For a device that can resolve m spatial and n spectral elements, this memory reruires mn bins and of the order of mn memory words.

(b) For each acquired reading $\eta_{k\ell}$ we perform a series of additions of values either $+\eta_{k\ell}$ or $-\eta_{k\ell}$, one to each of the ψ_{ij} memory bins. But before that can be done, we need to decide on the assignment of + or - needed for a given bin. This is done in the following way.

We store the sequence of + and - signs in one column of $\underline{s}^{-1}$ and in one row of $\underline{S}^{-1}$ and in one cycled permutation of each of these vectors. Let us designate these signs by their positions in these two vectors, as $\underline{s}_i^{-1}$ and $\underline{S}_j^{-1}$, respectively, i=1,... m; j=1,... n. (Since each of these sequences is cyclic it can, respectively, be brought into its kth and ℓth cycling position after a measurement $\eta_{k\ell}$). The elements of the two vectors then are multiplied in all possible combinations to give a matrix having mn elements.

$$\Sigma_{ij} = s_i^{-1} S_j^{-1} \qquad i=1 \cdots m;\ j=1 \cdots n$$

Each element Σ_{ij} is either + or - depending only on whether the signs s^{-1} and S_j^{-1} are similar or dissimilar for a particular combination of i and j values.

The additions $+\eta_{k\ell}$ or $-\eta_{k\ell}$ to the bins ψ_{ij} are made as successive elements, Σ_{ij} are computed, so that the elements Σ_{ij} need never be stored. Figure (5-3) shows the relation of Σ_{ij} to a superarray containign the set of all elements that are constructed at various stages of the computation.

When only a restricted number of spectral elements are of interest, we need to compute elements ψ_{ij} representing only selected j values. This might be useful, for example, if only certain atmospheric CO_2 absorption lines needed to be studied, and the spectral elements between were of lesser interest. In that case only $\Sigma_{k+i-1,\ell+j-1}$ elements corresponding to given j values need to be used, and the computing time decreases as p/n, where n is the total number of available spectral elements, and p is the actual number of interest.

One starts with the inverse of the codes, s^{-1} and S^{-1}, for the entrance and exit masks stored in the computer. One stores 509 elements of the exit mask, i.e., the 255 elements exhibited in the first mask position plus an additional 254 elements representing the further cycling of this mask. Similarly one stores twenty-nine elements for the entrance mask,

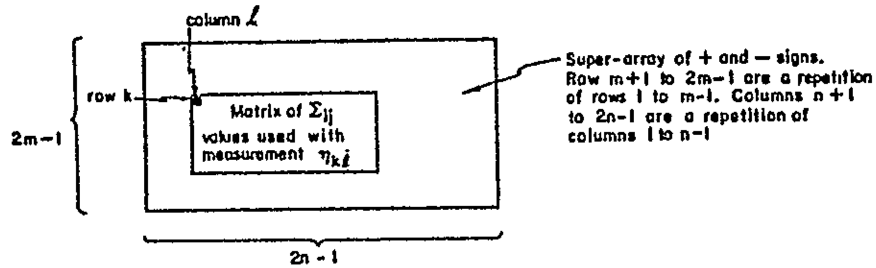

Figure 5-3. Matrices generated by the computer during the reduction of the spectral data.

representing the first fifteen elements used, plus the further cycling of fourteen elements.

For each reading $\eta_{k\ell}$ one essentially makes use of the matrix (figure 5-3) making use of elements k to k+14 of the stored entrance code and elements ℓ to ℓ+254 of the stored exit code. This matrix consists of + and - signs. When s^{-1}_{ik} and $S^{-1}_{\ell j}$ have the same sign, both being + or both being -, the matrix position ij is assigned a + sign, and the reading $\eta_{k\ell}$ is added to the accumulatively stored value of ψ_{ij}. If the elements s^{-1}_{ij} and $S^{-1}_{\ell j}$ have dissimilar signs, a - sign is assigned to ij and the reading $\eta_{k\ell}$ is subtracted from the stored ψ_{ij} values. This whole process takes ~100 msec, and is carried out while the succeeding intensity measurement is being made.

In pratice, we start with the first spatial element, i=1 and add or subtract the contributions to all the ψ_{1j} values, successively going from j=1 to j=255. We then repeat this procedure for i values going from 2 to 15. This whole procedure is carried out while the exit mask is moving from posiiton ℓ to ℓ+1 depending on whether the exit mask is moving forward or back. The entire process is then repeated for the next reading $\eta_{k,\ell+1}$. When the exit mask reaches its 255th position, ℓ remains unchanged, but the entrance mask moves from the position k to k+1.

For odd values of k, the exit mask moves in the direction of increasing ℓ values, and for even values of k, it moves toward decreasing values. In short, the exit mask moves back and forth as readings are taken. After the entrance mask has moved through all its fifteen positions, and the total 3825 readings have been taken and added onto or subtracted from the ψ_{ij} elements, the run is completed.

2. DATA: Instead of processing a data point immediately as it comes in, this program stores the data in the memory, so one can display the raw data points first, correct them if there are any obvious bad points, and then transform them. This program serves the same function as the inverse transform in the 1 x 255 system.

3. DISPLAY: The display program allows one to display the information in a number of different ways:

(a) One can call for the spectrum corresponding to any one of the entrance slit positions and display it individually.

(b) One can display the sum of the different spectra. In order to do this, one has to take into account that the spectrum for a given entrance slit is displaced by one spectral position from adjacent entrance slit position. In other words, the wavelength for element ψ^{-1}_{ij} corresponds to the wavelength for element $\psi_{\ell+1,j+1}$, because of the slightly displaced light paths through the spectrometer.

(c) Finally one can display all fifteen of these spectra simultaneously, with the zero baseline of each spectrum vertically displaced from the next one. While this format is somewhat crowded, it does allow a quick comparison of the individual spectra.

(C) Correction Program:

This program is shown in Appendix D written in BASIC language. It corrects the error introduced by the imperfect mask. Instead of correcting the mask which in practice is not possible, the program corrects the final spectrum. That is much easier.

As seen in section II-D, for any spectral line I_o, the distorted spectrum shows a line $I_o^{'}=I_o(1-\varepsilon)$, two positive blips with amplitude $(1/2)(\varepsilon I_o^{'}/1-\varepsilon)$ adjacent to the line on both sides, and two negative blips with same amplitude, i.e. $(\varepsilon/2)(I_o^{'}/1-\varepsilon)$ at 24, 25 elements to the left. The correction program takes the intensity of every element, $I_o^{'}$, multiplies it by $\varepsilon/2$, adds it to the elements 24 and 25 positions to the left, and subtracts it from the two adjacent elements, one on each side of the line. The final spectrum is complete except for a different normalization factor. This is a linearized correction procedure valid only for small values of ε, $\varepsilon \ll 1$.

CHAPTER VI

ASTRONOMICAL OBSERVATION

(A) Correction Procedure

The correction of the spectra for telluric absorption and for instrumental response is a critical procedure. The correction is carried out by comparing the source spectrum (either stellar or planetary) with a lunar or solar spectrum which is taken on the same day at an airmass as close as possible to the star. The following procedures are used in the data reduction:

(1) Correct the raw star spectrum and lunar spectrum (or sun) for negative dip due to the imperfect mask as described in section II-D.

(2) Correct for different entrance slit width if necessary because different slit widths will give different resolution.

(3) Most of the astronomical infrared sources to be observed are weak sources, hence a positive offset is always added to the signal to prevent the signal becoming negative. (The electronics are confused by negative signals.) The correction procedure shown previously also take out this offset. One can take out the offset from the raw spectrum if one knows how large the offset is. Another way to correct this is by substracting a constant intensity from the stellar spectrum until the ratio of the stellar spectrum over the Moon spectrum,

around any large telluric absorption reigon, such as the ozone band, is optimally corrected. By optimal correction we mean that the atmospheric feature appears as neither a positive, nor a negative band. The Moon is a strong infrared signal and does not require an offset, so the result can be used as a calibration for base line.

(4) Align the stellar spectrum and the lunar spectrum by the telluric absorption feature. The final stellar spectrum is obtained by taking the ratio of the stellar spectrum and the lunar spectrum and multiplying it by the black body temperature of the Moon. The lunar temperature is obtained by noting the phase angle of the lunar east limb where it has usually been observed, and extrapolating the temperature from the value given by Linsky (1973). This procedure assumes the lunar infrared emissivity at 8-14μm as unity, which is not true. Murcray et al's (1970) results for the lunar emissivity of 8-14μm region are shown in figure (6-1). The observation was done from a balloon. The strong feature centered at 9.6μm is a result of telluric ozone absorption. Murcray's result has not been used in our analysis because in the region to be discussed, 8.5μm-14μm, the Moon's emissivity is about constant except for the ozone absorption.

(B) Observation of α-Orionis

The observations of α-orionis were carried out with the 50" infrared telescope at Kitt Peak National Observatory, Arizona, in May 1974. The beam size is 18 sec. x 47 sec. The Kitt Peak 50" telescope bolometer was used with the Hadamard spectrometer. The dewer has a band pass of 8 - 14μm. The spec-

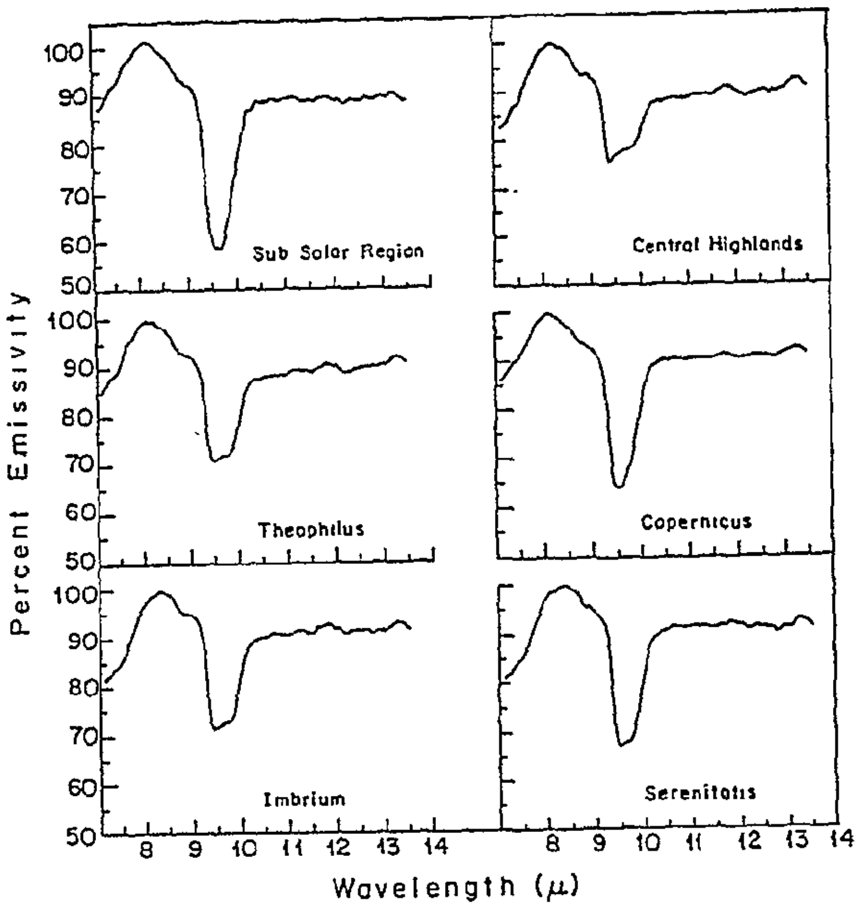

Figure 6-1. The spectral emissivity of various regions as calculated from the flight data (Murcray *et al*, 1970).

trometer operated in the 8-11μm region with a resolution $\lambda/\Delta\lambda$ around 500. The chopping frequency was 10 cycles per second.

Three runs were taken. Each run consisted of 10 scans of the sources. Two lunar spectra were taken on the same day for correction purposes. For the lunar temperature we used 383°K. Figure (6-2) shows the raw spectra of α-orionis and the Moon. The α-orionis spectrum is the sum of two independent runs.

Figure (6-3) shows the ratio spectrum of α-orionis corrected for lunar temperature. Except for the region immediately around the ozone band all the telluric absorption features are gone. The region between 9.35μm to 9.7μm is unreliable because the ozone band has a very low transmission.

α-orionis is a late type super-giant with temperature around 3000°K. A stellar continuum corresponding to a 3000°K blackbody is also shown in figure(6-3), normalized to arbitrary units. The broad emission feature around 10μm, which is due to silicate emission, is clearly shown in the spectrum. This 10μm 'silicate' emission feature of α-orionis has been previously discussed by others.

Woolf and Ney (1969) renormalized Gillett et al's spectra (1968) of α-orionis and interpreted the 10μm emission as coming from circumstellar dust which absorbs starlight and reradiates at infrared wavelengths. Since the emission is far more sharply peaked than a black body, the wavelength dependence of the emission probably closely mimics the wavelength dependence of the opacity of the material. In the same paper, Woolf and Ney

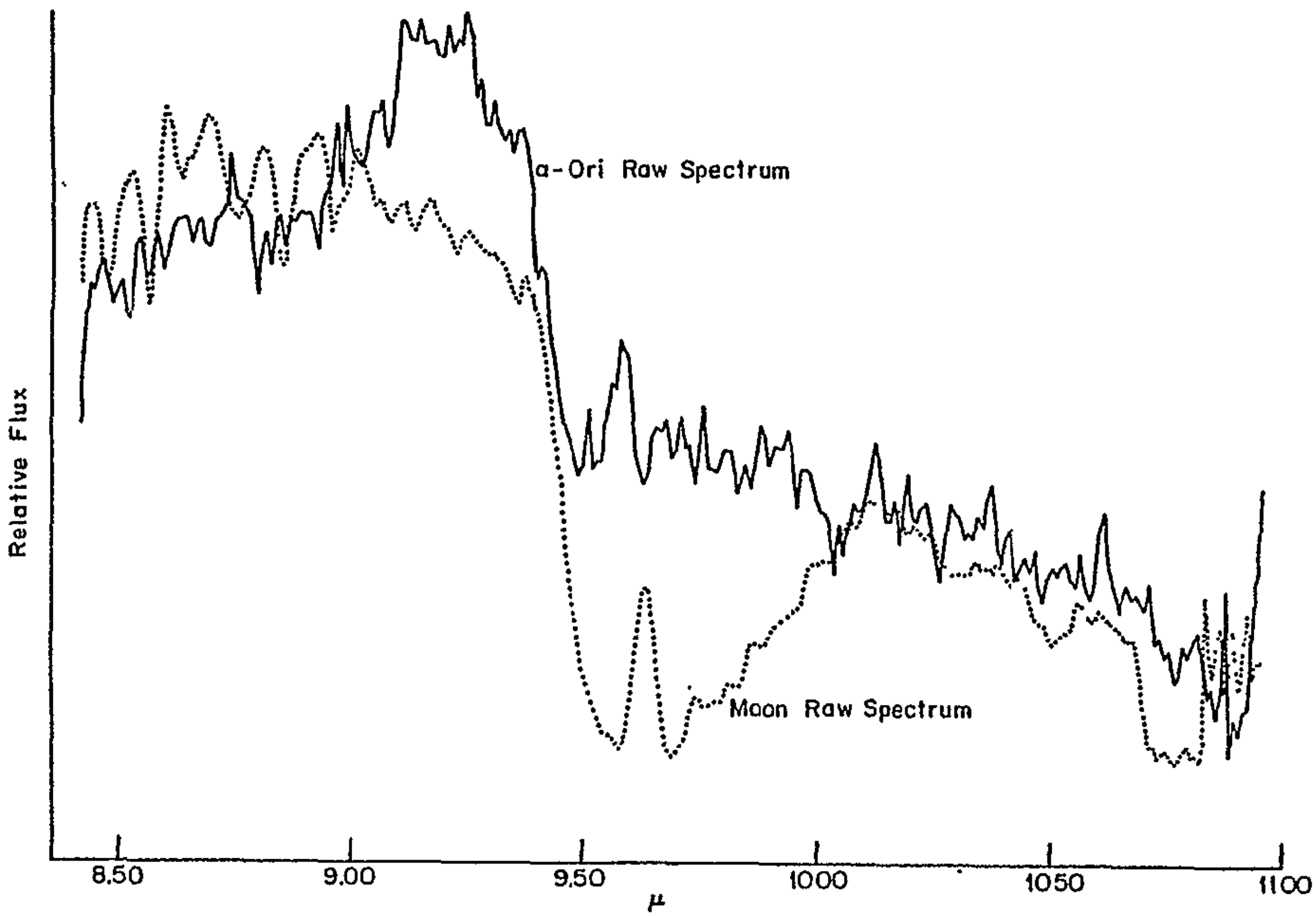

Figure 6-2. The raw spectra of α-orionis and the Moon.

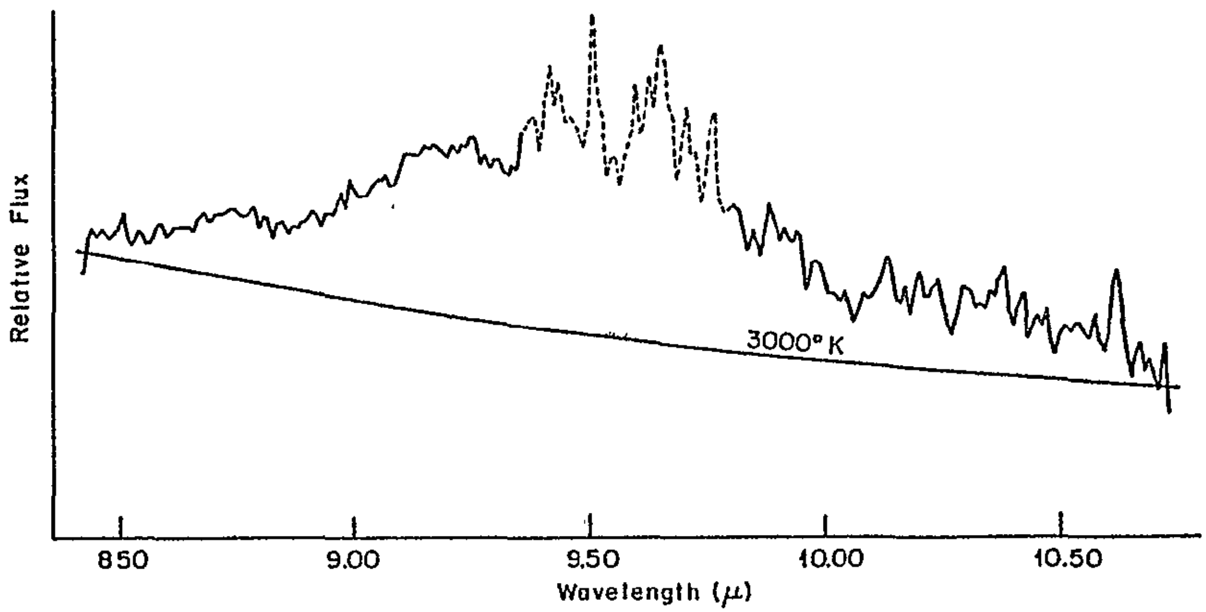

Figure 6-3. The ratio spectrum of α-orionis to the Moon corrected for lunar temperature.

also proposed that it is silicate grains which one is observing in the circumstellar dust cloud. This suggestion has been strengthened by high resolution spectra of Gamown _et al_ (1972) with resolution $\lambda/\Delta\lambda=250$ from 850 cm^{-1} to 1100 cm^{-1}. The emissivity of silicate grains should have a second peak near 20μm. This second emission feature was observed by Low and Swamy (1970) in narrow-band photometry of α-orionis. Another supporting piece of evidence for the silicate model of the α-orionis dust cloud comes from observations of silicon monoxide (SiO). Silicon monoxide is expected to be among the most abundant molecules present in the atmospheres of cool stars of normal composition. It is also a reagent in the condensation mechanism thought to produce circumstellar silicate grains (Mass _et al_, 1970). The presence of silicon monoxide in α-orionis was confirmed by Cuduback _et al_ (1971). They observed SiO absorption features around 4μm.

The silicates are expected to form from the material ejected by cool stars. Gilman (1969) calculated what solids would condense from gas of stellar composition as it moved away from a star and cooled. This is critically dependent on the ratio of oxygen to carbon in the gas. These elements first combine to form carbon monoxide; the subsequent development depends on which of the two is left over when all the other has been used up in this way. If carbon predominates, graphite will be the principal condensate, or under certain circumstances silicon carbide. If oxygen wins, the grains which should form are the silicates of calcium, magnesium, aluminium and iron;

combinations of these are responsible for the 10 and 20μm spectral features. Aluminium and calcium silicate may be rare because of the low cosmic abundance of aluminium and calcium. Woolf and Ney (1969) expected magnesium silicate, $MgSiO_3$, with some iron silicate, $FeSiO_3$, to be most abundant. For recent work on dust grains one can refer to Salpeter's paper (1974 a) on the theory of nucleation and dust grains in carbon-rich stellar atmosphere and his paper (1974 b) on formation and flow of dust grains in cool stellar atmospheres.

Laboratory spectra exist for silicate absorption features (Day, 1974). Any fine feature of the astronomically observed silicate emission may be washed out by different particle sizes and shapes, uncertainty in temperature and mixture of composition. Gammon et al (1972) examined the excess in XY Seg and O Cet and concluded that the type of silicates involved are basic rather than acidic. Day (1974) synthesized the amorphous magnesium silicate and obtained an absorption band quite similar to the material causing the interstellar 10μm absorption feature. He suggested that the existance of disordered structures seems a more reasonable expectation than crystalline terrestrial-type minerals. For the momnet, the nature of the silicates is certainly at an unsettled stage.

Penman (1976) had measured the middle infrared reflectivities of five silicate minerals, and used Kramers-Konig analysis to obtain the optical constants of the samples. He then used the optical constants in Mie computations of the absorption properties of very small mineral grains. The final absorption cross-section spectra compared to the observed 10μm silicate of the source W3/IRS5. All the calculated spectra have sharper features than the astronomical features due to the application of Mie theory. However, the hydrated silicate, Chloritite (hydrated Mg/Fe/Al silicate) and serpenlenite (hydrated Mg/Fe silicate) fits the observed astronomical positions correctly. They fall almost exactly at the center of the astronomical features.

To the author's knowledge only two spectra of α-orionis in 8-14μm exist in the literature. Gillett et al (1968) (figure 6-4a) obtained results in the wavelength region from 2.8 to 14μm, with a resolution $\lambda/\Delta\lambda=50$. Treffers and Cohen (1973) (figure 6-4 b) obtained a spectrum from 8-14μm, and in the 20μm region with resolution 1000. Gillett's and Treffers and Cohen's spectra are shown in figure (6-4). Compared with our result, all show the 10μm emission feature if Gillett's black body curve is lowered instead of being drawn tangent to the observed data at 10μm. Our spectrum shows a rather rapid dip at wavelengths beyond 10μm while Treffers and Cohen show a slower nearly constant decline. Further high resolution observations should clear this matter up. Our own instrument now operates at a resolution similar to that of Treffers and Cohen, and if used on a telescope as large as the 120 inch Lick Observatory reflector that they used, sufficiently high signal to noise ratios should be obtained.

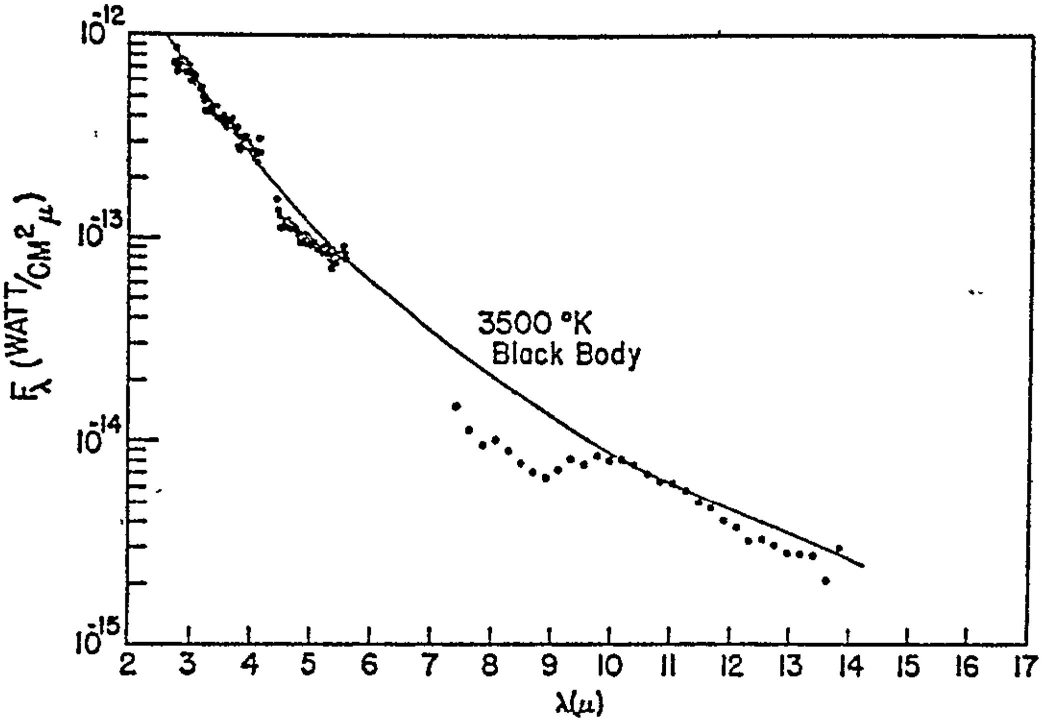

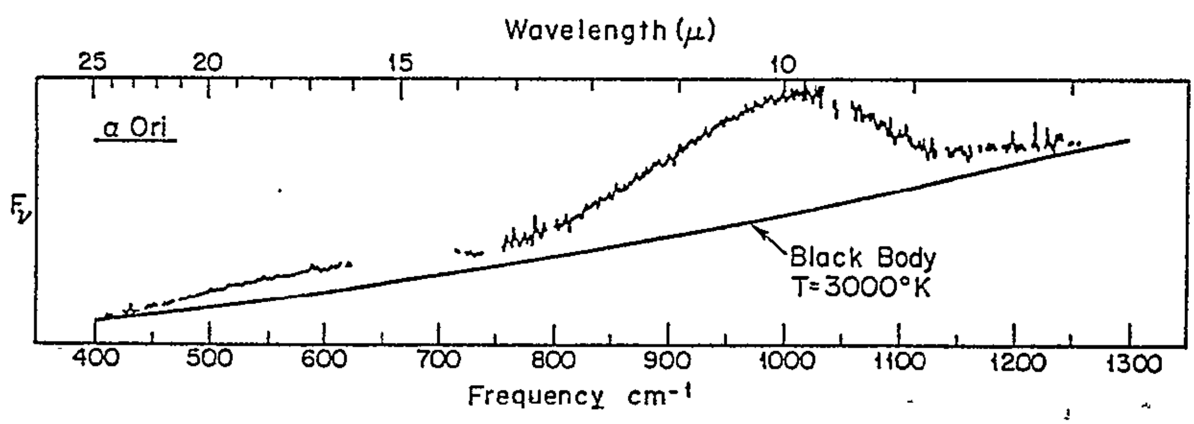

Figure 6-4. (a) Low resolution spectrum taken by Gillett et al(1969). Different symbols represent spectra taken on different nights. (b) High resolution spectrum taken by Treffers and Cohen (1973).

(C) Observations of Jupiter

The observations of Jupiter were also carried out with the 50" infrared telescope at Kitt Peak. The beam size is 18" x 47". The Kitt Peak bolometer assigned to the 50" telescope with band pass 8-14μm was used with the Hadamard spectrometer. For our Jupiter observations, the spectrometer operated in the 10.8-13.4μm region with an effective resolution $\lambda/\Delta\lambda$ around 250. The chopping frequency was 10 cycles per second.

Two runs were taken. Each run consisted of twelve scans of the whole Jovian disk. Two lunar spectra were taken on the same day for correction purposes. For the lunar temperature we used a value of 383°K. Figure (6-5) shows the raw spectrum of Jupiter and the Moon. Both the Jovian and lunar spectra are the sums of two independent runs. Figure (6-6) shows the ratio spectrum of Jupiter corrected for lunar temperature. The arrows labeled by H_2O show the position of telluric water vapor features. Most of the telluric features have been cancelled properly.

Jupiter is covered by clouds which in the visible part of the spectrum are seen from earth. Current models show three distinct cloud layers (figure 6-7, Ingersoll). The lowest layer is water ice, with maximum density at about 270°K. The middle cloud is solid ammonium hydrosulfide (NH_4SH) at about 200°K. Lewis and Prinn (1970) suggested that ultraviolet radiation from 2200 to 2700 Å is not absorbed by H_2, He, CH_4 and absorbed a little by NH_3. Therefore, the radiation in this

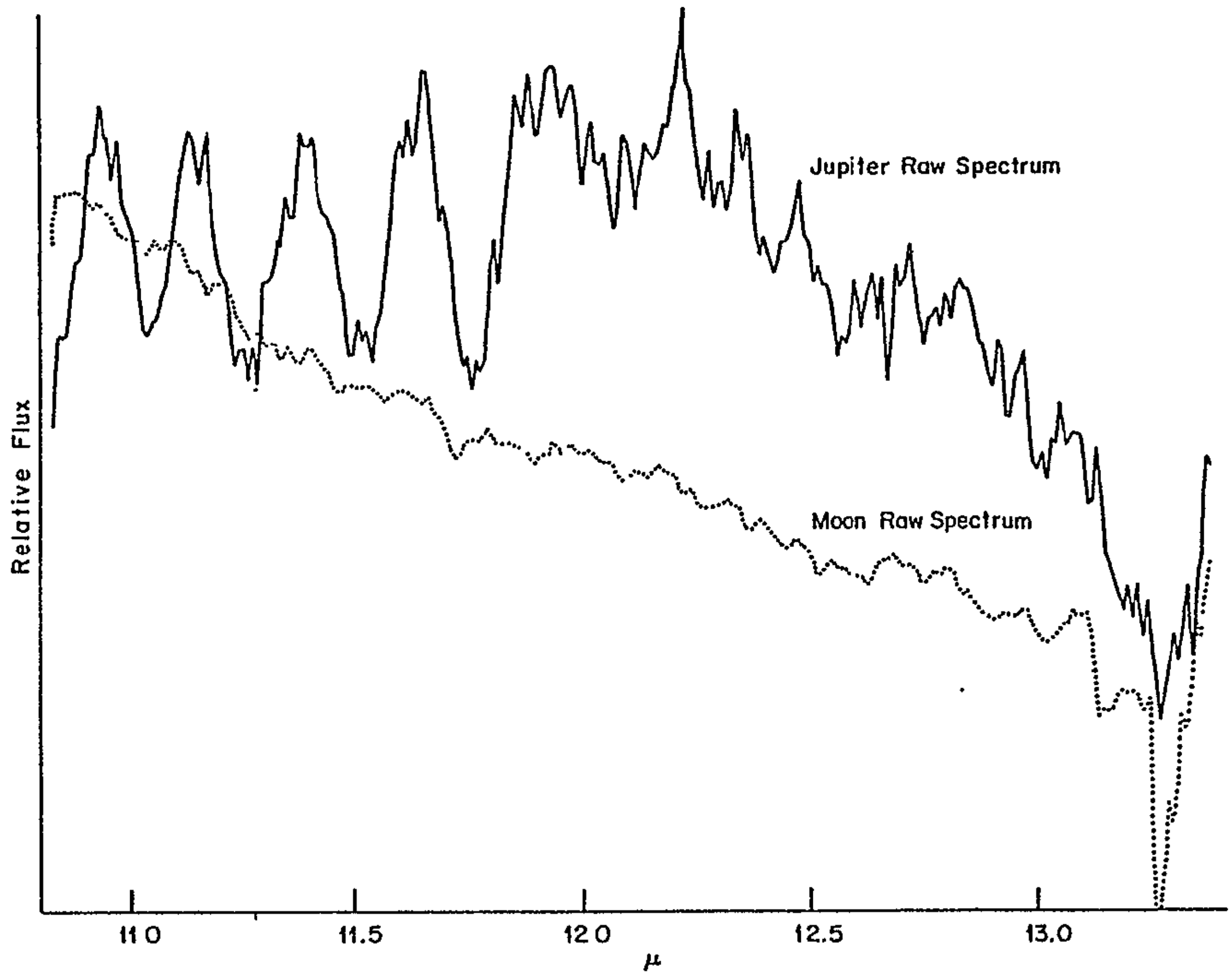

Figure 6-5. The raw spectrum of Jupiter and the Moon.

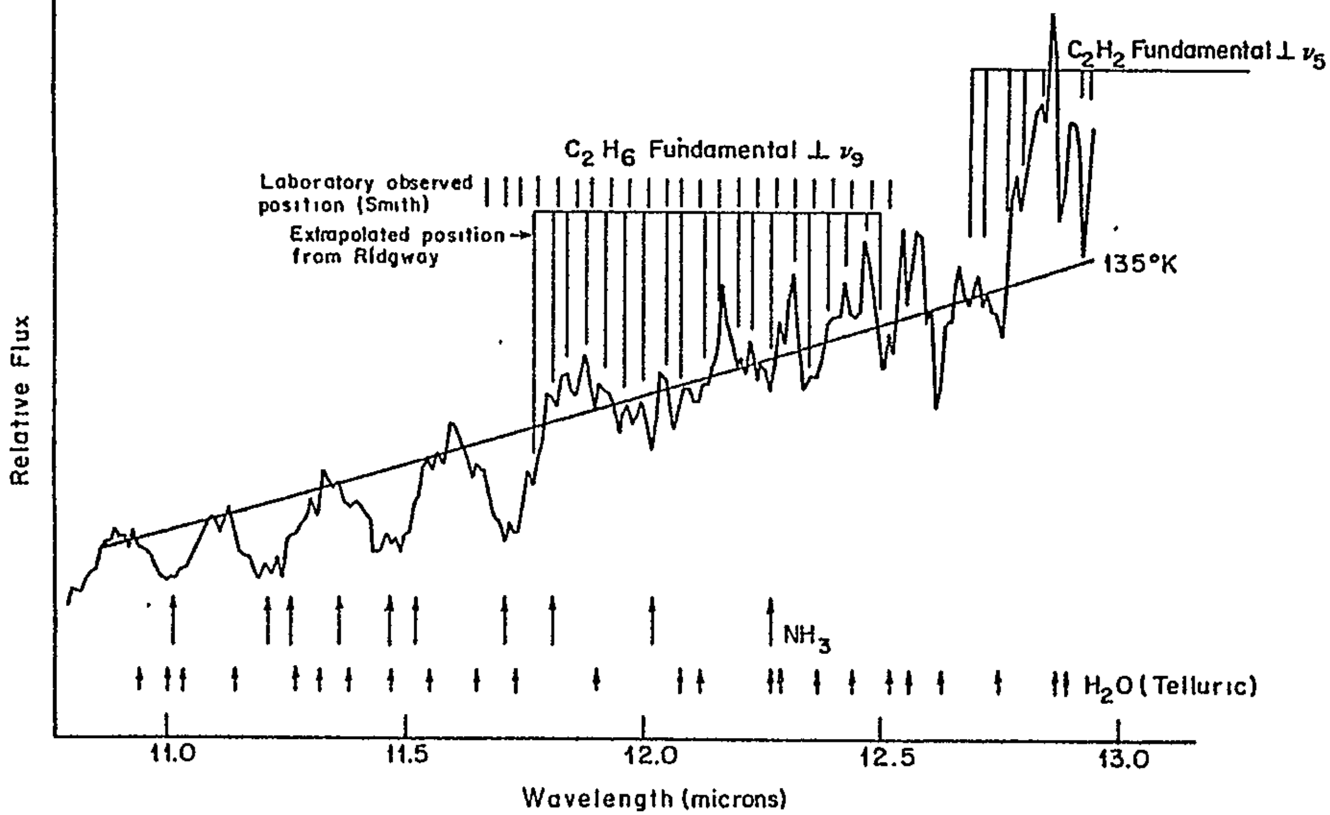

Figure 6-6. The ratio spectrum of Jupiter to the Moon corrected for lunar temperature.

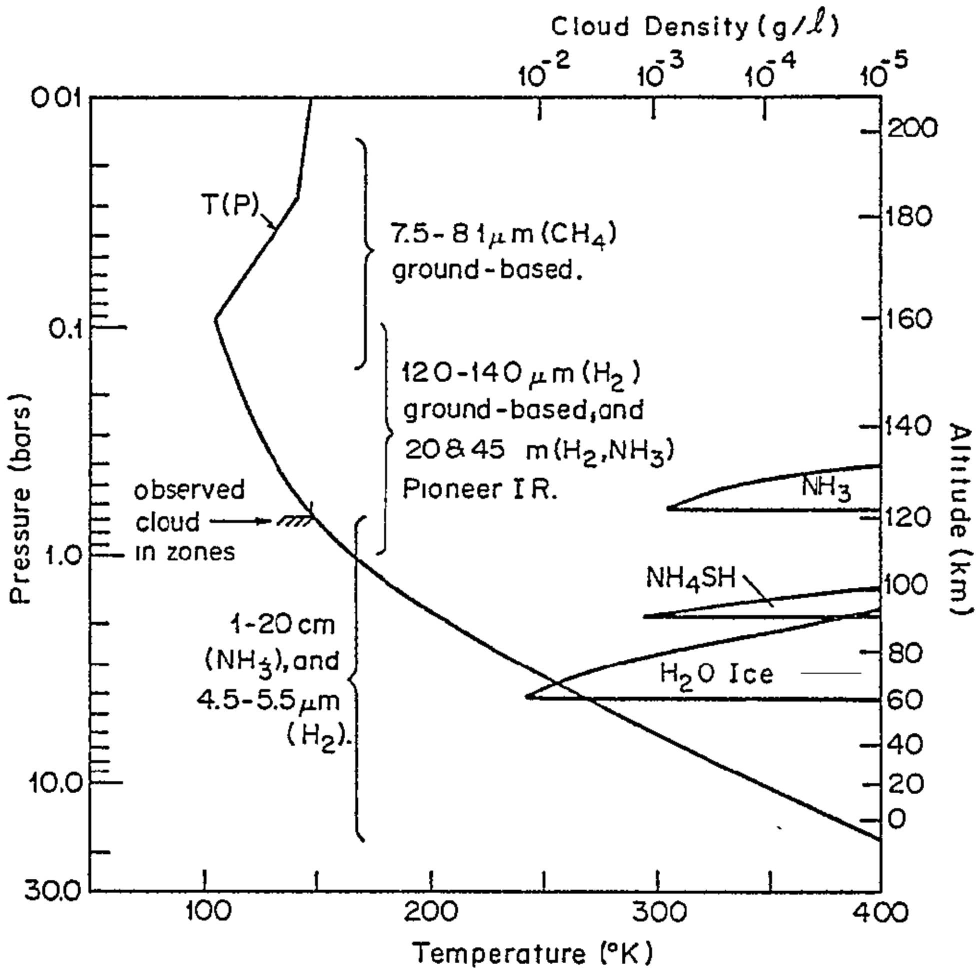

Figure 6-7. The atmospheric profile of Jupiter for a solar-composition model.

region may reach the ammonium hydrogen cloud and photolyze hydrogen sulfide there into hydrogen polysulfides (H_2S_x), elemental sulfur, and ammonium polysulfides $\left[(NH_4)_2S_x\right]$. All of these species are yellow, orange, or brown and may explain the color of zones. However, Sagan and Salpeter (1976) suggested that even under the most optimistic assumption that every H_2S photo dissociation event leads to polymerics, the implied optical depth falls short by two orders of magnitude from matching the observed values. Moreover, pure polymeric sulfur fits the observed optical properties of the Jovian red chromophores only poorly (Rages and Sagan, 1977). The upper cloud is solid ammonia at around 150°K. Solid ammonia is whitish and probably forms the white zones on the Jovian disk. The color of the Great Red Spot may be due to high altitude ultraviolet photolysis of phosphine (PH_3) into P_2H_4 and amorphous red phosphorus. The total depth of the cloud system is about 70 Km, and the pressure range probably runs from about 0.5 bar at the top to 4.5 bar at the cloud base. It is the cloud tops and above where the 10μm infrared radiation originates. Our spectrum measures a color temperature of 135°K which is consistent with Ingersoll's picture. The radiation should come from the cloud tops because the Jovian atmosphere at 10.5 to 13μm has appreciable opacity, as discussed in the next paragraph.

The main constituents of the Jovian atmosphere are hydrogen molecules, helium molecules, methane and ammonia, with minor constituents hydrogen sulfide, water, ethane and acetylene. Table 6-1 shows their observed abundance ratio by number.

TABLE 6-1

Solar composition atmosphere (fraction by number)

Species	(1)	(2)
H_2	0.886	0.870
He	0.112	0.128
H_2O	1.05×10^{-3}	8.80×10^{-4}
CH_4	6.30×10^{-4}	6.17×10^{-4}
NH_3	1.52×10^{-4}	1.49×10^{-4}
H_2S	2.90×10^{-5}	2.56×10^{-5}

(1) Weidenschilling and Lewis (1973).

(2) Podolak and Cameron (1974); Cameron (1973).

The table is taken from Ingrosell.

The abundances of hydrogen, methane, ammonia, and helium seem consistent judged from solar atomic abundances. For detailed information one can refer to McElroy (1973).

The opacity due to hydrogen molecules is caused by pressure induced dipole absorption. The hydrogen molecule has no permanent dipole moment, and consequently, no permanent dipole spectrum. Gaseous H_2, however, has a weak pressure - induced dipole spectrum which absorbs significantly over the long path lengths and low pressure of the Jovian atmosphere. The induced dipole moment results from two distinct physical process (Kranendonk and Kiss, 1959). The first takes place when the permanent quadrapole moment of one molecule induces a dipole moment in another molecule by virtue of the neighbor's polarizability. This is a long range interaction. The second physical process takes place when the overlap forces of the two adjacent molecules cause an asymmetrical distortion of their electronic charge clouds. The net induced dipole moment is modulated by the relative translational and rotational motion of the colliding pair and this modulation produces the absorption of infrared radiation. The translational spectrum is predominant at long wavelengths with its peak at 100μm at 100^{o}K (Trafton and Munch, 1969). In our wavelength region (10.5 - 13μm) its contribution to the opacity is negligible. The rotational hydrogen collisional spectrum, however, has its peak at 17μm and contributes a continuous opacity in our wavelength region (Th. Encrenaz, 1972).

The helium molecule also has no permanent dipole moment.

Its opacity comes from the collision with the hydrogen molecules and resembles the H_2-H_2 collision process. The collision is less important due to the smaller abundances of helium.

Ammonia is an important source of opacity at 10μm under Jovian atmospheric conditions. The 10μm band of ammonia arises from transitions through the ν_2 mode. In the ν_2 mode of vibration, the nitrogen atom oscillates vertically relative to the plane of the hydrogen atoms (figure 6-8a). The nitrogen atom is able to penetrate through the potential barrier to the other side of the hydrogen plane. This inverted position leads to inversion splitting of the levels of the ammonia molecules. The splitting generates both symmetric and antisymmetric energy levels with a given vibrational quantum number. The 10μm band of ammonia arises from transitions from the ground vibrational state to the first excited state in the ν_2 mode (figure 6-8b). Another transition, from the first excited symmetric vibrational state to the second excited asymmetric state is also in 10μm range, but the contribution due to this "hot band" is small for the low temperature in the Jovian atmosphere.

The ammonia is clearly seen in abosrption in the spectrum. The centers of the bands are shown by the arrows labeled NH_3. The ammonia absorption has been observed by different groups.

Gillett _et al_ (1969)(figure 6-9) observed Jupiter from 2.8-14μm with low resolution $\lambda/\Delta\lambda=50$. Briefly, their results show the following: The spectrum has a depression at 3.3μm caused by CH_4. Solar heating of the upper atmosphere via this band results in warming of the upper atmospheric layers. This

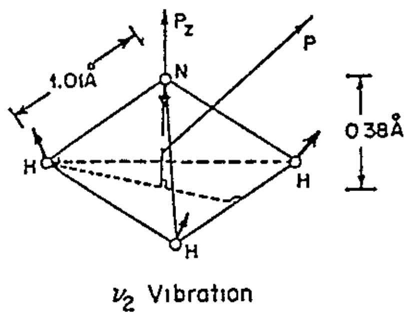

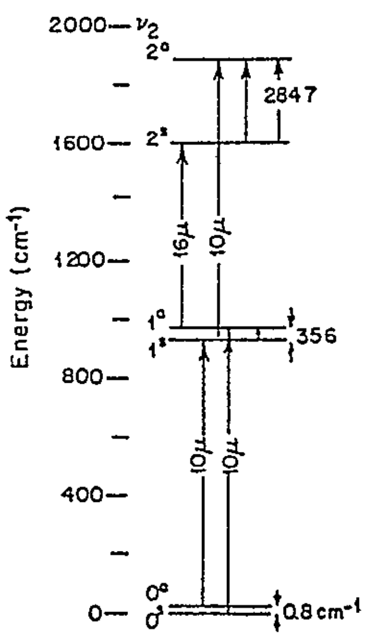

Figure 6-8. (a) Schematic representation of the NH_3 molecule. The components of angular momentum and the motion in the ν_2 vibrational mode are also shown. (b) Energy levels of the ν_2 vibrational mode of ammonia. Superscripts a and s refer to the antisymmetric and symmetric levels which arise due to inversion splitting.

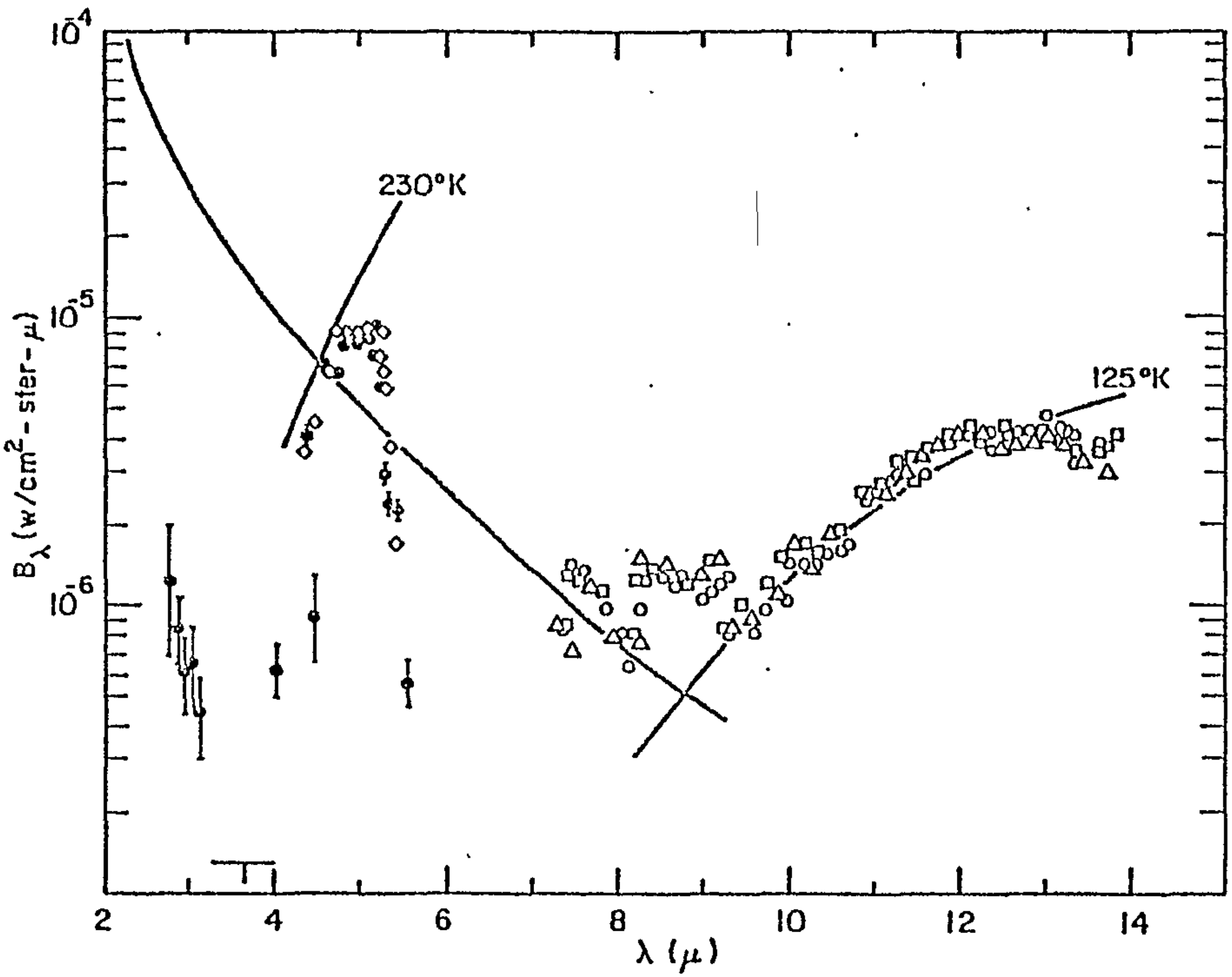

Figure 6-9. Low resolution spectrum taken by Gillett et al (1969). Different symbols represent spectrum taken on different nights. This figure is taken from their paper.

proceeds until energy is radiated at the same rate via the 7.7μm band of CH_4. Ammonia absorption around 10μm was also detected. Judging from the CH_4 emission, these authors were the first to suggest a temperature inversion on Jupiter caused by solar heating of the 3.3μm band of CH_4. They also showed that the NH_3 band at 10μm is saturated, and calculated that the H_2 abundance at 12.5μm, assuming a temperature of 125°K, is 12 km-atm. with a pressure $P_{H_2} \sim 1/4$atm.

Aitken and Jones (1972) obtained a Jovian spectrum from 8 - 13μm at a resolution $\lambda/\Delta\lambda \sim 143$(figure 6-10). The ammonia absorption band is again seen. They estimated that the ammonia abundance in the band is about 2.7 cm-atm. and a lapse rate $\Gamma = \frac{\partial T}{\partial h}$ at 13μm given by H=-30K, where H is the scale height ∿20km.

The most recent published infrared spectrum is by Lacy et al (1975) who used the Lick Observatory 120" telescope. High resolution spectra were obtained at 890 cm^{-1}(11.24μm) with $\lambda/\Delta\lambda=1780$. Medium resolution data were observed from 1000 cm^{-1} to 850 cm^{-1}(10 ∿ 12.75μm) with $\lambda/\Delta\lambda$ from 250 to 333 (figure 6-11 a,b). The authors also calculated synthetic spectra, assuming that NH_3 and H_2 are the only sources of opacity. Their conclusions from comparison between observed and computed spectra follow: All of the prominent lines in their observed spectrum are saturation NH_3 bands broadened to a width many times the pressure - broadened line width. The observed 135°K continuum is primarily formed by the wings of the NH_3 line. The H_2 opacity may be important if NH_3 is unsaturated

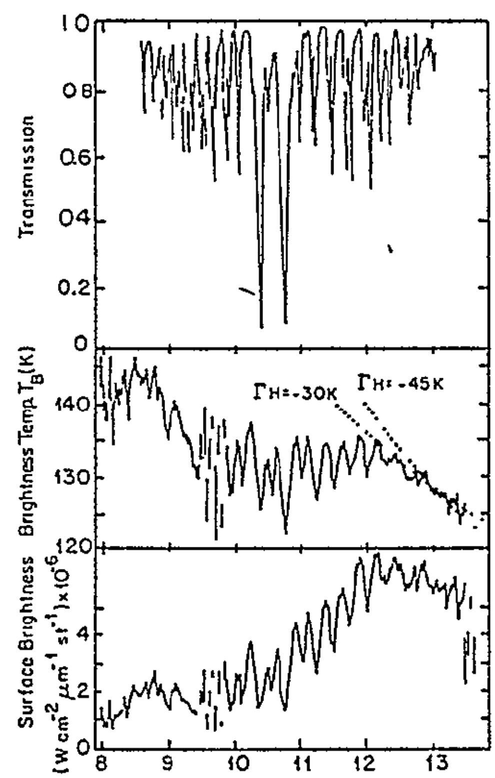

Figure 6-10. (a) Room temperature absorption spectrum of ammonia, p=0.06 atmos, w=0.6 cm atmos. (b) Brightness temperature; (c) Surface brightness of the central region of Jupiter from 8 to 13.5μm. (Taken from Aitken and Jones).

near 135°K. A pressure of 0.125 atm. at 135°K is required to form the continuum. The minimum temperature in their synthetic model is 118±5°K while the observed minimum temperature is 123°K, about 5°K larger than the derived temperature due to incomplete resolution of the features. The lapse rate at 135°K is 7.5±2.5°K/SH. Gillett et al (1969) estimated the lapse rate at the NH_3 saturation level is 4°K/SH. A discrepancy occurs in the comparision of the medium resolution data between 870 and 890 cm^{-1}. In this region the Jovian spectrum seems to be depressed by about 2°K relative to the calculated curve. The authors suggested that it may be due to an as yet unidentified minor constituent of the Jovian atmosphere.

Our spectrum has about the same resolution as the medium spectra of Lacy et al's and so the two spectra can be compared. The line positions match well. The vertical matching shows a drift towards longer wavelength. Figure (6-11a) is obtained by matching points A and B. The short wavelength side matches but the end of the long wavelength side is about 1.5 times higher. Also our spectrum seems to match the theoretical curve better at 870 to 890 cm^{-1}. Figure (6-11b) is obtained by matching A' and B'. Then the long wavelength side matches better than before but the short wavelength side is different. Also now our spectrum matches better with Lacy et al's observed result at 870 - 890 cm^{-1}. A conclusion about the discrepancy at 870 cm^{-1} between Lacy's observed and calculated spectra can not be reached at present until there is a better way for matching our and Lacy's et al's spectrum. Also it is not clear

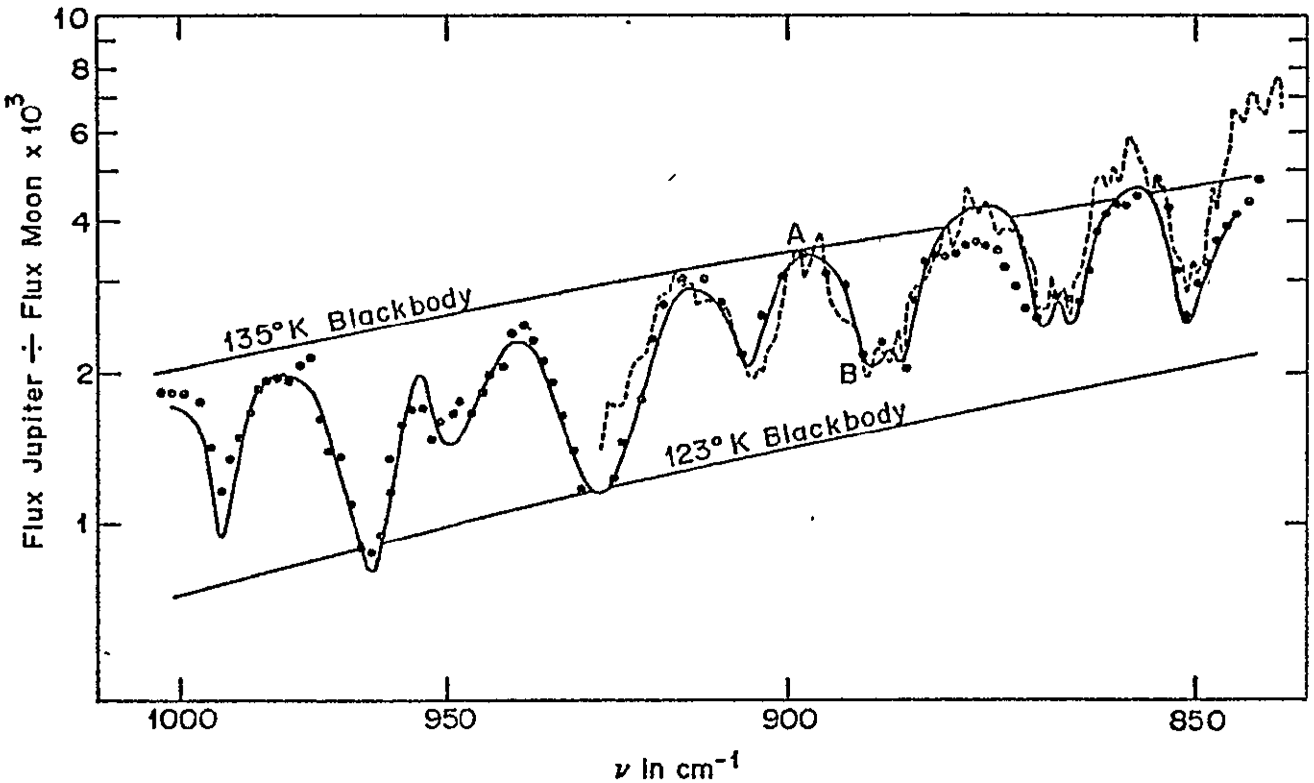

Figure 6-11a. Spectrum of the N and S polar regions of Jupiter at 3-4 cm^{-1} resolution divided by the spectrum of the Moon. Data points are shown as solid circles, and the solid line represents the best fitting synthetic spectrum calculated from the model calculated by Lacy et al (1975)(The graph is taken from Lacy et al). The dotted curve is our observed spectrum by matching Lacy's spectrum at points A and B.

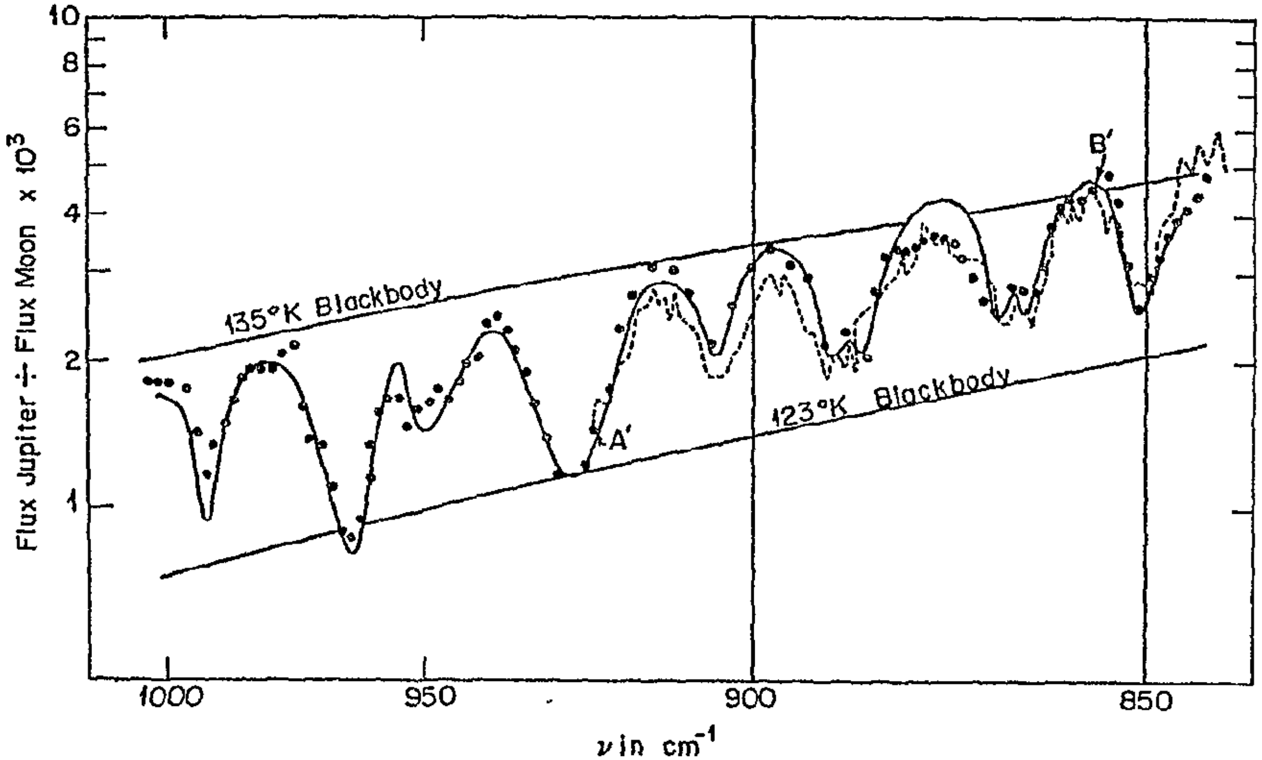

Figure 6-11b. Same as 6-11a except matching our spectrum with Lacy's at A' and B'.

whether the difference in matching of our spectrum and Lacy <u>et al</u>'s between long wavelength and short wavelength is real or not. There could be several reasons for the difference. It could be due to the inaccuracy of the end of the spectra, because the short wavelength side is the end of our spectrum and the long wavelength side is the end of Lacy's spectrum; or it may just be due to the matching technique. More effort is needed to clearify this point.

The absorption due to NH_3 is much less important beyond 12μ, so one may be able to use the H_2 opacity to estimate the lapse rate in that region. The lapse rate can be estimated by the equation

$$T_B(\lambda_1) - T_B(\lambda_2) = \frac{\Gamma H}{2} \text{lu} \frac{a(\lambda_1)}{a(\lambda_2)}$$

where $T_B(\lambda_1)$ is the brightness temperature at λ_1

$T_B(\lambda_2)$ is the brightness temperature at λ_2

Γ is the lapse rate

$a(\lambda_1)$ is the absorption coefficient at λ_1

$a(\lambda_2)$ is the absorption coefficient at λ_2

H is the scale height

If one chooses λ_1=11.95, λ_2=12.34 with measured brightness temperature T_1=133.94, T_2=133.64, $\alpha(\lambda_1)$, $\alpha(\lambda_2)$ are taken from Calpa and Ketebaar (1957), one obtains a result ΓH=-43.2°K for an H_2 opacity dominated atmosphere. Gillett <u>et al</u> (1969) calculated the adiabatic lapse rate (ΓH)ad=-42°K for an H_2 atmosphere, while Aitken and Jones (1972) measured a value of ΓH=-30°K from their spectrum. Our value seems closer to the value calculated by Gillett rather than to Aitken's. It is emphasized here that the estimate is based on the assumption that the H_2 opacity is the dominant opacity at wavelengths 11.95μ and 12.34μ, which may not be true.

Methane has a strong emission band at 7.7μ but does not have any band structure in our region. Methane has two important contribution to the overall thermal structure of the Jovian atmosphere. The first one is that methane has an absorption band at 3.3μm which absorbs solar energy and reradiates at 7.7μm producing an inversion temperature layer with a maximum temperature of 150°K at an altitude 160 - 200 km. Secondly, methane is photo dissociated by ultraviolet light in the upper atmosphere. This results in products such as ethane (C_2H_6), acetylene (C_2H_2), and ethylene (C_2H_4). Strobel (1973) estimated that column densities of C_2H_6, C_2H_2, C_2H_4 above the cloud top are approximately 10^{21}, 3×10^{16}, $3 \times 10^{15} cm^{-2}$ respectively. C_2H_6 and C_2H_2 were first observed by Ridgway (1973) using the 60" Kitt Peak solar telescope in the 750 - 875 cm^{-1} (11.42 - 13.33μm)range with resolution $\lambda/\Delta\lambda=770$,(figure 6-12a). The lines are shown in strong emission at the 140°K temperature. The apparent lines are superpositions of many lines, each group corresponding to a subband. Ridgway calculated that the mixing ratios are $N(C_2H_6)/N(H_2)=4 \times 10^{-3}$ and $N(C_2H_2)/N(H_2)=8 \times 10^{-5}$. The ratio $N(C_2H_6)/N(C_2H_2)=50$ where Strobel predicts about 200. Combes <u>et al</u> (1974)'s (figure 6-12b) observation confirms the presence of very strong emission lines of C_2H_2 and C_2H_6. The abundance of

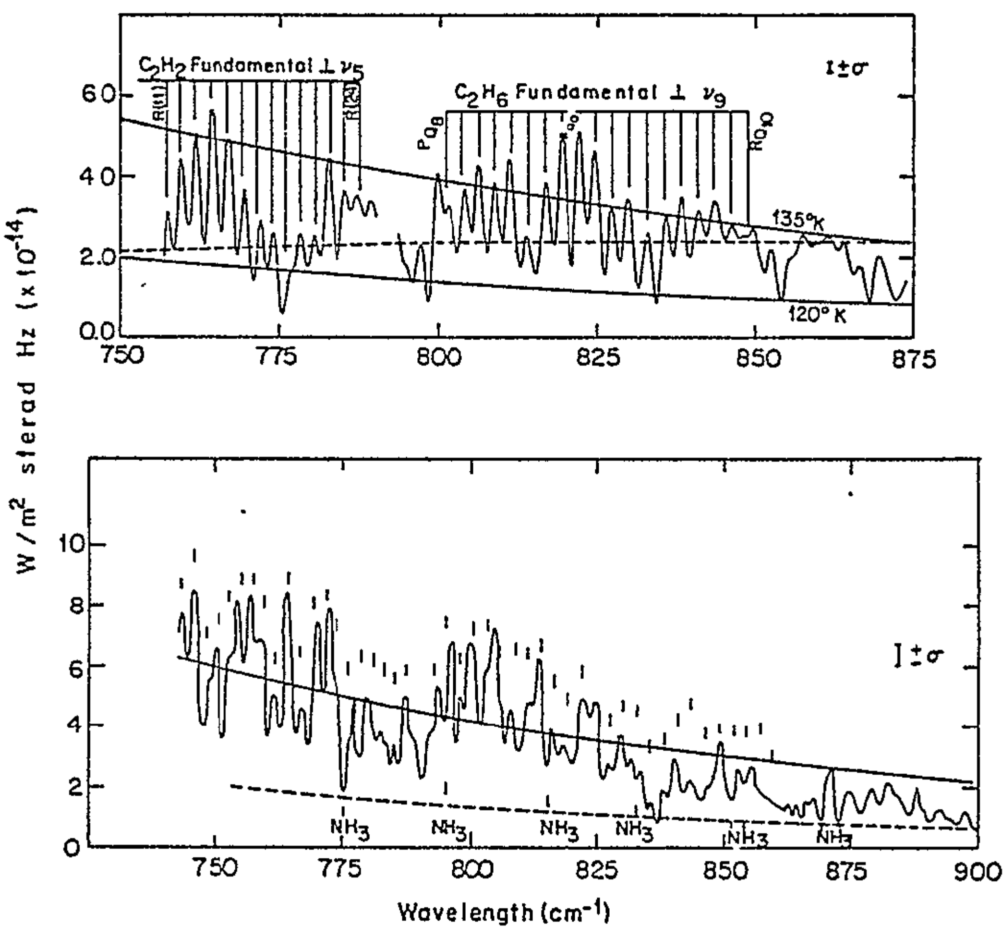

Figure 6-12. (a) Thermal emission spectrum of Jupiter corrected for absorption in the earth's atmosphere observed by Ridgway (1973). The dashed line is the predicted form of the H_2 continuum. (b) The ratio of the Jovian spectrum to the atmospheric absorption spectrum observed by Combes et at (1974). The solid and dashed lines are the blackbody curves at 135°K and 120°K respectively.

ethane estimated from Ridgway's spectra depends strongly on the distribution of gas temperature, which is not well-determinded. If the temperature in the mesospheric inversion layer turns out to have a maximum value of 150°K, the observations indicate ~ (Ridgway 1974) 2×10^{-2} gm cm^{-1} of ethane in this high temperature region. Sagan and Salpeter (1976) estimate the column density of ethane molecules to be 3×10^{-3} gm cm^{-2} by assuming that ethane is produced by photolysis of methane by solar ultraviolet photon and destroyed mainly by eddy diffusion into the troposphere, followed by pyrolysis in deeper, hotter layers. This would be in very serious conflict with the observations, especially since only a small fraction of the theoretical column density refer to the hotter inversion region.

The ethane emission band is also shown in our spectrum (figure 6-6). In the figure the indicated emission line position was extrapolated from Ridgway's spectrum, and the laboratory observed position by Smith (1949) are also shown for comparison. Our positions agree with Ridgway's reasonable well, while Smith's seem displaced from ours by 0.01μm,possibly due to a uncertainty in position calibration. Only a portion of the C_2H_2 spectrum can be seen in our spectral coverage. The abundance of C_2H_6 is not estimated here because the absolute amplitude of our spectrum is not well calibrated.

Our spectrum contains both ammonia and ethane features while other observers have not shown both. This will be useful because one can compute the synthetic spectra including both. Ammonia will provide us with information about the top of the cloud layer while ethane provides us with the information about the inversion layer. A synthetic spectrum including both ethane and acetylene would be interesting because the inclusion of these new gases would affect the models, especially around the inversion. Acetylene would appear around 13μm. The absorption of solar radiation by CH_4 at 3.3μm used to be thought to be radiated solely by CH_4 at 7.7μm. The 7.7μm emission intensity is a critical test of a temperature inversion model and the emission intensity calculated by Wallace et al (1974) is within 25% of the value observed by Gillett et al (1969). If ethane and acetylene do contribute to emission in the thermal infrared, there must be some additional source of solar absorption in order to produce the observed inversion temperature. Additional absorption at this altitude, perhaps due to particles, is suggested by the low ultraviolet albedo of Jupiter in the wavelength region 2100 to 3600 Å (Wallace, Caldwell and Savage, 1972).

Terrile and Westphal (1976) had imaged Jupiter at high spatial resolution at 8 - 14μm. All images reveal a belt and zone structure similar to visible photographs. In the 8 - 14μm broad-band data, belts appear to be about 2^{o}K hotter than the zone. The lowest belt-zone contrast is found in the hydrogen opacity dominated region at 12.5μm, while images at 9.5μm have the greatest contrast. This is consistant with the dynamic picture that zones are rising columns of air and belts are sinking columns of air. Ammonia gas being carried upward in zones will freeze out and form a thick cloud on top of the zones, giving a low infrared temperature to the zones, and the crystalized NH_3 particle will be carried down to the deep atmosphers in the belt where they will get sublimated. One can look deeper into clouds in the belt because of the lack of the ammonia cloud on top of it and therefore see a higher infrared temperature. Although there are a number of high resolution spectra of good spectra for methane. The observation of methane will be interesting not only because it provides us with information about the inversion layer, it is also useful to find out the temperature profile. If the temperature profile of the Jovian atmosphere is known, one can use it to find the ammonia abundance profile. Ammonia itself is not a very good tool for probing the temperature profile because it has a low vapor pressure and its variation is very sensitive to temperature changes. Observations of methane at 3.3μm and 7.7μm, should be able to accomplish this.

The Hadamard transform spectrometer described in this thesis would be able to make these observations, with small modifications that would permit observations to be made at these wavelength. In addition, observations should be undertaken at 8.0 to 9.5 microns where neither ammonia nor methane have strong absorption features. At these wavelengths one would be observing the clouds. In this 8.0 to 9.5 micron region our instrument should be able to image the bands and zones of Jupiter, to probe for spectral differences and cloud features. Such observations should increase our understanding of Jupiter's cloud structure.

(D) Observations of Mercury

The observations of Mercury were made with the newly built Cornell 25" telescope at Mount Pleasant, Ithaca, New York. The telescope has a focal ratio f/13.5 . The spectrometer's acceptance beam size is 7.8" x 78" . The dewar described in section III-B was used with the spectrometer. The spectrometer operated in the 10.5∿13μm region with a resolution $\lambda/\Delta\lambda$ around 300. The chopping frequency was 10 cycles per second.

The observational procedure was carried out a little differently from the observations of α-orionis and Jupiter. First, Sun spectra were used for correction spectra rather than lunar spectra. There are no known molecular lines in this region. Its temperature at 11.10μm is 5030°K(Saildy & Goody). The observations were made on August 3, 1976. At that time the Sun was about an hour away from Mercury, and was observed through roughly the same air mass as Mercury. Secondly, Mercury is so faint in broad day light that we were unable to see it in visible light. The way to find Mercury was the following: We pointed the telescope in the correct region and scanned for the infrared signal. The signal is so strong that one can see it go off scale on the synchronous demodulator. The pointing accuracy of the telescope is 6 sec. of time in right ascension and 25 sec. of arc in declination. Thirdly, since we could not see Mercury visually for tracking, we adapted a different method for tracking Mercury. Since our computer programming is set up in such a way that the data taken when the mask is moving forward and moving backward are stored in different areas, we only took data when the mask was moving forward. When the mask was moving backward we maximized the signal to assure correct pointing and waited for the next forward pass. Any noise introduced when moving the telescope for maximizing the signal would have gone into the backward-pass data bins and those data points were thrown away anyway. Since each pass takes 51 sec. only, Mercury remained at essentially the same position during the forward data taking pass.

Two runs of Mercury and two runs of the Sun were taken. Each run consisted of ten scans of the sources. Figure (6-13) shows the raw spectra of Mercury and the Sun. Since Ithaca has a lot of moisture in the air during the summer time, the correction for atmospheric features is more difficult than at Kitt Peak and is done in a different way. A constant was added to the Mercury spectra such that atmospheric features in the Mercury/Sun ratio spectrum were minimized. This step ensures that the atmospheric features are largely corrected. The Mercury spectrum which has a constant added to it was then multiplied by another constant to make its amplitude as close to that of the solar spectrum as possible. The solar spectrum was then subtracted from the modified Mercury spectrum. The multiplication of the Mercury spectrum by a constant assured that atmospheric features in the two spectra had similar amplitudes before the subtraction step. This difference spectrum was then added to a "perfect" solar spectrum which is calculated according to the blackbody function appropriate to the solar temperature. What one gets from these procedures is:

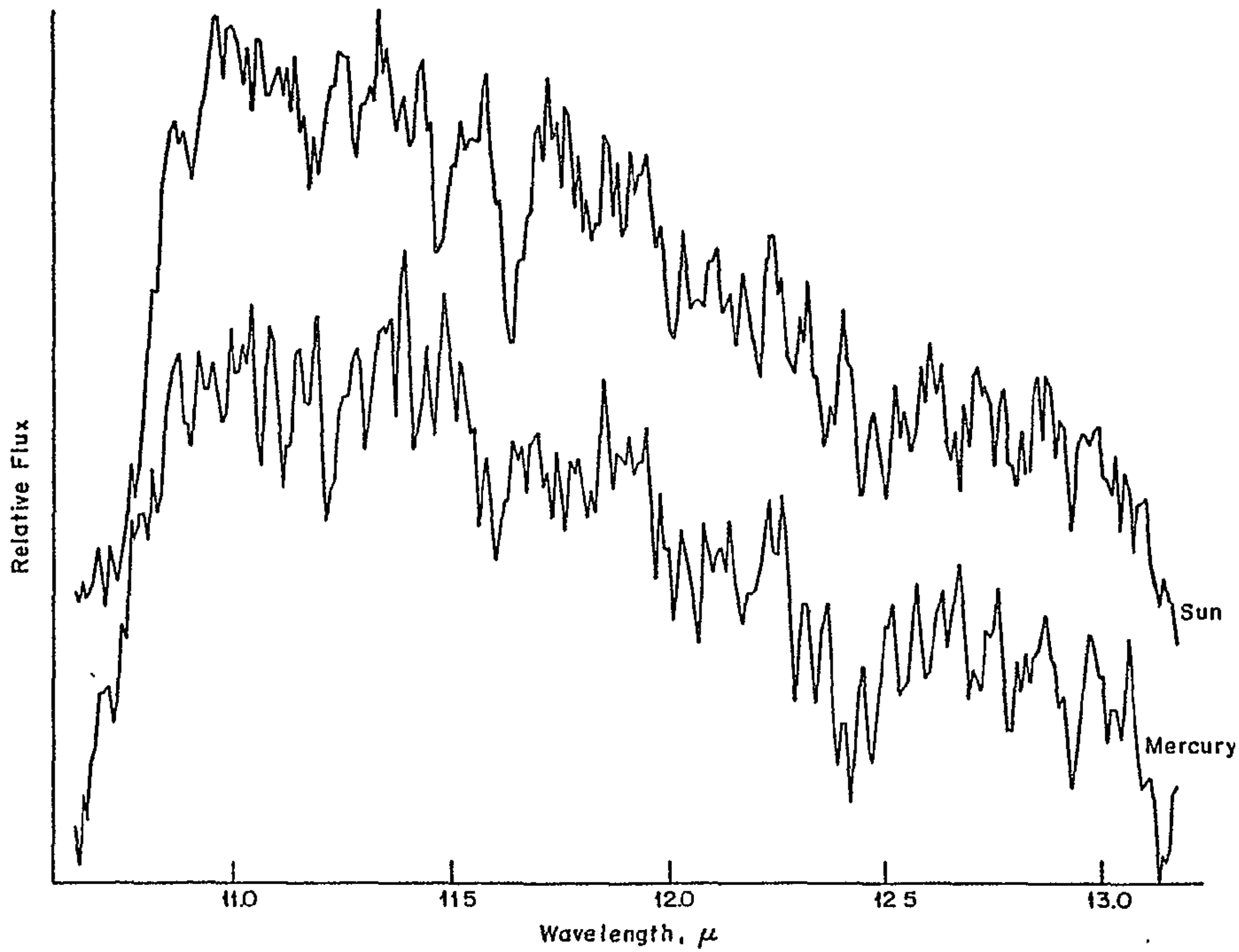

Figure 6-13. The raw spectra of Mercury and the Sun.

Final Mercury Spectrum

= observed corrected Mercury spectrum - observed solar spectrum + perfect solar spectrum

= ("perfect" Mercury spectrum + noise in the Mercury spectrum) - ("perfect" solar spectrum + noise in the solar spectrum) + "perfect" solar spectrum

= "perfect" Mercury spectrum + (noise in the Mercury spectrum - noise in the solar spectrum)

Any systematic noise such as emission and absorption due to the sky or to the telescope will be subtracted away. The advantage of this method is that the final spectrum is obtained through subtraction rather than by division. Division, in the low signal portion of the spectrum, produces deceptive high noise spikes in the ratio spectrum. The method we have used tends to eliminate these.

Since this will be the first high resolution Mercury spectrum obtained, we will calculate Mercury's disk integrated infrared temperature and compare this temperature with the observed one. Morrison and Sagan (1967) had calculated the infrared brightness temperature of the center-of-disk as a function of phase angle and heliocentric longitude, but there is no disk integrated infrared temperature available in the literature. In the following we will discuss the factors that may affect the brightness temperature, and then present a method of calculating the disk integrated infrared brightness and compare it with our observation. A good review of thermophysics of Mercury is given by Morrison (1970).

In 1965, Pettingill and Dyce (1965) used radar to discover that Mercury has a rotation period of 59 days, two thirds of the orbital period, instead of an 88 day synchronous rotation around the Sun. This implies that Mercury has a solar day, on the planet, about 176 terrestrial days long, equal to two orbital revolutions in three rotations. Mercury's non-synchronous rotation leads to time-dependent thermal emission of the planet due to the diurnal variation of the insolation. This diurnal variation would not happen for a synchronously rotating Mercury. The diurnal variation changes the brightness temperature as a function of both phase angle and heliocentric longitude. It also allows a measurement of the thermal properties of Mercury's surface.

Because of the high eccentricity of Mercury's orbit, (e=0.2), the diurnal cycle of insolation is markedly different from longitude to longitude, and can differ by a factor of 2.5. The eccentricity enters in two ways. First, the variation in distance from the Sun produces a solar constant that varies by more than a factor of 2 from perihelion to aphelion. Second, the changing orbital angular velocity causes the apparent speed of the Sun across the sky to vary; near perihelion the angular velocity of revolution actually slightly exceeds the angular velocity of rotation, and the apparent planetocentric solar motion is retrograde (figure 6-14, Soter and Ulrichs, 1967). The two effects of the eccentricity reinforce one another, with the larger flux coming at a time when the angular rate of the Sun across the sky is largest. The two longitudes (180° apart)

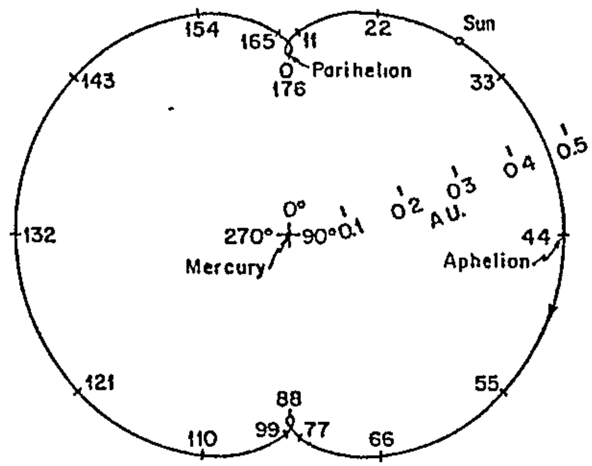

<u>Figure 6-14</u>. Diurnal path of the Sun about Mercury, drawn to scale. The relative positions of the Sun are marked at 11 day intervals with the planet held as a fixed reference. Planeto-graphic longitude are indicated for Mercury. (Taken from Soter and Ulrichs, 1967).

that see the Sun overhead at perihelion receive more than two and a half as much energy per period as the longitude 90° away, where the Sun is always small and rapidly moving while near the zenith.

Besides the insolation geometry, a possible atmosphere on Mercury will also affect the thermal emission. CO_2 is a major product for a possible secondary atmosphere, furthermore, since CO_2 could have been photodissociated and reduced to CO by preferential loss of oxygen, Fink et al (1973) had set up a search for a possible Mercury atmosphere of CO_2 and CO. They set up an upper limit 1.0×10^{-4} mb surface pressure for CO_2 and 2.0×10^{-5}mb for CO. Mariner 10's results also suggest that Mercury has no atmosphere although it may have a thin layer of He and other inert gas trapped by Mercury's magnetic field.

The optical observations of Mercury show that the integral spectral reflectivity of Mercury is quite similar to that for the integral moon (McCord and Adams, 1972). The Bond albedo of Mercury (de Vancouleurs, 1964) is 0.058.

In our model calculation we assume the following things. This model has been described by Murdock (1974):

1. The emission from the dark side at the phase angle we observed is negligible. On the day we made our observations, August 3, 1976, the illuminated portion amounted to 0.973 of the total disk and the dark portion was 0.017. The dark side temperature is about 110°K, which at 10μm has a flux 6.7181×10^{-8}watt-cm^{-2}-μ^{-1}-sr^{-1}. The flux for 500°K at 10μm is 7.1007×10^{-3}watt-cm^{-2}-μ^{-1}-sr^{-1}, so the contribution from the dark side

is negligible.

2. At infrared wavelengths, the radiation that reaches the observer originates very near the surface, so the infrared temperature is assumed equal to the insolation temperature. Soter and Ultichs' (1967) results show that the day time temperature is independent of the thermal properties of the surface material and determined largely by the insolation temperature.

3. The infrared emissivity we assumed was 0.9, which is the lunar value. We choose this value since Mercury's surface may be similar to the lunar surface.

In figure (6-15) we choose two coordinate systems on Mercury surface. The unprimed system is the "solar system" with the z-axis pointing towards the Sun. A is the subsolar point. The hemisphere above the plane BCD facing the Sun is the illuminated part. The primed system is the "earth system' with the z'-axis pointing towards the earth. A' is the subearth point. The hemisphere above the plane B'C'D' facing the earth is the portion that is being seen from earth. The two systems are different by an angle α with the x-axis as the common axis.

If the surface is in equilibrium with sunlight and cannot conduct heat away, the subsolar point temperature is:

$$T_o = \left[\frac{S(1-A)}{\sigma\varepsilon R^2}\right]^{1/4} \qquad (6\text{-}1)$$

where S is solar constant at earth, equal to 1.360×10^{6} erg $cm^{-2}s^{-1}$

A is the Bond albedo for Mercury, assumed to be 0.058.

σ is the stefan-Boltzmann constant equal to 5.67×10^{-5} erg $cm^{-2}s^{-1}$

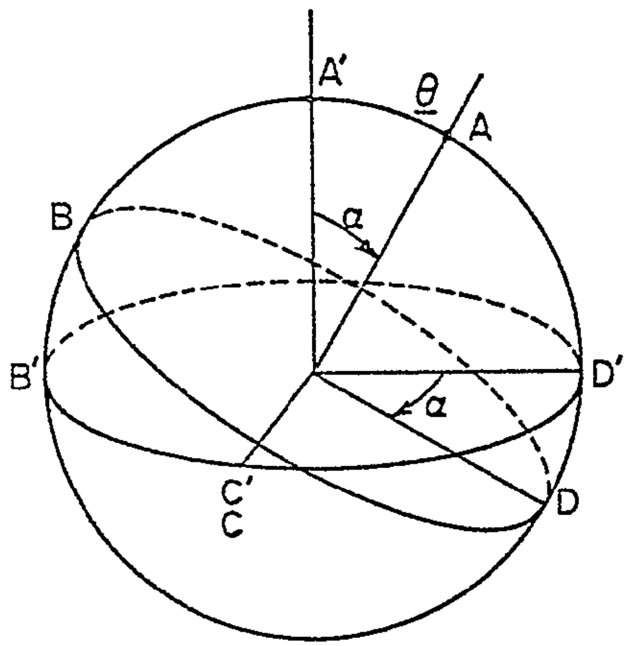

Figure 6-15. Two coordinate systems on the surface of Mercury. The unprimed system is the "solar system" with the Z-axis pointing towards the Sun. A is the subsolar point. The primed system is the "earth system" with the Z'-axis pointing towards the earth. A' is the sub-earth point.

ε is the infrared emissivity at 10μm from the surface, assumed to be 0.9

R is the distance between Mercury and the Sun in astronomical units

Mercury's subsolar point temperature varies with distance from the Sun as $R^{-1/2}$ and therefore is a function of heliocentric longitude due to the eccentricity we discuss above.

In the unprimed system the temperature distribution on the surface will be concentric isothermal bands around the subsolar point. The temperature of a band at colatitude θ is given by

$$T(\theta) = T_o \cos^{1/4}\theta \qquad (6\text{-}2)$$

The total intensity at any wavelength region will be composed of the contributions at that wavelength from many isothermal regions each with its own apparent area.

Since one is interested in the flux coming to the earth one will have,

$$dF'_\lambda = I_\lambda(\theta',\phi')\, dA' \qquad (6\text{-}3)$$

$$= I_\lambda(\theta',\phi')\, r^2 \sin\theta' d\theta' d\phi' \qquad (6\text{-}4)$$

$$= E_\lambda(\theta',\phi') \cos\theta' r^2 \sin\theta' d\theta' d\phi' \qquad (6\text{-}5)$$

where dF'_λ is the flux at wavelength λ coming from the area dA'

I_λ is the intensity at (θ',ϕ')

dA' is the differential area on Mercury

r is the radius of Mercury

$\Xi_\lambda(\theta',\phi') = I_\lambda(\theta',\phi')/\cos\theta'$ is the component of flux that radiates toward the earth.

$\Xi_\lambda(\theta',\phi')$ is a complicated function of (θ',ϕ') bacause the temperature distribution is a complicated function of (θ',ϕ'). However, one can convert the system to the "sun coordinate" where $\Xi_\lambda(\theta,\phi)$ is a simple function.

Since $dA' = dA$ (6-6)

$$\cos\theta' = \cos\theta\cos\alpha - \sin\theta\sin\phi\sin\alpha \qquad (6\text{-}7)$$

equation(6-5) becomes

$$dF_\lambda = \Xi_\lambda(\theta)\left[\cos\theta\cos\alpha - \sin\theta\sin\phi\sin\alpha\right] r^2\sin\theta d\theta d\phi$$

where

$$\Xi_\lambda(\theta) = \frac{C_1}{\lambda^5}\,\frac{1}{e^{C_2/kT(\theta)}-1} \qquad (6\text{-}8)$$

where $C_1 = 1.1909 \times 10^4$ watt $cm^{-1}\mu^{-1}sr^{-1}$

$C_2 = 1.4388 \times 10^4 \mu K$

and $T(\theta)$ is given by (6-2)

so

$$F_\lambda = r^2\int d\theta\int d\phi\ \Xi_\lambda(\theta)(\sin\theta\cos\theta\cos\alpha - \sin^2\theta\sin\phi\sin\alpha) \qquad (6\text{-}9)$$

The integral (6-9) can be separated into two parts, for $\theta \le \underline{\theta}$

where $\underline{\theta} = \frac{\pi}{2} - \alpha$ (6-10)

is the limit of the cap shared by both the Sun and the earth, i.e. the limit of integration over $d\theta$ can ϕ go from 0 to 2π. For $\theta > \underline{\theta}$, the limit of the integral over d is constrained by the physical condition that some part on ϕ that is illuminated by the Sun can not be seen from the earth.

So (6-9) becomes

$$F_\lambda = r^2\int_0^{\theta} d\theta\int_0^{2\pi} d\phi\ \Xi_\lambda(\theta)(\sin\theta\cos\theta\cos\alpha - \sin^2\alpha\sin\phi\sin\alpha)$$

$$+ r^2\int_{\underline{\theta}}^{\frac{\pi}{2}} d\theta\int_{\phi_1(\theta)}^{\phi_2(\theta)} d\phi\ \Xi_\lambda(\theta)(\sin\theta\cos\theta\cos\alpha - \sin^2\theta\sin\phi\sin\alpha) \quad (6\text{-}11)$$

To find $\phi_1(\theta)$ and $\phi_2(\theta)$ one notices that ϕ is given when $\theta'=90^\circ$. From (6-7)

$$\cos\theta' = \cos\theta\cos\alpha - \sin\theta\sin\phi\sin\alpha$$

$$\theta' = \frac{\pi}{2} \Rightarrow \sin\phi = \cot\alpha\cot\theta \quad (6\text{-}12)$$

and

$$\phi = \sin^{-1}(\cot\alpha\cot\theta) \quad (6\text{-}13)$$

Since ϕ will also be symmetric about the y-axis, equation (6-11) can be rewritten as:

$$F_\lambda = r^2\int_0^{\frac{\pi}{2}-\alpha} d\theta\int_0^{2\pi} d\phi\ \Xi_\lambda(\theta)(\sin\theta\cos\theta\cos\alpha - \sin^2\theta\sin\phi\sin\alpha)$$

$$+ \int_{\frac{\pi}{2}-\alpha}^{\frac{\pi}{2}} d\theta\int_{\pi-\sin^{-1}(\cot\alpha\cot\theta)}^{2\pi+\sin^{-1}(\cot\alpha\cot\theta)} \Xi_\lambda(\theta)(\sin\theta\cos\theta\cos\alpha - \sin^2\theta\sin\phi\sin\alpha) \quad (6\text{-}14)$$

After evaluating the integral one obtains the following:

$$F_\lambda = 2\pi r^2\cos\alpha\left[\Xi_\lambda(\theta)\frac{\sin^2\theta}{2}\right]_0^{\frac{\pi}{2}-\alpha} + \pi r^2\cos\alpha\left[\Xi_\lambda(\theta)\frac{\sin^2\theta}{2}\right]_{\frac{\pi}{2}-\alpha}^{\frac{\pi}{2}}$$

$$+ 2r^2 \int_{\frac{\pi}{2}-\alpha}^{\frac{\pi}{2}} d\theta \sin^{-1}(\cot\alpha\cot\theta) \sin\theta\cos\theta\cos\alpha\ \Xi_\lambda(\theta)$$

$$+ r^2 \left[\overline{\Xi_\lambda(\theta)(\cos\theta\sqrt{\sin^{-2}\alpha - \cos^2\theta} + \sin^{-2}\alpha\sin^{-1}\frac{\cos\theta}{|\sin\alpha|}} \right]_{\frac{\pi}{2}}^{\frac{\pi}{2}-\alpha}$$

(6-15)

where $\left[\overline{\Xi_\lambda(\theta)\ \frac{\sin^2\theta}{2}} \right]_0^{\frac{\pi}{2}-\alpha}$

is the mean of ($\Xi_\lambda(\theta)\ \frac{\sin^2\theta}{2}$) in the interval of θ from 0 to $\frac{\pi}{2}-\alpha$. The same meaning applies to the third term of (6-15).

As a check of equation (6-15), if α=0, that means when subsolar point and subearth point coinside, let $\Xi(\theta)$=constant evaluating (6-15) gives:

$$F = \pi r^2 \Xi$$

If $\alpha = \frac{\pi}{2}$, that means the subsolar point and subearth point are 90° apart. With $\Xi(\theta)$ assumed to be constant, equation (6-15) gives

$$F = \frac{\pi r^2}{2} \Xi$$

which is as one expects since one is seeing half of Mercury.

Equation (6-15) can be readily integrated on a computer. It is applied to our case with the following physical parameters:

Date: August 3, 1976 .

Phase Angle: 53°

Radius vector: 0.414 A.U.

Orbital longitude: 198.09°

Mercury perihelion point: 0.3075 A.U.

Subsolar temperature at perihelion point: 700°K

Subsolar temperature at $\alpha=53°$: 603°K

Equation (6-15) was computed on a LSI mini computer at each wavelength, from 10.6 to 13.2μm. The program and the result are shown in the Appendix D. The integral was divided into twenty steps. $\Xi(\theta)$ was evaluated from equation (6-8)

$$\Xi_\lambda(\theta) = \frac{C_1}{\lambda^5} \frac{1}{e^{C_2/kT(\theta)}-1}$$

where $T(\theta) = T_o \cos^{1/4}\theta$

The calculated spectrum is a measure of color temperature and is used to compare with the observed spectrum. Figure (6-16) shows the final Mercury spectrum conected for solar temperature, with a number of blackbody slopes shown to match. The calculated spectrum (cross) matches the blackbody temperature 525°K, which also matches the observed spectrum. We concluded that the best fit lies in the 500°K region. Murdock (1974) measured a effective brightness temperature at 10.8μm at the same phase angle to be around 650°K. Our results disagree with his results.

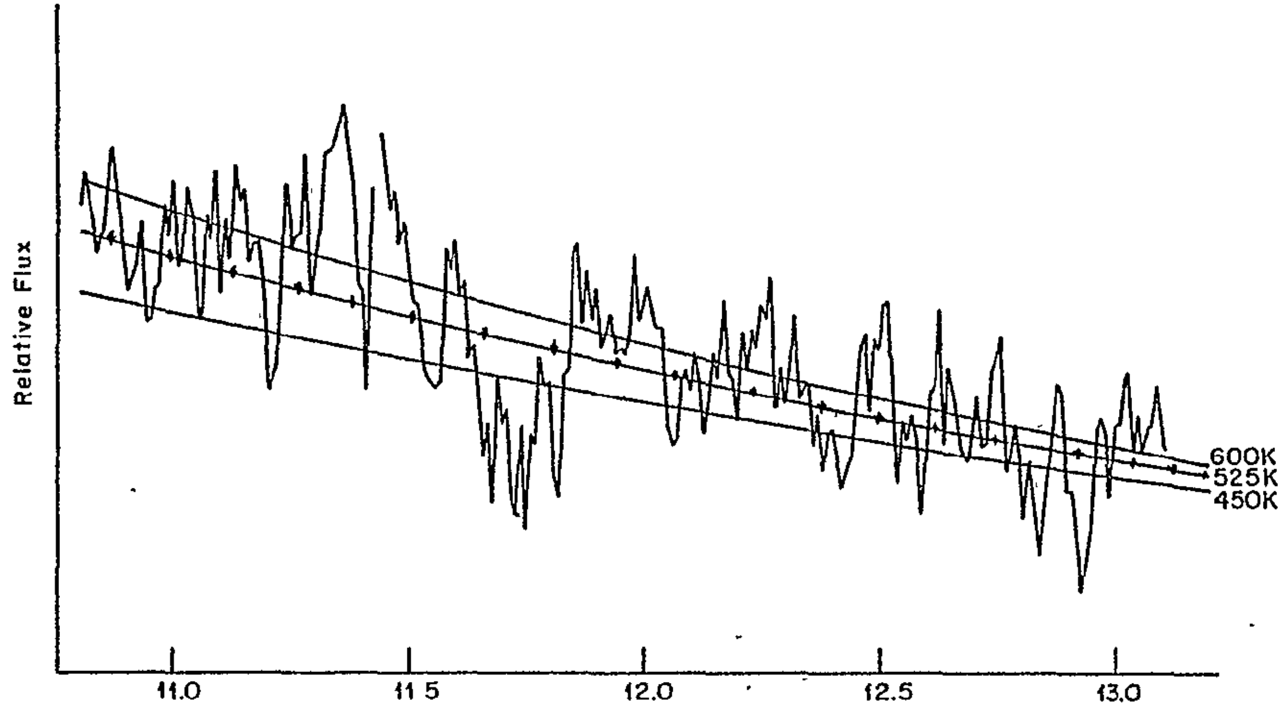

Figure 6-16. The final Mercury spectrum, corrected for solar temperature, with a number of blackbody slopes shown to match.

APPENDIX A

ESTIMATE OF CODING ERROR FOR FOURIER TRANSFORM SPECTROMETRY

Let ξ be the path difference in a two beam interferometer. $P(\nu)$ is the power at wavelength ν, (i.e. the spectral density function) ν here is taken to be $1/\lambda$. $S(\xi)$ is the power received for path difference ξ. Then (p.96 Stewart)

$$S(\xi) = \int_0^\infty P(\nu) \cos^2(2\pi\xi\nu)\, d\nu \qquad \text{A-1}$$

$$= 1/2P_o + 1/2\int_0^\infty P(\nu) \cos(4\pi\xi\nu)\, d\nu \qquad \text{A-2}$$

The reciprocal Fourier property is (Morse and Feshback P.454) that if

$$F(\xi) = \sqrt{\frac{2}{\pi}} \int_0^\infty \cos(\xi\nu) f(\nu) d\nu$$

Then $$f(\nu) = \sqrt{\frac{2}{\pi}} \int_0^\infty \cos(\xi\nu) F(\xi) d\xi$$

which implies, neglecting the constant term, that

$$P(\nu) = 16\int_0^\infty \cos(4\pi\xi\nu) s(\xi) d\xi \qquad \text{A-3}$$

Suppose we take measurement at (N+1) equally seperated steps in the variable ξ. Let the step length be τ, then

$$\xi = n\tau$$

In general τ is chosen such that

$$\tau = \frac{1}{4(\nu_{max} - \nu_{min})} \qquad \text{A-4}$$

which, if $\nu_{min} << \nu_{max}$, effectively implies sampling twice per cycle (Stewart, p.303).

One can now write the integral for $P(\nu)$ as

$$P(\nu) = 16\sum_{n=0}^{N} \tau S(n\tau) \cos(4\pi\nu n\tau) \qquad \text{A-5}$$

Now consider frequency $\nu = \nu_{min} + m\delta$

where $$\delta = \frac{\nu_{max} - \nu_{min}}{N} \qquad \text{A-6}$$

and m is an integer. $m = 0, 1 \cdots N$

The $\delta P(\nu)$ is the power in the resolved spectral band width δ about frequency ν

$$\delta P(\nu) = 16\tau\delta \sum_{n=0}^{N} S(n\tau) \cos(4\pi\nu n\tau) \qquad \text{A-7}$$

but $$\tau\delta = \frac{\delta}{4(\nu_{max} - \nu_{min})}$$

$$= \frac{\delta}{4N\delta}$$

$$= \frac{1}{4N} \qquad \text{A-8}$$

Therefore

$$\delta P(\nu) = \frac{4}{N} \sum_{n=0}^{N} S(n\tau) \cos(4\pi\nu n\tau) \qquad \text{A-9}$$

Writing this out in matrix form, with $\theta_1 = 4\pi\tau\nu_{min}$, $\theta_2 = 4\pi\tau(\nu_{min}+\delta)$ and with $\pi(\nu_{min}) \equiv \delta P(\nu_{min})$ we have

$$\begin{bmatrix} \pi(\nu_{min}) \\ \pi(\nu_{min}+\delta) \\ \cdot \\ \cdot \\ \cdot \\ \cdot \\ \pi(\nu_{max}-\delta) \\ \pi(\nu_{max}) \end{bmatrix} \equiv \delta \begin{bmatrix} P(\nu_{min}) \\ P(\nu_{min}+\delta) \\ \cdot \\ \cdot \\ \cdot \\ \cdot \\ P(\nu_{max}-\delta) \\ P(\nu_{max}) \end{bmatrix} - \frac{4}{N} \begin{bmatrix} 1 & \cos\theta_1 \cdots\cdots & \cos N\theta_1 \\ 1 & \cos\theta_2 \cdots\cdots & \cos N\theta_2 \\ \cdot & & \\ \cdot & & \\ \cdot & & \\ \cdot & & \\ 1 & \cos\theta_{N-1} \cdots & \cos N\theta_{N-1} \\ 1 & \cos\theta_n \cdots\cdots & \cos N\theta_N \end{bmatrix} \begin{bmatrix} S(0) \\ S(1) \\ \cdot \\ \cdot \\ \cdot \\ \cdot \\ \cdot \\ S(N) \end{bmatrix}$$

or $$\pi = W^{-1} S \qquad \text{A-10}$$

From (2-8)

$$\begin{aligned} \Delta_j &= (A_{j1} + \cdot \cdot \cdot + A_{jN})^{1/2} \\ &= \sqrt{\frac{16}{N^2}} (1 + \cos^2\theta_j + \cdot \cdot \cdot + \cos^2 N\theta_j)^{1/2} \\ &= \frac{4}{N} \left(\sum_{n=0}^{N} \cos^2 n\theta_j \right)^{1/2} \\ &\sim \frac{4}{N} \sqrt{\frac{N+1}{2}} \\ &\sim \sqrt{\frac{8}{N}} \qquad \text{for } N>>1 \qquad \text{A-11} \end{aligned}$$

The SNR improvement is the reciprocal of this quantity.

APPENDIX B

```
                          NAM    CMND
                          EXTR   IER,ØTT,ØTL,CRLF
                          EXTR   ERR,XEQ,ØFPA
                          EXTR   XA,XB,FIX,FLT
0100                      ABS    :100
                 *PRINT NAME
0100   0110               ZAR
0101   F900               JST    ØTL
       0000
0102   017B               DATA   NAME
0103   F201               JMP    $+2
                 *
                 *CØMMAND INTERPRETER
                 *
0104   0800      CMND     ENT
0105   0A00               EIN
0106   4005               CIE                ENABLE PANIC BUTTØN
0107   F900               JST    CRLF        PRINT PRØMPT CHARACTER
       0000
0108   C687               LAP    :87
0109   F900               JST    ØTT
       0000
010A   C6AA               LAP    '*'
010B   F900               JST    ØTT
       0000
010C   1200               RØV                CLEAR MATH FLAG
010D   0108               ZXR
010E   F900               JST    IER         INPUT CØMMAND
       0000
010F   C0D3               CAI    'S'
0110   F25C               JMP    STATUS
0111   C0D4               CAI    'T'
0112   E24E               LDX    TRANS
0113   C0D2               CAI    'R'
0114   E24D               LDX    READ
0115   C0C3               CAI    'C'
0116   E24C               LDX    CLEAR
0117   3809               JXN    ØKF
0118   1400               SØV                SET MATH FLAG
0119   C0D0               CAI    'P'
011A   E249               LDX    PUNCH
011B   C0C7               CAI    'G'
011C   E248               LDX    GRAPH
011D   C0D6               CAI    'V'
011E   E249               LDX    CRT
011F   3801               JXN    ØKF
0120   F900      BAD      JST    ERR
       0000
0121   EA48      ØKF      STX    FUNC        SAVE CALL ADDRESS
0122   0108               ZXR
0123   F900               JST    IER         FETCH BEAM
       0000
0124   C0AB               CAI    '+'
```

```
0125  E24C          LDX   NP
0126  C0AD          CAI   '-'
0127  E24F          LDX   NM
0128  3335          JXN   ØKB
0129  3249          JØR   BAD         IF MATH FLAG CLEAR
012A  0523          XRP               RESET INDICES
012B  E900          STX   XA
      0000
012C  E900          STX   XB
      0000
012D  EB1D          STX   *XC
012E  C5FF          LXM   255         RESET CØUNT
012F  EA3B          STX   CNT
0130  0108          ZXR
0131  C0C4          CAI   'D'
0132  E233          LDX   FSB
0133  C0D2          CAI   'R'
0134  E232          LDX   FDV
0135  2855          JXZ   BAD
0136  EA35          STX   MATH        SAVE MATH PØINTER
0137  F900          JST   XEQ         WAHT FØR GØ
      0000
                *MATH LØØP
0138  FB33    MLP   JST   *MATH
0139  9002          DATA  :9002,:9202,:9402
013A  9202
013B  9402
013C  D900          IMS   XA          BUMP CØUNTERS
      0000
013D  D900          IMS   XB
      0000
013E  211A          JAZ   ØKM         MATH ØK?
013F  1340          SAØ               NØ!
0140  C6D2          LAP   'R'         PRINT ERRØR MSG.
0141  3203          JØR   ØVFL
0142  F900          JST   ØTL
      0000
0143  0184          DATA  UNDER
0144  F202          JMP   FLØW
0145  F900    ØVFL  JST   ØTL
      0000
0146  0187          DATA  ØVER
0147  C600    FLØW  LAP   0
0148  F900          JST   ØTL
      0000
0149  018A          DATA  MSG
014A  F900          JST   FLT
      0000
014B          XC    REF
014C  0179          DATA  XCF
014D  F900          JST   ØFPA
      0000
014E  0179          DATA  XCF
```

```
014F   C68D             LAP    :8D
0150   F900             JST    ØTL
       0000
0151   0197             DATA   ZERØ
0152   B707             LDA    *XC         CLEAR BAD ELEMENT
0153   1050             ALA    1
0154   8A14             ADD    TP
0155   0043             TAX
0156   0110             ZAR
0157   9C00             STA    @0
0158   9C01             STA    @1
0159   DF0E    ØKM      IMS    *XC
015A   DA10             IMS    CNT
015B   F623             JMP    MLP
015C   E20C             LDX    TP
015D   F201             JMP    ØKB+1
015E   F900    ØKB      JST    XEQ         WAIT FØR GØ
       0000
015F   FB0A             JST    *FUNC       CALL FUNCTIØN
0160   F65B             JMP    CMND+1
0161           TRANS    REF
0162           READ     REF
0163           CLEAR    REF
0164           PUNCH    REF
0165           GRAPH    REF
0166           FSB      REF
0167           FDV      REF
0168           CRT      REF
0169   1400    TP       DATA   :1400
016A   0000    FUNC     DATA   0
016B   0000    CNT      DATA   0
016C   0000    MATH     DATA   0
016D   4006    STATUS   CID                KILL PANIC SWITCH
016E   0110             ZAR
016F   F900             JST    ØTL
       0000
0170   01A1             DATA   TATUS
0171   F900             JST    ØFPA
       0000
0172   1000    NP       DATA   :1000
0173   0110             ZAR
0174   F900             JST    ØTL
       0000
0175   01A7             DATA   NMM
0176   F900             JST    ØFPA
       0000
0177   1200    NM       DATA   :1200
0178   F673             JMP    CMND+1
0179   0000    XCF      RES    2,0
017B   8D3A    NAME     DATA   :8D3A,:8AA0
017C   8AA0
017D   C8D4             TEXT   'HTS: IX255'
017E   D3BA
```

```
      017F  A0B1
      0180  D8B2
      0181  B5B5
0133  0182  8D8A              DATA    :8D8A,0
      0183  0000
0134  0184  8AD5    UNDER     DATA    :8AD5
0135  0185  CEC4              TEXT    'NDER'
      0186  C5D2
0136  0187  8ACF    ØVER      DATA    :8ACF
0137  0188  D6C5              TEXT    'VER'
      0189  D2A0
0138  018A  C6CC    MSG       TEXT    'FLØW ØCCURRED'
      018B  CFD7
      018C  A0CF
      018D  C3C3
      018E  D5D2
      018F  D2C5
      0190  C4A0
0139  0191  C1D4              TEXT    'AT ELEMENT'
      0192  A0C5
      0193  CCC5
      0194  CDC5
      0195  CED4
0140  0196  A000              DATA    :A000
0141  0197  ACA0    ZERØ      TEXT    ', REPLACED'
      0198  D2C5
      0199  D0CC
      019A  C1C3
      019B  C5C4
0142  019C  A0C2              TEXT    ' BY ZERØ'
      019D  D9A0
      019E  DAC5
      019F  D2CF
0143  01A0  AE8D              DATA    :AE8D
0144  01A1  D4C1    TATUS     TEXT    'TATUS: N+='
      01A2  D4D5
      01A3  D3BA
      01A4  A0CE
      01A5  ABBD
0145  01A6  A000              DATA    :A000
0146  01A7  ACA0    NMM       TEXT    ', N-= '
      01A8  CEAD
      01A9  BDA0
0147  01AA  0000              DATA    0
0148                          END
0000 ERRØRS
```

```
                        NAM   TRANS
                        NAM   RTTR,RTØP
                        EXTR DISP
                        EXTR IKB,ØTL,ØFPA,CRLF,ERR
                        EXTR DPACC,DPFLT
                        EXTR DPN:,DPSUB:,DPDIV:,DPSM:
                        EXTR XB,XC,FAD
                        EXTR DPFIX
0000                    REL   0
                  *
                  *1X255 HTS PRØCESSØR
                  *
0000  0800  TRANS ENT
0001  E2BC        LDX   BPNT
0002  1328        LLX   1           INDIRECT BIT ØN
0003  1400        SØV
0004  11A8        RRX   1
0005  EA88        STX   BEAM
0006  EA88        STX   BEAM+1
0007  B2A0        LDA   ZCT         CLEAR BUFFERS
0008  9AA0        STA   CNT
0009  E2A1        LDX   NT
000A  0110        ZAR
000B  9C00  CLR   STA   @0
000C  0128        IXR
000D  DA9B        IMS   CNT
000E  F603        JMP   CLR
000F  C6BF        LAP   '?'
0010  F900        JST   ØTL
0011  0137        DATA MØDE
0012  F900        JST   IKB
0013  C0CD        CAI   'M'
0014  F205        JMP   MØN
0015  C0D4        CAI   'T'
0016  F208        JMP   TAPE
0017  C0C9        CAI   'I'
0018  F209        JMP   INVS
0019  F900        JST   ERR
001A  0110  MØN   ZAR
001B  0210        CAR
001C  9AA0        STA   TETR
001D  0110        ZAR
001E  F20D        JMP   NEXT
001F  0110  TAPE  ZAR
0020  9A9C        STA   TETR
0021  F202        JMP   T4
0022  C601  INVS  LAP   1
0023  9A99        STA   TETR
0024  0108  T4    ZXR
0025  F900        JST   IKB
0026  C0AB        CAI   '+'
0027  0408        CXR
0028  C0AD        CAI   '-'
0029  0108        ZXR
```

```
002A  EA8E         STX   TREM
002B  0110         ZAR
002C  E292  NEXT   LDX   MASK
002D  0128         IXR
002E  0210         CAR              CHANGE DIRECTIØN
002F  9A7F         STA   DIR
0030  C0FF         CAI   :FF
0031  F203         JMP   FØWD
0032  0030         TXA
0033  8A7A         ADD   H255
0034  0048         TAX
0035  EA76  FØWD   STX   MSK1
0036  C7F5         LAM   245
0037  9A79         STA   DCT2
0038  C7FF         LAM   255        START DATA CØUNT
0039  9A76         STA   DCT
003A  FAB1         JST   TURNØN     WAIT FØR LIGHT
            *INPUT LØØP
003B  FABB  ILP    JST   MØNS       INPUT
003C  9A6C         STA   CNT        &SAVE
003D  EA6C         STX   CNT+1
003E  C7FF         LAM   255        SPECTRUM CØUNT
003F  9A72         STA   SCT
0040  B26B         LDA   MSK1       RESET MASK PØINTER
0041  9A6B         STA   MSK2
0042  B271         LDA   IB         GET BUFFER PØINTER
0043  9A0F         STA   IBP
            *TRANSFØRM CØLUMN TØ INPUT BUFFER
0044  E265  TLP    LDX   CNT+1
0045  0110         ZAR
0046  D366         CMS   *MSK2
0047  F208         JMP   T1A
0048  B274         LDA   TETR
0049  2183         JAL   5+4
004A  0110         ZAR
004B  0108         ZXR
004C  F204         JMP   T1
004D  B25B         LDA   CNT
004E  F900         JST   DPN:
004F  F201         JMP   T1
0050  B258  T1A    LDA   CNT
0051  DA5B  T1     IMS   MSK2
0052  F900         JST   DPACC      ADD
0053  0000  IBP    DATA  0
0054  C202         AXI   2          BUMP PØINTER
0055  EE02         STX   IBP
0056  DA5B         IMS   SCT        DØNE?
0057  F613         JMP   TLP        NØ
0058  E253         LDX   MSK1       YES,MØVE CØLUMN
0059  0128         IXR              +1IF FWD
005A  B254         LDA   DIR
005B  C000         CAI   0
005C  C302         SXI   2          -1IF REV.
005D  EA4E         STX   MSK1
```

```
005E   DA52            IMS   DCT2
005F   F201            JMP   $+2
0060   40C7            SEL   24,7
0061   DA4E            IMS   DCT        END ØF RØW?
0062   F627            JMP   ILP        NØ
                *END ØF RØW STØP TEST
0063   B259            LDA   TETR
0064   2081            JAM   $+2
0065   F209            JMP   STØP
0066   3408            JSS   STØP       SS DØWN?
0067   48C7            SSN   :C7        NØ, STØP DØWN?
0068   F206            JMP   STØP       YES
0069   FA56            JST   ACC        NØ, SAVE DATA
006A   E24D            LDX   NØBM
006B   0110            ZAR
006C   F100            JMP   DISP
006D   B241    RTTR    LDA   DIR
006E   F642            JMP   NEXT
006F   E243    STØP    LDX   NI
0070   C601            LAP   1
0071   F100            JMP   DISP
0072   C6BF    RTØP    LAP   '?'
0073   F900            JST   ØTC
0074   011F            DATA  MSG
0075   F900            JST   IKB
0076   C0CE            CAI   'N'        ABØRT LAST PASS?
0077   F203            JMP   NØ         NØ
0078   C0D9            CAI   'Y'        YES
0079   F203            JMP   YES        YES
007A   F608            JMP   RTØP       WRØNG ENTRY
007B   FA44    NØ      JST   ACC        SAVE DATA
007C   F203            JMP   Y2
007D   C6AC    YES     LAP   ','        PRINT ABØRT
007E   F900            JST   ØTC
007F   0128            DATA  ABT
0080   B234    Y2      LDA   CT         SET CØUNTER
0081   9A30            STA   SCT
0082   0350            ARP              RESET SUBSCRIPTS
0083   9900            STA   XB
0084   9900            STA   XC
0085   E230            LDX   NPBM
                *ADD TØ BEAM ARRAY
0086   EE33    ALP     STX   IBP
0087   B400            LDA   @0         GET DATA
0088   E401            LDX   @1
0089   F900            JST   DPFLT      FLØAT IT
008A   9A21            STA   MSK1       SAVE IT
008B   EA21            STX   MSK2
008C   F900            JST   FAD        ADD TØ BEAM
008D   00AC            DATA  MSK1
008E   0000    BEAM    RES   2,0
0090   D900            IMS   XB         BUMP SUBSCRIPTS
0091   D900            IMS   XC
0092   E63F            LDX   IBP
```

```
0093  C202              AXI   2
0094  DA1D              IMS   SCT        DØNE?
0095  F60F              JMP   ALP        NØ
                  *PRINT PASS CØUNT
0096  F900              JST   CRLF
0097  C702              LAM   2
0098  9A23              STA   CØN1
0099  E21C              LDX   NPEM
009A  0110  MK          ZAR
009B  E401              LDX   @1
009C  F900              JST   DPFLT
009D  9A0E              STA   MSK1
009E  EA0E              STX   MSK2
009F  F900              JST   ØFPA
00A0  00AC              DATA  MSK1
00A1  0110              ZAR
00A2  F900              JST   ØTL
00A3  0130              DATA  RUNS
00A4  E212              LDX   NMEM
00A5  DA16              IMS   CØN1
00A6  F60C              JMP   MK
00A7  F7A7  T2          RTN   TRANS
                  *DATA STØRAGE
00A8  FA00  ZCT         DATA  -1536
00A9  0000  CNT         DATA  0,0
00AA  0000
00AB  1400  NT          DATA  :1400
00AC  0000  MSK1        DATA  0
00AD  0000  MSK2        DATA  0
00AE  00FF  H255        DATA  255
00AF  0000  DIR         DATA  0
00B0  0000  DCT         DATA  0
00B1  0000  DCT2        DATA  0
00B2  0000  SCT         DATA  0
00B3  1800  NI          DATA  :1800
00B4  1802  IB          DATA  :1802
00B5  FE00  CT          DATA  -512
00B6  1400  NPEM        DATA  :1400
00B7  1600  NMEM        DATA  :1600
00B8  0000  NØEM        DATA  0
00B9  0000  TREM        DATA  0
00BA  9002  PLS         DATA  :9002
00BB  9202  MINS        DATA  :9202
00BC  0000  CØN1        DATA  0
00BD  0000  TETR        DATA  0
00BE  1000  BPNT        DATA  :1000
00BF        MASK        REF
                  *
                  *ADD INPUT ARRAY TØ TEMP ARRAY
                  *
00C0  0800  ACC         ENT
00C1  B604              LDA   TETR
00C2  2083              JAM   $+4
00C3  B60A              LDA   TREM
```

```
00C4   0210             CAR
00C5   F201             JMP    $+2
00C6   B617             LDA    DIR
00C7   C000             CAI    0
00C8   F202             JMP    $+3
00C9   E613             LDX    NPEM
00CA   F201             JMP    $+2
00CB   E614             LDX    NMEM
00CC   EE14             STX    NØEM
00CD   DC01             IMS    @1       BUMP CØUNTER
00CE   C202             AXI    2
00CF   EA12             STX    TBP      SAVE TEMP PØINTER
00D0   C7FF             LAM    255      DATA CØUNT
00D1   9E28             STA    CNT
00D2   E61F             LDX    NI       INPUT PØINTER
00D3   C202    A1       AXI    2        BUMP CØUNTER
00D4   EE81             STX    IBP      +SAVE
00D5   B618             LDA    TETR
00D6   2188             JAL    T5
00D7   B400             LDA    @0
00D8   E401             LDX    @1
00D9   1328             LLX    1
00DA   1B86             LLR    7
00DB   13A8             LRX    1
00DC   1356             LLA    7
00DD   10D6             ARA    7
00DE   F202             JMP    T6
00DF   B400    T5       LDA    @0
00E0   E401             LDX    @1
00E1   F900    T6       JST    DPACC
00E2   0000    TBP      DATA   0
00E3   C202             AXI    2        BUMP TEMP
00E4   EE02             STX    TBP
00E5   E692             LDX    IBP
00E6   0110             ZAR
00E7   9C00             STA    @0
00E8   9C01             STA    @1
00E9   DE40             IMS    CNT      DØNE?
00EA   F617             JMP    A1       NØ
00EB   F72B             RTN    ACC
                *
                *WAIT.FØR ALIGNMENT PULSE
                *
00EC   0800    TURNØN   ENT
00ED   4006             CID             DISABLE AUTØ
00EE   48C1             SSN    :C1      LIGHT ØFF?
00EF   F601             JMP    $-1      NØ
00F0   0E00             SEM             YES BYTE ØN
00F1   49C1             SEN    :C1      LIGHT ØN?
00F2   F601             JMP    $-1      NØ
00F3   0F00             SWM             YES, BYTE ØFF
00F4   40C4             SEL    :C4      CLEAR FLAG
00F5   4005             CIE             ENABLE AUTØ
00F6   F70A             RTN    TURNØN
```

```
                    *
                    *INPUT FRØM MØNSANTØ
                    *  CØNVERT BCD TØ BINARY
                    *
00F7   0800   MØNS     ENT
00F8   B63B            LDA   TETR
00F9   208F            JAM   T3
00FA   C6FF            LAP   255
00FB   8E4B            ADD   DCT
00FC   1050            ALA   1
00FD   E644            LDX   TREM
00FE   3802            JXN   S+3
00FF   8A08            ADD   DMTR
0100   F201            JMP   S+2
0101   8A05            ADD   DPTR
0102   0048            TAX
0103   B400            LDA   @0
0104   E401            LDX   @1
0105   F900            JST   DPFIX
0106   F70F            RTN   MØNS
0107   1002   DPTR     DATA  :1002
0108   1202   DMTR     DATA  :1202
0109   49C6   T3       SEN   :C6        FLAG
010A   F601            JMP   S-1        NØ
010B   5AC6            INX   :C6        YES, INPUT TØ X
010C   2843            JXZ   S-3        IGNØRE ZERØES
010D   C704            LAM   4          SET DIGIT CØUNT
010E   9E65            STA   CNT
010F   0110            ZAR              CLEAR TALLY
0110   9E63            STA   MSK2
0111   F206            JMP   M2
0112   1350   M1       LLA   1          X10
0113   9E66            STA   MSK2
0114   1351            LLA   2
0115   8E68            ADD   MSK2
0116   9E69            STA   MSK2
0117   0110            ZAR
0118   1B03   M2       LLL   4          GET NEXT DIGIT
0119   8E6C            ADD   MSK2       ADD TØ TALLY
011A   DE71            IMS   CNT        LAST DIGIT?
011B   F609            JMP   M1         NØ
011C   0048            TAX
011D   0110            ZAR
011E   F727            RTN   MØNS       YES
                    *TEXT STØRAGE
011F   8D8A   MSG      DATA  :8D8A
0120   C1C2            TEXT  'ABØRT LAST RUN?'
0121   CFD2
0122   D4A0
0123   CCC1
0124   D3D4
0125   A0D2
0126   D5CE
0127   BFA0
```

```
0317   0128   8D8A   ABT     DATA :8D8A
0318   0129   B1A0           TEXT '1 RUN ABØRTED,'
       012A   D2D5
       012B   CEA0
       012C   C1C2
       012D   CFD2
       012E   D4C5
       012F   C4AC
0319   0130   A0D2   RUNS    TEXT ' RUNS KEPT'
       0131   D5CE
       0132   D3A0
       0133   CBC5
       0134   D0D4
0320   0135   8D8A           DATA :8D8A,0
       0136   0000
0321   0137   8D8A   MØDE    DATA :8D8A
0322   0138   CDCF           TEXT 'MØNSANTØ,TAPE ØR INVERSE?'
       0139   CED3
       013A   C1CE
       013B   D4CF
       013C   ACD4
       013D   C1D0
       013E   C5A0
       013F   CFD2
       0140   A0C9
       0141   CED6
       0142   C5D2
       0143   D3C5
       0144   BFA0
0323                         END
0000   ERRØRS
```

```
                        NAM   IKB,IER,BIPT,XEQ
                        NAM   ØTT,ERR,CRLF
                        NAM   ØTL,ØFPA
0000                    REL   0
                  *
                  * PANIC SWITCH
                  *
0000   FB00             JST   *CMND
0001              CMND  REF
                  *
                  *KEYBØARD INPUT
                  *
0002   0800       IKB   ENT
0003   4038             SEL   7,0     AUTØ-ECHØ
0004   4039             SEL   7,1     KBD MØDE
0005   5939             RDA   7,1     READ ØN FLAG
0006   403C             SEL   7,4     RESET
0007   F705             RTN   IKB
0008   0800       IER   ENT
0009   FE07             JST   IKB
000A   C0DF             CAI   :DF     BACK ARRØW?
000B   FF0A             JST   *CMND   YES
000C   C08A             CAI   :8A     LINE FEED?
000D   FF0C             JST   *CMND   YES
000E   F706             RTN   IER     NEITHER,RETURN
                  *
                  *PAPER TAPE INPUT
                  *   DS0 = 0 FØR TTY
                  *         1 FØR HSR
                  *
000F   0800       BIPT  ENT
0010   5801       BIP2  ISA           READ SWITCHES
0011   13D0             LRA   1       DS0 UP FØR TTY
0012   220A             JØS   HSR     DØWN FØR HSR
0013   493B             SEN   7,3     TTY BUSY?
0014   F604             JMP   BIP2    YES
0015   403A             SEL   7,2     NØ,STEP READER
0016   4839       WT    SSN   7,1     FLAG?
0017   F203             JMP   IT      YES
0018   0150             IAR           NØ,BUMP CØUNT
0019   2149             JAZ   BIP2    RESTART IF TIME UP
001A   F604             JMP   WT      ELSE CHECK FLAG AGAIN
001B   5838       IT    INA   7,0     INPUT FRØM TTY
001C   F70D             RTN   BIPT    & RETURN
001D   4933       HSR   SEN   6,3     HSR BUSY?
001E   F60E             JMP   BIP2    YES
001F   4032             SEL   6,2     NØ, STEP READER
0020   4835       WH    SSN   6,5     FLAG?
0021   F203             JMP   IH      YES
0022   0150             IAR           NØ, BUMP CØUNT
0023   2153             JAZ   BIP2    RESTART IF TIME UP
0024   F604             JMP   WH      ELSE CHECK FLAG AGAIN
0025   5835       IH    INA   6,5     INPUT FRØM HSR
```

```
0026  F717          RTN   BIPT      & RETURN
                *
                *WAIT FØR EXECUTE SIGNAL
                *
0027  0800  XEQ     ENT
0028  FE20          JST   IER       INPUT
0029  C08D          CAI   :8D       CARRIAGE RETURN?
002A  F703          RTN   XEQ       YES, RETURN
002B  F603          JMP   XEQ+1     NØ, GET MØRE
                *
                *ØUTPUT TØ TTY
                *
002C  0800  ØTT     ENT
002D  403C          SEL   7,4       RESET INTERFACE
002E  6D3B          WRA   7,3       WRITE ØN NØT BUSY
002F  493B          SEN   7,3       DØNE?
0030  F601          JMP   $-1       NØ
0031  F705          RTN   ØTT       YES
                *
                *CØMMAND ERRØR EXIT
                *
0032  0800  ERR     ENT
0033  C6DF          LAP   :DF       PRINT ARRØW
0034  FE08          JST   ØTT
0035  FF34          JST   *CMND     RESTART CØMMAND
                *
                *CARRIAGE-RETURN,LINE FEED
                *
0036  0800  CRLF    ENT
0037  C68D          LAP   :8D       CR
0038  FE0C          JST   ØTT
0039  C68A          LAP   :8A       LF
003A  FE0E          JST   ØTT
003B  F705          RTN   CRLF
                *
                *ØUTPUT TEXT FRØM BUFFER
                *
003C  0800  ØTL     ENT
003D  8A0F          ADD   CAI       MAKE CØMPARE INSTRUCTIØN
003E  9A06          STA   ØT2       &SAVE IT
003F  9A09          STA   ØT3
0040  E704          LDX   *ØTL      GET TEXT PØINTER
0041  DE05          IMS   ØTL       SET RETURN ADDRESS
0042  B400  ØT1     LDA   @0        GET WØRD
0043  11D7          RRA   8         PRINT FIRST BYTE
0044  FE18          JST   ØTT
0045  C000  ØT2     CAI   0         LAST ØNE
0046  F70A          RTN   ØTL       YES, RETURN
0047  1157          RLA   8         PRINT SECØND BYTE
0048  FE1C          JST   ØTT
0049  C000  ØT3     CAI   0         LAST ØNE?
004A  F70E          RTN   ØTL       YES RETURN
004B  0128          IXR             BUMP PØINTER
```

```
004C  F60A         JMP   ØTI     LØØP
004D  C000  CAI    CAI   0
            *
            *ØUTPUT FLØATING PØINT NUMBER
            *
004E  0800  ØFPA   ENT
004F  E701         LDX   *ØFPA   GET PØINTER
0050  DE02         IMS   ØFPA    SET RETURN ADDRESS
0051  EA01         STX   ØPT     SAVE PØINTER
0052  FB0E         JST   *FAS    CØNVERT TØ ASCII
0053  0000  ØPT    DATA  0
0054  0059         DATA  BUF
0055  0110         ZAR           SET END FLAG
0056  FE1A         JST   ØTL     PRINT NUMBER
0057  0059         DATA  BUF
0058  F70A         RTN   ØFPA
0059  0000  BUF    RES   8,0
0061        FAS    REF
                   END
0000 ERRØRS
```

```
0001                          NAM    READ,CLEAR
0002                          NAM    PUNCH,GRAPH
0003                          EXTR   IKB,ØTT,BIPT
0004                          EXTR   ØTL,CRLF,FPLØT,ØFPA
0005                          EXTR   XA,XB,XC,FAD
0006  0000                    REL    0
0007                   *
0008                   * READ PAPER TAPE & ADD TØ BUFFER
0009                   *
0010  0000  0800       READ   ENT
0011                   *INITIALIZE VARIABLES
0012  0001  1128              RLX    1           SET INDEX BIT
0013  0002  1400              SØV
0014  0003  11A8              RRX    1
0015  0004  EA33              STX    R5          & SAVE PØINTER
0016  0005  EA34              STX    R5+2
0017  0006  0528              XRP                RESET SUBSCRIPTS
0018  0007  E900              STX    XA
            0000
0019  0008  E900              STX    XB
            0000
0020  0009  E900              STX    XC
            0000
0021  000A  B236              LDA    TP          SET INPUT BUFFER PØINTER
0022  000B  9A38              STA    MPT
0023  000C  B235              LDA    CT          SET INPUT CØUNT
0024  000D  9A37              STA    CNT
0025                   *SKIP LEADER & LABEL
0026  000E  C68A              LAP    :8A         LINE FEED
0027  000F  F900              JST    ØTT
            0000
0028  0010  F900              JST    BIPT
            0000
0029  0011  2141              JAZ    $-1         SKIP LEADER
0030  0012  F900       R1     JST    ØTT         ECHØ LABEL
            0000
0031  0013  F900              JST    BIPT        READ TAPE
            0000
0032  0014  C092              CAI    :92         END ØF LABEL?
0033  0015  F201              JMP    R2          YES
0034  0016  F604              JMP    R1          NØ
0035  0017  F900       R2     JST    BIPT        READ TAPE
            0000
0036  0018  C0FF              CAI    :FF         FILE MARK?
0037  0019  F201              JMP    R3          YES
0038  001A  F603              JMP    R2          NØ
0039                   *READ LØØP
0040  001B  F900       R3     JST    BIPT        LØWER BYTE
            0000
0041  001C  1B87              LLR    8           SAVE
0042  001D  F900              JST    BIPT        UPPER BYTE
            0000
0043  001E  1B07              LLL    8           RESTØRE
```

```
001F  E224              LDX    MPT          SAVE LØW BITS
0020  9C01              STA    @1
0021  F900              JST    BIPT         LØWER BYTE
      0000
0022  1B87              LLR    8
0023  F900              JST    BIPT         UPPER BYTE
      0000
0024  1B07              LLL    8
                  *CØNVERT BASIC-F.P. TØ CAI-F.P.
0025  2109              JAZ    Z1           0=0=0
0026  0048              TAX                 SAVE SIGN
0027  3081              JAP    S+2          ABS. VAL.
0028  0310              NAR
0029  1B87              LLR    8            REMØVE MSB
002A  1328              LLX    1
002B  8A17              ADD    D64          FIX CHARACTERISTIC
002C  1B07              LLL    8
002D  13C0              LAØ                 RECØVER SIGN
002E  11D0              RRA    1
002F  9B14        Z1    STA    *MPT         SAVE HI BITS
0030  DA13              IMS    MPT          BUMP PØINTER
0031  DA12              IMS    MPT          TWICE!
0032  DA12              IMS    CNT          MØRE?
0033  F618              JMP    R3           YES
                  *ADD INPUT BUFFER TØ BEAM ARRAY
                  *PANIC SWITCH DISABLED FØR DURATIØN
0034  4006              CID                 DISABLE AUTØ
0035  B20C              LDA    CT           RESET CØUNTER
0036  9A0E              STA    CNT
0037  F900        R4    JST    FAD          F.P. ADD
      0000
0038  0000        R5    DATA   0,:9400,0
0039  9400
003A  0000
003B  D900              IMS    XA           BUMP SUBSCRIPTS
      0000
003C  D900              IMS    XB
      0000
003D  D900              IMS    XC
      0000
003E  DA06              IMS    CNT          MØRE?
003F  F608              JMP    R4           YES
0040  F740              RTN    READ
                  *STØRAGE
0041  1400        TP    DATA   :1400
0042  FF00        CT    DATA   -256
0043  0040        D64   DATA   64
0044  0000        MPT   DATA   0
0045  0000        CNT   DATA   0
                  *
                  *CLEAR BEAM ARRAY
                  *
0046  0800        CLEAR ENT
```

```
0047  B605          LDA   CT      SET CØUNT
0048  9E03          STA   CNT
0049  0110          ZAR           CLEAR
004A  9C00   C1     STA   @0      HI BITS
004B  9C01          STA   @1      LØ BITS
004C  C202          AXI   2       BUMP PØINTER
004D  DE08          IMS   CNT     DØNE?
004E  F604          JMP   C1      NØ
004F  F709          RTN   CLEAR
                    *
                    *PUNCH BEAM ARRAY - BASIC FØRMAT
                    *
0050  0800   PUNCH  ENT
0051  FA22          JST   LEAD    LEADER
0052  B610          LDA   CT      START CØUNTER
0053  9E0E          STA   CNT
0054  F900   P1     JST   IKB     ECHØ LABEL
      0000
0055  C092          CAI   :92     CTRL/TAPE?
0056  F201          JMP   P2      YES
0057  F603          JMP   P1      NØ
0058  C6FF   P2     LAP   :FF     PUNCH FILE MARK
0059  F900          JST   ØTT
      0000
005A  B401   P3     LDA   @1      PUNCH LØ BITS
005B  F900          JST   ØTT
      0000
005C  13D7          LRA   8
005D  F900          JST   ØTT
      0000
005E  B400          LDA   @0      GET HI BITS
005F  C202          AXI   2       BUMP PØINTER
0060  EE1C          STX   MPT     AND SAVE
                    *CØNVERT CAI-F.P. TØ BASIC-F.P.
0061  210A          JAZ   Z2      0=0=0
0062  0048          TAX           SAVE SIGN
0063  1350          LLA   1       CLEAR A15
0064  1B87          LLR   8       SPLIT
0065  9622          SUB   D64     FIX CHARACTERISTIC
0066  1400          SØV           INSERT MSB
0067  1150          RLA   1
0068  1B06          LLL   7       RE-FØRMAT
0069  1329          LLX   2       RECØVER SIGN
006A  3201          JØR   $+2     CØRRECT FØR IT
006B  0310          NAR
006C  F900   Z2     JST   ØTT     PUNCH HI BITS
      0000
006D  1B87          LLR   8
006E  F900          JST   ØTT
      0000
006F  E62B          LDX   MPT     RECØVER PØINTER
0070  DE2B          IMS   CNT     DØNE?
0071  F617          JMP   P3      NØ
```

```
0072  FA01          JST    LEAD        YES, PUNCH LEADER
0073  F723          RTN    PUNCH
                *PUNCH 5" ØF LEADER
0074  0800  LEAD    ENT
0075  C732          LAM    50
0076  9E31          STA    CNT
0077  0110          ZAR
0078  F900  L2      JST    ØTT
      0000
0079  DE34          IMS    CNT
007A  F602          JMP    L2
007B  F707          RTN    LEAD
                *
                *PLØT DATA ARRAY
                *
007C  0800  GRAPH   ENT
007D  EA06          STX    T           SAVE CØUNT PØINTER
007E  C202          AXI    2
007F  EA08          STX    PT          SAVE DATA PØINTER
0080  0110          ZAR                PRINT CØUNT
0081  F900          JST    ØTL
      0000
0082  008A          DATA   CTX
0083  F900          JST    ØFPA
      0000
0084  0000  T       DATA   0
0085  F900          JST    CRLF
      0000
0086  C7FF          LAM    255         PLØT DATA
0087  F900          JST    FPLØT
      0000
0088  0000  PT      DATA   0
0089  F70D          RTN    GRAPH
008A  8A8A  CTX     DATA   :8A8A
008B  C3CF          TEXT   'CØUNT = '
008C  D5CE
008D  D4A0
008E  BDA0
008F  0000          DATA   0
                    END
0000 ERRØRS
```

```
                  *
                  *  FPLØT - FLØATING POINT PLØTTER
                  *
                  *       CALLING SEQUENCE:
                  *                                LDA MDIN
                  *                                JST *FPLØT
                  *                                DATA ARRAY
                  *                               (RETURN)
                  *
                          NAM    FPLØT
0000                      REL    0
0000  0800   FPLØT        ENT
0001  9A4C                STA    NRØW
0002  9A4C                STA    CNT
0003  B703                LDA    *FPLØT
0004  9A1F                STA    RP3
0005  9A24                STA    RP4
0006  A249                IØR    B15
0007  9A05                STA    RP1
0008  9A03                STA    RP2
0009  0350                ARP
000A  9B4F                STA    *XA
000B  F204                JMP    MØVE
000C  FB4E   LP1          JST    *FCP
000D  0000   RP1          DATA   0,MAX
000E  0051
000F  2183                JAL    INC
0010  FB4B   MØVE         JST    *FMV
0011  0000   RP2          DATA   0,MAX
0012  0051
0013  DB46   INC          IMS    *XA
0014  DA3A                IMS    CNT
0015  F609                JMP    LP1
0016  FB41                JST    *CRLF
0017  FB40                JST    *CRLF
0018  C6BD                LAP    '='
0019  FB3F                JST    *ØTL
001A  0061                DATA   SF
001B  FB43                JST    *FDV
001C  0055                DATA   F50,MAX,SCALE
001D  0051
001E  0053
001F  FB40                JST    *ØFPA
0020  0053                DATA   SCALE
0021  FB36                JST    *CRLF
0022  FB35                JST    *CRLF
0023  FB3C   LP2          JST    *ØFPA
0024  0000   RP3          DATA   0
0025  DE01                IMS    RP3
0026  DE02                IMS    RP3
0027  C6A0                LAP    ' '
0028  FB2E                JST    *ØTT
0029  FB34                JST    *FMP
```

```
002A   0000   RP4     DATA   0,SCALE,MAX
002B   0053
002C   0051
002D   DE03           IMS    RP4
002E   DE04           IMS    RP4
002F   FB2D           JST    *FIX
0030   0051           DATA   MAX,CNT
0031   004F
0032   B21C           LDA    CNT
0033   0048           TAX
0034   3085           JAP    PØS
0035   C6AD           LAP    '-'
0036   FB20           JST    *ØTT
0037   C6B0           LAP    '0'
0038   FB1E           JST    *ØTT
0039   F20E           JMP    ØUT
003A   C6A0   PØS     LAP    ' '
003B   FB1B           JST    *ØTT
003C   2809           JXZ    MARK
003D   C6B0           LAP    '0'
003E   FB18           JST    *ØTT
003F   0508           NXR
0040   EA0E           STX    CNT
0041   C6AA           LAP    '*'
0042   F201           JMP    $+2
0043   FB13           JST    *ØTT
0044   DA0A           IMS    CNT
0045   F602           JMP    $-2
0046   C6AA   MARK    LAP    '*'
0047   FB0F           JST    *ØTT
0048   FB0F   ØUT     JST    *CRLF
0049   DA04           IMS    NRØW
004A   F627           JMP    LP2
004B   FB0C           JST    *CRLF
004C   DE4C           IMS    FPLØT
004D   F74D           RTN    FPLØT
004E   0800   NRØW    HLT
004F   0800   CNT     HLT
0050   8000   B15     DATA   :8000
0051   0000   MAX     RES    2,0
0053   0000   SCALE   RES    2,0
0055   4348   F50     DATA   :4348,0
0056   0000
0057          ØTT     REF
0058          CRLF    REF
0059          ØTL     REF
005A          XA      REF
005B          FCP     REF
005C          FMV     REF
005D          FIX     REF
005E          FMP     REF
005F          FDV     REF
0060          ØFPA    REF
```

```
0099   0061   D3C3   SF      TEXT    'SCAL FACTOR ='
       0062   C1CC
       0063   85C6
       0064   C1C3
       0065   D4CF
       0066   D2A0
       0067   BDA0
0100                         END
```

```
                 *
                 *CRT - FLØATING POINT PLØTTER
                 *
                 *      CALLING SEQUENCE:
                 *                    JST *CRT
                 *                    (RETURN)
                 *
                       NAM   CRT
0000                   REL   0
0000  0800  CRT        ENT
0001  C7FF             LAM   255
0002  9A5F             STA   NRØW
0003  9A5F             STA   CNT
0004  49C4             SEN   24,4
0005  F601             JMP   $-1
0006  40C7             SEL   24,7
0007  C202             AXI   2
0008  0030             TXA
0009  A261             IØR   B15
000A  9A0B             STA   RP1
000B  9A0E             STA   RP2
000C  9A10             STA   RP3
000D  9A13             STA   RP4
000E  9A36             STA   RP5
000F  0110             ZAR
0010  9A54             STA   MIN
0011  9A54             STA   MIN+1
0012  0350             ARP
0013  9B5B             STA   *XA
0014  F204             JMP   MØVE
0015  FB5A  LP1        JST   *FCP
0016  0000  RP1        DATA  0,MAX
0017  0067
0018  2183             JAL   INC1
0019  FB57  MØVE       JST   *FMV
001A  0000  RP2        DATA  0,MAX
001B  0067
001C  FB53  INC1       JST   *FCP
001D  0000  RP3        DATA  0,MIN
001E  0065
001F  3083             JAP   INC2
0020  FB50             JST   *FMV
0021  0000  RP4        DATA  0,MIN
0022  0065
0023  DB4B  INC2       IMS   *XA
0024  DA3E             IMS   CNT
0025  F610             JMP   LP1
                 *
0026  FB4F             JST   *CRLF
0027  FB4E             JST   *CRLF
0028  C6BD             LAP   '='
0029  FB4D             JST   *ØTL
002A  0079             DATA  SF
```

```
                     *
002B  FB46                 JST    *FSB
002C  0067                 DATA   MAX,MIN,MAX
002D  0065
002E  0067
002F  FB43                 JST    *FDV
0030  006C                 DATA   F250,MAX,SCALE
0031  0067
0032  0069
0033  FB44                 JST    *ØFPA
0034  0069                 DATA   SCALE
0035  FB40                 JST    *CRLF
                     *
0036  FB3D                 JST    *FMP
0037  0069                 DATA   SCALE,MIN,MAX
0038  0065
0039  0067
003A  FB3A                 JST    *FIX
003B  0067                 DATA   MAX,MIN
003C  0065
003D  B227                 LDA    MIN
003E  0310                 NAR
003F  3081                 JAP    $+2
0040  0110                 ZAR
0041  9A22                 STA    X
0042  0350                 ARP
0043  9B2B                 STA    *XA
                     *
0044  FB2F           LP2   JST    *FMP
0045  0000           RP5   DATA   0,SCALE,MAX
0046  0069
0047  0067
0048  DB26                 IMS    *XA
0049  FB2B                 JST    *FIX
004A  0067                 DATA   MAX,CNT
004B  0063
004C  E217                 LDX    X
004D  B215                 LDA    CNT
004E  49C4           DØT   SEN    24,4
004F  F601                 JMP    $-1
0050  49C2                 SEN    24,2
0051  F601                 JMP    $-1
0052  6EC2                 ØTX    24,2
0053  2107                 JAZ    DØNE
0054  3183                 JAG    PØS
0055  00A8                 DXR
0056  0150                 IAR
0057  F609                 JMP    DØT
0058  0128           PØS   IXR
0059  00D0                 DAR
005A  F60C                 JMP    DØT
005B  B208           DØNE  LDA    X
005C  8A11                 ADD    H256
```

```
005D  9A06           STA    X
005E  DA03           IMS    NRØW
005F  F61B           JMP    LP2
0060  FB15           JST    *CRLF
0061  F761           RTN    CRT
                *
0062  0000      NRØW DATA   0
0063  0000      CNT  DATA   0
0064  0000      X    DATA   0
0065  0000      MIN  RES    2, 0
0067  0000      MAX  RES    2, 0
0069  0000      SCALE RES   2, 0
006B  8000      B15  DATA   :8000
006C  447A      F250 DATA   :447A, 0
006D  0000
006E  0100      H256 DATA   256
                *
006F            XA   REF
0070            FCP  REF
0071            FMV  REF
0072            FSB  REF
0073            FDV  REF
0074            FMP  REF
0075            FIX  REF
0076            CRLF REF
0077            ØTL  REF
0078            ØFPA REF
                *
0079  D3C3      SF   TEXT   'SCALE FACTØR ='
007A  C1CC
007B  C5A0
007C  C6C1
007D  C3D4
007E  CFD2
007F  A0BD
                *
                     END
0000 ERRØRS
```

```
                          NAM   VIEW
                          EXTR  DPN:, DPSUB:, DPDIV:, DPSM:
                          NAM   DISP
                          EXTR  RTTR, RTØP
0000   0800   VIEW        ENT
0001   9A71   DISP        STA   VEVR
0002   C202               AXI   2
0003   EA66               STX   RP1D      PØINTER
0004   EA66               STX   RP2D
0005   C7FF               LAM   255
0006   9A6A               STA   CNT
0007   9A64               STA   NRØW
0008   0110               ZAR             INITIALIZE MAX AND MIN
0009   9A63               STA   MIN
000A   9A63               STA   MIN+1
000B   9A63               STA   MAX
000C   9A63               STA   MAX+1
000D   B400   STCM        LDA   @0
000E   D260               CMS   MAX
000F   F20A               JMP   MIN1      A1<MAX
0010   F205               JMP   MAX1      A1>MAX
0011   B401               LDA   @1        A1=MAX
0012   D25D               CMS   MAX+1
0013   F206               JMP   MIN1      A1=MAX  A2<MAX+1
0014   9A5B               STA   MAX+1     A1=MAX  A2>MAX+1
0015   F211               JMP   FICM
0016   9A58   MAX1        STA   MAX
0017   B401               LDA   @1
0018   9A57               STA   MAX+1
0019   F20D               JMP   FICM
001A   B400   MIN1        LDA   @0
001B   D251               CMS   MIN
001C   F206               JMP   MIN2      A1<MIN
001D   F209               JMP   FICM      A1>MIN
001E   B401               LDA   @1        A1=MIN
001F   D24E               CMS   MIN+1
0020   F202               JMP   MIN2      A1=MIN  A2<MIN+1
0021   F205               JMP   FICM      A1=MIN  A2>MIN+1
0022   F204               JMP   FICM      A1=MIN  A2=MIN+1
0023   B400   MIN2        LDA   @0
0024   9A48               STA   MIN
0025   B401               LDA   @1
0026   9A47               STA   MIN+1
0027   E242   FICM        LDX   RP1D
0028   C202               AXI   2
0029   EA40               STX   RP1D
002A   DA46               IMS   CNT
002B   F61E               JMP   STCM
              *
002C   B242               LDA   MAX
002D   E242               LDX   MAX+1
002E   F900               JST   DPSUB:
       0000
```

```
002F   006D            DATA   MIN
0030   1050            ALA    1
0031   1329            LLX    2
0032   3201            JØR    $+2
0033   0150            IAR
0034   13A3            LRX    1
0035   9A39            STA    MAX
0036   EA39            STX    MAX+1
                *
0037   B235            LDA    MIN
0038   E235            LDX    MIN+1
0039   F900            JST    DPDIV:
       0000
003A   006F            DATA   MAX
003B   9A2D            STA    TEM
003C   10D1            ARA    2
003D   0310            NAR
003E   8A2A            ADD    TEM
003F   10D5            ARA    6
                *
0040   0310            NAR
0041   3081            JAP    $+2
0042   0110            ZAR
0043   9A2E            STA    X
                *
0044   E226            LDX    RP2D
0045   B400     LPD    LDA    @0
0046   E401            LDX    @1
0047   F900            JST    DPDIV:
       0000
0048   006F            DATA   MAX
0049   9A1F            STA    TEM
004A   10D1            ARA    2
004B   0310            NAR
004C   8A1C            ADD    TEM
004D   10D5            ARA    6
                *
004E   E223            LDX    X
004F   49C4     DØT    SEN    24,4
0050   F601            JMP    $-1
0051   49C2            SEN    24,2
0052   F601            JMP    $-1
0053   6EC2            ØTX    24,2
0054   2107            JAZ    DØNE
0055   3183            JAG    PØS
0056   00A8            DXR
0057   0150            IAR
0058   F609            JMP    DØT
0059   0128     PØS    IXR
005A   00D0            DAR
005B   F60C            JMP    DØT
                *
005C   B215     DØNE   LDA    X
```

```
005D  8A16             ADD    H256
005E  9A13             STA    X
005F  E20B             LDX    RP2D
0060  C202             AXI    2
0061  EA09             STX    RP2D
0062  DA09             IMS    NRØW
0063  F61E             JMP    LPD
0064  B20E             LDA    VEVR
0065  2101             JAZ    $+2
0066  F100             JMP    RTØP
      0000
0067  F100             JMP    RTTR
      0000
0068  F768             RTN    VIEW
0069  0000   TEM       DATA   0
006A  0000   RP1D      DATA   0
006B  0000   RP2D      DATA   0
006C  0000   NRØW      DATA   0
006D  0000   MIN       RES    2,0
006F  0000   MAX       RES    2,0
0071  0000   CNT       DATA   0
0072  0000   X         DATA   0
0073  0000   VEVR      DATA   0
0074  0100   H256      DATA   256
                       END
0000 ERRØRS
```

```
                        NAM     DPACC
                        NAM     DPFLT
                        NAM     DPFIX
                        EXTR    DPN:
                        EXTR    DPN
0000                    REL     0
                *
                *DØUBLE PRECISIØN ACCUMULATE
                *
0000    0800    DPACC   ENT
0001    9A10            STA     TEMP
0002    0030            TXA
0003    E703            LDX     *DPACC
0004    1200            RØV
0005    8C01            ADD     @1
0006    820C            AND     MASK
0007    9C01            STA     @1
0008    B209            LDA     TEMP
0009    3204            JØR     DC1
000A    1200            RØV
000B    0150            IAR
000C    3201            JØR     DC1
000D    0110            ZAR
000E    8C00    DC1     ADD     @0
000F    9C00            STA     @0
0010    DE10            IMS     DPACC
0011    F711            RTN     DPACC
0012    0000    TEMP    DATA    0
0013    7FFF    MASK    DATA    :7FFF
                *
                *DØUBLE PRECISIØN TØ CAI-F. P.
                *
0014    0800    DPFLT   ENT
0015    3801            JXN     DPF1
0016    2113            JAZ     DPF4
0017    BA13    DPF1    EMA     BITS
0018    0110            ZAR
0019    BA11            EMA     BITS
001A    9A11            STA     SIGN
001B    3081            JAP     DPF2
001C    F900            JST     DPN:
        0000
001D    1328    DPF2    LLX     1
001E    1B00    DPF3    LLL     1
001F    DA0B            IMS     BITS
0020    3242            JØR     DPF3
0021    1B88            LLR     9
0022    BA08            EMA     BITS
0023    0310            NAR
0024    8A08            ADD     D160
0025    1356            LLA     7
0026    A204            IØR     BITS
0027    BA04            EMA     SIGN
```

```
0028   8205          AND    DPM
0029   A202          IØR    SIGN
002A   F716   DPF4   RTN    DPFLT
002B   0000   BITS   DATA   0
002C   0000   SIGN   DATA   0
002D   00A0   D160   DATA   160
002E   8000   DPM    DATA   :8000
002F   0800   DPFIX  ENT
0030   9E04          STA    SIGN
0031   821C          AND    DPP
0032   13D6          LRA    7
0033   9606          SUB    D160
0034   9E09          STA    BITS
0035   B609          LDA    SIGN
0036   8218          AND    MANT
0037   A218          IØR    SBIT
0038   BE0D          EMA    BITS
0039   2109          JAZ    DPFX2
003A   3190          JAG    DPFX4
003B   BE10          EMA    BITS
003C   1B07          LLL    8
003D   1B30   DPFX1  LLR    1
003E   DE13          IMS    BITS
003F   F602          JMP    DPFX1
0040   1B00          LLL    1
0041   13A8          LRX    1
0042   F201          JMP    $+2
0043   BE18   DPFX2  EMA    BITS
0044   BE18          EMA    SIGN
0045   3083          JAP    DPFX3
0046   BE1A          EMA    SIGN
0047   F900          JST    DPN:
       0000
0048   F201          JMP    $+2
0049   BE1D   DPFX3  EMA    SIGN
004A   F71B          RTN    DPFIX
004B   0118   DPFX4  ZAX
004C   1400          SØV
004D   F71E          RTN    DPFIX
004E   7FFF   DPP    DATA   :7FFF
004F   007F   MANT   DATA   :7F
0050   0080   SBIT   DATA   :80
                     END
0000 ERRØRS
```

APPENDIX C

```
                         NAM    CMND
                         EXTR   IER,ØTT,ØTL,CRLF
                         EXTR   ERR,XEQ
0100                     ABS    :100
               *PRINT    NAME
0100  0110               ZAR
0101  F900               JST    ØTL
      0000
0102  012B               DATA   NAME
0103  F201               JMP    $+2
               *
               *COMMAND INTERPRETER
               *
0104  0800     CMND      ENT
0105  0A00               EIN
0106  4005               CIE               ENABLE PANIC BUTTØN
0107  F900               JST    CRLF       PRINT PRØMPT CHARACTER
      0000
0108  C687               LAP    :87
0109  F900               JST    ØTT
      0000
010A  C6AA               LAP    '*'
010B  F900               JST    ØTT
      0000
010C  0108               ZXR
010D  F900               JST    IER        INPUT CØMMAND
      0000
010E  C0D4               CAI    'T'
010F  E213               LDX    TRANS
0110  C0D2               CAI    'R'
0111  E212               LDX    READ
0112  C0C3               CAI    'C'
0113  E211               LDX    CLEAR
0114  380A               JXN    ØKF
0115  C0D0               CAI    'P'
0116  E20F               LDX    PUNCH
0117  C0C7               CAI    'G'
0118  E20F               LDX    FPLØT
0119  C0D6               CAI    'V'
011A  E20E               LDX    CRT
011B  C0C4               CAI    'D'
011C  E20A               LDX    DATUM
011D  3801               JXN    ØKF
011E  F900     BAD       JST    ERR
      0000
011F  EA0A     ØKF       STX    FUNC       SAVE CALL ADDRESS
0120  F900               JST    XEQ        WAIT FØR GØ
      0000
0121  FB08               JST    *FUNC      CALL FUNCTIØN
0122  F61D               JMP    CMND+1
0123           TRANS     REF
0124           READ      REF
0125           CLEAR     REF
```

```
0047  0126        PUNCH  REF
0048  0127        DATUM  REF
0049  0128        FPLØT  REF
0050  0129        CRT    REF
0051  012A  0000  FUNC   DATA   0
0052  012B  B1B5  NAME   TEXT   '15*255 FULL HTS'
      012C  AAB2
      012D  B5B5
      012E  A0C6
      012F  D5CC
      0130  CCA0
      0131  C8D4
      0132  D3A0
0053  0133  8D3A         DATA   :8D3A, 0
      0134  0000
0054                     END
0000 ERRØRS
```

```
                          NAM    TRANS
                          NAM    RTTR
                          EXTR   DISP
0000                      REL    0
0000  0800   TRANS        ENT
0001  C6BF                LAP    '?'
0002  F900                JST    *ØTL
      8127
0003  013E                DATA   MØTA
0004  F900                JST    *IKB
      8128
0005  1200                RØV
0006  C0CD                CAI    'M'
0007  F203                JMP    MØN
0008  C0D4                CAI    'T'
0009  F204                JMP    TAP
000A  F900                JST    *ERR
      812A
000B  F900   MØN          JST    *CRLF
      8129
000C  0108                ZXR
000D  F20F                JMP    BEG
000E  F900   TAP          JST    *CRLF
      8129
000F  C68A                LAP    :8A
0010  F900                JST    *ØTT
      8126
0011  F900                JST    *BIPT
      8125
0012  2141                JAZ    $-1
0013  F900   T1           JST    *ØTT
      8126
0014  F900                JST    *BIPT
      8125
0015  C092                CAI    :92
0016  F201                JMP    T2
0017  F604                JMP    T1
0018  F900   T2           JST    *BIPT
      8125
0019  C0FF                CAI    :FF
001A  F201                JMP    T4
001B  F603                JMP    T2
001C  C401   T4           LXP    1
001D  E900   BEG          STX    TETR
      012B
001E  B100                LDA    MASK0
      0122
001F  9AF3                STA    MASK1
0020  F900                JST    *CRLF
      8129
0021  C6BF                LAP    '?'
0022  F900                JST    *ØTL
      8127
```

```
0023   0130          DATA   DIRE
0024   F900          JST    *IKB
       8128
0025   C0C6          CAI    'F'
0026   F205          JMP    FØRD
0027   C0C2          CAI    'B'
0028   F208          JMP    BACK
0029   C0CF          CAI    'Ø'
002A   F20A          JMP    BØTH
002B   FBFE          JST    *ERR
002C   C71E   FØRD   LAM    30
002D   9AE2          STA    CNT2
002E   0108          ZXR
002F   0408          CXR
0030   F207          JMP    TKF
0031   C71E   BACK   LAM    30
0032   9ADD          STA    CNT2
0033   0108          ZXR
0034   F203          JMP    TKF
0035   C70F   BØTH   LAM    15
0036   9AD9          STA    CNT2
0037   0358          AXP
0038   EAF5   TKF    STX    DIR1
0039   E2F1          LDX    TETR
003A   2802          JXZ    $+3
003B   C70F          LAM    15
003C   9AD3          STA    CNT2
003D   B2D4          LDA    ZCT
003E   9AD2          STA    CNT3
003F   E2E3          LDX    IBC
0040   0110          ZAR
0041   9C00   CLR    STA    @0
0042   0128          IXR
0043   DACD          IMS    CNT3
0044   F603          JMP    CLR
0045   EAD1          STX    IBP
0046   E2D4          LDX    TETR
0047   2803          JXZ    NEXT
0048   E2E5          LDX    DIR1
0049   3801          JXN    NEXT
004A   0210          CAR
004B   E2D8   NEXT   LDX    MASK
004C   0128          IXR
004D   0210          CAR
004E   C000          CAI    0
004F   C2FF          AXI    255
0050   EAB8          STX    MSK1
0051   9ABA          STA    DIR
0052   C7F5          LAM    245
0053   9ACC          STA    DCT2
0054   C7FF          LAM    255
0055   9AB7          STA    DCT
0056   B2D4          LDA    TETR
```

```
0057  2107          JAZ   TUR1
0058  FBCC  T3      JST   *BIPT
0059  1357          LLA   8
005A  9AD4          STA   TEMT
005B  FBC9          JST   *BIPT
005C  A2D2          IØR   TEMT
005D  9AB0          STA   VAL
005E  F209          JMP   PRØC
005F  FA89  TUR1    JST   TURNØN
0060  FA93  ILP     JST   MØNS
0061  9AAC          STA   VAL
0062  B2CB          LDA   DIR1
0063  C001          CAI   1
0064  F203          JMP   PRØC
0065  D2A6          CMS   DIR
0066  F235          JMP   FINØNE
0067  F234          JMP   FINØNE
0068  C70F  PRØC    LAM   15
0069  9AA5          STA   CNT1
006A  B2A8          LDA   MASK1
006B  9AA8          STA   MASK2
006C  B2B6          LDA   IBC
006D  9AA8          STA   IB
006E  C7FF  SPA     LAM   255
006F  9AA5          STA   SCT
0070  B298          LDA   MSK1
0071  9A98          STA   MSK2
0072  B2A3          LDA   IB
0073  9AA3          STA   IBP
0074  0110          ZAR
0075  D39E          CMS   *MASK2
0076  F201          JMP   $+2
0077  F213          JMP   TLP2
0078  E295  TLP1    LDX   VAL
0079  0110          ZAR
007A  D38F          CMS   *MSK2
007B  F201          JMP   $+2
007C  0508          NXR
007D  0030          TXA
007E  8B98          ADD   *IBP
007F  9B97          STA   *IBP
0080  DA89          IMS   MSK2
0081  DA95          IMS   IBP
0082  DA92          IMS   SCT
0083  F60B          JMP   TLP1
0084  DA8F          IMS   MASK2
0085  C6FF          LAP   255
0086  8A8F          ADD   IB
0087  9A8E          STA   IB
0088  DA86          IMS   CNT1
0089  F61B          JMP   SPA
008A  F211          JMP   FINØNE
008B  E282  TLP2    LDX   VAL
```

```
008C  0110          ZAR
008D  D37C          CMS   *MSK2
008E  0508          NXR
008F  0030          TXA
0090  8B86          ADD   *IBP
0091  9B85          STA   *IBP
0092  DA77          IMS   MSK2
0093  DA83          IMS   IBP
0094  DA80          IMS   SCT
0095  F60A          JMP   TLP2
0096  DA7D          IMS   MASK2
0097  C6FF          LAP   255
0098  8A7D          ADD   IB
0099  9A7C          STA   IB
009A  DA74          IMS   CNT1
009B  F62D          JMP   SPA
009C  E26C  FINØNE  LDX   MSK1
009D  0128          IXR
009E  B26D          LDA   DIR
009F  C000          CAI   0
00A0  C302          SXI   2
00A1  EA67          STX   MSK1
00A2  DA7D          IMS   DCT2
00A3  F201          JMP   $+2
00A4  40C7          SEL   24,7
00A5  DA67          IMS   DCT
00A6  F201          JMP   TUR2
00A7  F204          JMP   TUR3
00A8  B282  TUR2    LDA   TETR
00A9  2101          JAZ   $+2
00AA  F652          JMP   T3
00AB  F64B          JMP   ILP
00AC  C7FF  TUR3    LAM   255
00AD  9A6E          STA   CNT7
00AE  E263          LDX   IBP
00AF  0110          ZAR
00B0  9C00  CLR1    STA   @0
00B1  0128          IXR
00B2  DA69          IMS   CNT7
00B3  F603          JMP   CLR1
00B4  C7F1          LAM   241
00B5  9A63          STA   CNT4
00B6  C70F          LAM   15
00B7  9A62          STA   CNT5
00B8  9A62          STA   CNT6
00B9  B269          LDA   IBC
00BA  9A63          STA   IBD
00BB  C70E          LAM   14
00BC  9A60          STA   HM14
00BD  B260  NXBIN   LDA   IBD
00BE  9A60          STA   IBE
00BF  B35F  NXRØW   LDA   *IBE
00C0  10D3          ARA   4
```

```
00C1   8B55            ADD    *IBP
00C2   9B54            STA    *IBP
00C3   B254            LDA    H256
00C4   8A5A            ADD    IBE
00C5   9A59            STA    IBE
00C6   DA53            IMS    CNT5
00C7   F608            JMP    NXRØW
00C8   B252            LDA    CNT6
00C9   9A50            STA    CNT5
00CA   DA53            IMS    IBD
00CB   DA4B            IMS    IBP
00CC   DA4C            IMS    CNT4
00CD   F610            JMP    NXBIN
00CE   B24B            LDA    CNT5
00CF   0150            IAR
00D0   9A4A            STA    CNT6
00D1   9A48            STA    CNT5
00D2   C701            LAM    1
00D3   9A45            STA    CNT4
00D4   DA48            IMS    HM14
00D5   F618            JMP    NXBIN
00D6   0110            ZAR
00D7   9A49            STA    ØFFSET
00D8   F100            JMP    DISP
       0000
00D9   B251    RTTR    LDA    TETR
00DA   2104            JAZ    T5
00DB   B252            LDA    DIR1
00DC   3184            JAG    T6
00DD   0210            CAR
00DE   F206            JMP    T7
00DF   B24E    T5      LDA    DIR1
00E0   2182            JAL    $+3
00E1   B22A    T6      LDA    DIR
00E2   F202            JMP    T7
00E3   B228            LDA    DIR
00E4   3101            JAN    $+2
00E5   DA2D    T7      IMS    MASK1
00E6   DA29            IMS    CNT2
00E7   F69C            JMP    NEXT
00E8   F7E8            RTN    TRANS
00E9   0800    TURNØN  ENT
00EA   4006            CID
00EB   48C1            SSN    :C1
00EC   F601            JMP    $-1
00ED   0E00            SBM
00EE   49C1            SEN    :C1
00EF   F601            JMP    $-1
00F0   0F00            SWM
00F1   40C4            SEL    :C4
00F2   4005            CIE
00F3   F70A            RTN    TURNØN
00F4   0800    MØNS    ENT
```

```
00F5  49C6          SEN    :C6
00F6  F601          JMP    $-1
00F7  5AC6          INX    :C6
00F8  2843          JXZ    $-3
00F9  C704          LAM    4
00FA  9A10          STA    CNT
00FB  0110          ZAR
00FC  9A0D          STA    MSK2
00FD  F206          JMP    M2
00FE  1350  M1      LLA    1
00FF  9A0A          STA    MSK2
0100  1351          LLA    2
0101  8A08          ADD    MSK2
0102  9A07          STA    MSK2
0103  0110          ZAR
0104  1B03  M2      LLL    4
0105  8A04          ADD    MSK2
0106  DA04          IMS    CNT
0107  F609          JMP    M1
0108  F714          RTN    MØNS
0109  0000  MSK1    DATA   0
010A  0000  MSK2    DATA   0
010B  0000  CNT     DATA   0
010C  0000  DIR     DATA   0
010D  0000  DCT     DATA   0
010E  0000  VAL     DATA   0
010F  0000  CNT1    DATA   0
0110  0000  CNT2    DATA   0
0111  0000  CNT3    DATA   0
0112  F010  ZCT     DATA   -4080
0113  0000  MASK1   DATA   0
0114  0000  MASK2   DATA   0
0115  0000  SCT     DATA   0
0116  0000  IB      DATA   0
0117  0000  IBP     DATA   0
0118  0100  H256    DATA   256
0119  0000  CNT4    DATA   0
011A  0000  CNT5    DATA   0
011B  0000  CNT6    DATA   0
011C  0000  CNT7    DATA   0
011D  FFF2  HM14    DATA   -14
011E  0000  IBD     DATA   0
011F  0000  IBE     DATA   0
0120  0000  DCT2    DATA   0
0121  0000  ØFFSET  DATA   0
0122        MASK0   REF
0123        IBC     REF
0124        MASK    REF
0125        BIPT    REF
0126        ØTT     REF
0127        ØTL     REF
0128        IKB     REF
0129        CRLF    REF
```


C-3

```
0303  012A              ERR     REF
0304  012B   0000       TETR    DATA    0
0305  012C   0000       TEDA    DATA    0
0306  012D   0FF0       TCT1    DATA    4080
0307  012E   0000       DIR1    DATA    0
0308  012F   0000       TEMT    DATA    0
0309  0130   8D8A       DIRE    DATA    :8D8A
0310  0131   C6CF               TEXT    'FØRWARD, BACKWARD, ØR BØTH?'
      0132   D2D7
      0133   C1D2
      0134   C4AC
      0135   C2C1
      0136   C3CB
      0137   D7C1
      0138   D2C4
      0139   ACCF
      013A   D2A0
      013B   C2CF
      013C   D4C8
      013D   BFA0
0311  013E   8D8A       MØTA    DATA    :8D8A
0312  013F   C6D2               TEXT    'FRØM MØNSANTØ ØR FRØM TAPE?'
      0140   CFCD
      0141   A0CD
      0142   CFCE
      0143   D3C1
      0144   CED4
      0145   CFA0
      0146   CFD2
      0147   A0C6
      0148   D2CF
      0149   CDA0
      014A   D4C1
      014B   D0C5
      014C   BFA0
0313                            END
0000 ERRØRS
```

```
                          NAM    DATUM, RTDA
                          EXTR   DISD
0000  0300  DATUM         ENT
0001  C6BF                LAP    '?'
0002  FB63                JST    *ØTL
0003  0067                DATA   DIRE
0004  FB71                JST    *IKB
0005  C0C6                CAI    'F'
0006  F205                JMP    FØRD
0007  C0C2                CAI    'B'
0008  F208                JMP    BACK
0009  C0CF                CAI    'Ø'
000A  F20A                JMP    BØTH
000B  FB6C                JST    *ERR
000C  C71E  FØRD          LAM    30
000D  9A73                STA    DNT2
000E  0108                ZXR
000F  0408                CXR
0010  F207                JMP    PKF
0011  C71E  BACK          LAM    30
0012  9A6E                STA    DNT2
0013  0108                ZXR
0014  F203                JMP    PKF
0015  C70F  BØTH          LAM    15
0016  9A6A                STA    DNT2
0017  0353                AXP
0018  EA60  PKF           STX    DIR1
0019  B260                LDA    ZCT1
001A  9A60                STA    CT1
001B  E25B                LDX    IBC
001C  EA5F                STX    IB
001D  0110                ZAR
001E  9C00  CLR           STA    @0
001F  0128                IXR
0020  DA5A                IMS    CT1
0021  F603                JMP    CLR
0022  9A61                STA    RØN
0023  0210  NEXT          CAR
0024  9A58                STA    DIR0
0025  C7F5                LAM    245
0026  9A58                STA    DDT2
0027  C7FF                LAM    255
0028  9A55                STA    DDT
0029  FA19                JST    DURNØN
002A  FA23  DLP           JST    DØNS
002B  9A54                STA    DAT
002C  B24C                LDA    DIR1
002D  C001                CAI    1
002E  F203                JMP    STØ
002F  D24D                CMS    DIR0
0030  F232                JMP    DLP2
0031  F231                JMP    DLP2
0032  B24D  STØ           LDA    DAT
```

```
0033  E248            LDX   IB
0034  9C00            STA   @0
0035  DA46            IMS   IB
0036  DA48            IMS   DDT2
0037  F201            JMP   $+2
0038  40C7            SEL   24,7
0039  DA44            IMS   DDT
003A  F610            JMP   DLP
003B  DA48            IMS   RØN
003C  B247  DLP1      LDA   RØN
003D  2101            JAZ   $+2
003E  F100            JMP   DISD
      0000
003F  B23D  RTDA      LDA   DIRO
0040  DA40            IMS   DNT2
0041  F61E            JMP   NEXT
0042  F742            RTN   DATUM
0043  0800  DURNØN    ENT
0044  4006            CID
0045  43C1            SSN   :C1
0046  F601            JMP   $-1
0047  0E00            SBM
0048  49C1            SEN   :C1
0049  F601            JMP   $-1
004A  0F00            SWM
004B  40C4            SEL   :C4
004C  4005            CIE
004D  F70A            RTN   DURNØN
004E  0800  DØNS      ENT
004F  49C6            SEN   :C6
0050  F601            JMP   $-1
0051  5AC6            INX   :C6
0052  2843            JXZ   $-3
0053  C704            LAM   4
0054  9A2D            STA   CNT
0055  0110            ZAR
0056  9A2C            STA   MSK2
0057  F206            JMP   M2
0058  1350  M1        LLA   1
0059  9A29            STA   MSK2
005A  1351            LLA   2
005B  8A27            ADD   MSK2
005C  9A26            STA   MSK2
005D  0110            ZAR
005E  1B03  M2        LLL   4
005F  8A23            ADD   MSK2
0060  DA21            IMS   CNT
0061  F609            JMP   M1
0062  F714            RTN   DØNS
0063  DA1A  DLP2      IMS   DDT
0064  F63A            JMP   DLP
0065  F629            JMP   DLP1
0066        ØTL       REF
```

```
0106   0067   8D3A   DIRE    DATA    :8D3A
0107   0068   C6CF           TEXT    'FØRWARD, BACKWARD ØR BØTH?'
       0069   D2D7
       006A   C1D2
       006B   C4AC
       006C   C2C1
       006D   C3CB
       006E   D7C1
       006F   D2C4
       0070   A0CF
       0071   D2A0
       0072   C2CF
       0073   D4C8
       0074   BFA0
0108   0075          CRLF    REF
0109   0076          IKB     REF
0110   0077          IBC     REF
0111   0078          ERR     REF
0112   0079   0000   DIR1    DATA    0
0113   007A   F00B   ZCT1    DATA    -4085
0114   007B   0000   CT1     DATA    0
0115   007C   0000   IB      DATA    0
0116   007D   0000   DIRO    DATA    0
0117   007E   0000   DDT     DATA    0
0118   007F   0000   DDT2    DATA    0
0119   0080   0000   DAT     DATA    0
0120   0081   0000   DNT2    DATA    0
0121   0082   0000   CNT     DATA    0
0122   0083   0000   MSK2    DATA    0
0123   0084   0000   RØN     DATA    0
0124                         END
0000 ERRØRS
```

```
                  NAM    IKB,IER,BIPT,XEQ
                  NAM    ØTT,ERR,CRLF
                  NAM    ØTL,ØFPA,ØDEC
0000              REL    0
            *
            * PANIC SWITCH
            *
0000  FB00        JST    *CMND
0001        CMND  REF
            *
            *KEYBØARD INPUT
            *
0002  0800  IKB   ENT
0003  4038        SEL    7,0      AUTØ-ECHØ
0004  4039        SEL    7,1      KBD MØDE
0005  5939        RDA    7,1      READ ØN FLAG
0006  403C        SEL    7,4      RESET
0007  F705        RTN    IKB
0008  0800  IER   ENT
0009  FE07        JST    IKB
000A  C0DF        CAI    :DF      BACK ARRØW?
000B  FF0A        JST    *CMND    YES
000C  C08A        CAI    :8A      LINE FEED?
000D  FF0C        JST    *CMND    YES
000E  F706        RTN    IER      NEITHER,RETURN
            *
            *PAPER TAPE INPUT
            * DS0 = 0 FØR TTY
            * 1 FØR HSR
            *
000F  0800  BIPT  ENT
0010  5801  BIP2  ISA             READ SWITCHES
0011  13D0        LRA    1        DS0 UP FØR TTY
0012  220A        JØS    HSR      DØWN FØR HSR
0013  493B        SEN    7,3      TTY BUSY?
0014  F604        JMP    BIP2     YES
0015  403A        SEL    7,2      NØ,STEP READER
0016  4839  WT    SSN    7,1      FLAG?
0017  F203        JMP    IT       YES
0018  0150        IAR             NØ,BUMP CØUNT
0019  2149        JAZ    BIP2     RESTART IF TIME UP
001A  F604        JMP    WT       ELSE CHECK FLAG AGAIN
001B  5838  IT    INA    7,0      INPUT FRØM TTY
001C  F70D        RTN    BIPT     & RETURN
001D  4933  HSR   SEN    6,3      HSR BUSY?
001E  F60E        JMP    BIP2     YES
001F  4032        SEL    6,2      NØ, STEP READER
0020  4835  WH    SSN    6,5      FLAG?
0021  F203        JMP    IH       YES
0022  0150        IAR             NØ, BUMP CØUNT
0023  2153        JAZ    BIP2     RESTART IF TIME UP
0024  F604        JMP    WH       ELSE CHECK FLAG AGAIN
0025  5835  IH    INA    6,5      INPUT FRØM HSR
```

```
0026  F717         RTN   BIPT     & RETURN
                *
                *WAIT FØR EXECUTE SIGNAL
                *
0027  0800   XEQ   ENT
0028  FE20         JST   IER      INPUT
0029  C08D         CAI   :8D      CARRIAGE RETURN?
002A  F703         RTN   XEQ      YES, RETURN
002B  F603         JMP   XEQ+1    NØ, GET MØRE
                *
                *ØUTPUT TØ TTY
                *
002C  0800   ØTT   ENT
002D  403C         SEL   7,4      RESET INTERFACE
002E  6D3B         WRA   7,3      WRITE ØN NØT BUSY
002F  493B         SEN   7,3      DØNE?
0030  F601         JMP   $-1      NØ
0031  F705         RTN   ØTT      YES
                *
                *CØMMAND ERRØR EXIT
                *
0032  0800   ERR   ENT
0033  C6DF         LAP   :DF      PRINT ARRØW
0034  FE03         JST   ØTT
0035  FF34         JST   *CMND    RESTART CØMMAND
                *
                *CARRIAGE-RETURN,LINE FEED
                *
0036  0800   CRLF  ENT
0037  C68D         LAP   :8D      CR
0038  FE0C         JST   ØTT
0039  C68A         LAP   :8A      LF
003A  FE0E         JST   ØTT
003B  F705         RTN   CRLF
                *
                *ØUTPUT TEXT FRØM BUFFER
                *
003C  0800   ØTL   ENT
003D  8A0F         ADD   CAI      MAKE CØMPARE INSTRUCTIØN
003E  9A06         STA   ØT2      &SAVE IT
003F  9A09         STA   ØT3
0040  E704         LDX   *ØTL     GET TEXT PØINTER
0041  DE05         IMS   ØTL      SET RETURN ADDRESS
0042  B400   ØT1   LDA   0        GET WØRD
0043  11D7         RRA   8        PRINT FIRST BYTE
0044  FE13         JST   ØTT
0045  C000   ØT2   CAI   0        LAST ØNE
0046  F70A         RTN   ØTL      YES, RETURN
0047  1157         RLA   8        PRINT SECØND BYTE
0048  FE1C         JST   ØTT
0049  C000   ØT3   CAI   0        LAST ØNE?
004A  F70E         RTN   ØTL      YES RETURN
004B  0128         IXR            BUMP PØINTER
```

```
004C  F60A         JMP   ØT1       LØØP
004D  C000  CAI    CAI   0
            *
            *ØUTPUT FLØATING PØINT NUMBER
            *
004E  0800  ØFPA   ENT
004F  E701         LDX   *ØFPA     GET PØINTER
0050  DE02         IMS   ØFPA      SET RETURN ADDRESS
0051  EA01         STX   ØPT       SAVE PØINTER
0052  FB0E         JST   *FAS      CØNVERT TØ ASCII
0053  0000  ØPT    DATA  0
0054  0059         DATA  BUF
0055  0110         ZAR             SET END FLAG
0056  FE1A         JST   ØTL       PRINT NUMBER
0057  0059         DATA  BUF
0058  F70A         RTN   ØFPA
0059  0000  BUF    RES   8,0
0061        FAS    REF
            *
            * ØDEC ØUTPUT DECIMAL (+/-DDDDD)
            ** ØDEC CØNVERTS THE BINARY VALUE IN THE
            *A REG AND PRINTS IT AS A SIGNED 5
            * DIGIT DECIMAL NUMBER ØN THE TELETYPE.
            * AR AND OV ARE DESTRØYED.
            *
            * LDA VAL AR = VALUE
            * SWM  MUST BE IN WØRD MØDE
            * JST *ØDEC CALL RØUTINE
            * *** RETURN XR UNCHANGED
0062  0800  ØDEC   ENT
0063  EA19         STX   S         SAVE XR
0064  C4AB         LXP   '+'
0065  3082         JAP   $+3
0066  0310         NAR             MAKE VALUE +
0067  C202         AXI   2         MAKE SIGN -
0068  9A15         STA   V         SAVE VALUE
0069  0030         TXA
006A  FE3E         JST   ØTT       PRINT SIGN
006B  B215         LDA   STRT
006C  9A13         STA   PTR       INITIALIZE TBL PTR
006D  C705         LAM   5
006E  9A10         STA   T         SET FØR 5 DIGITS
006F  B20E  Ø1     LDA   V
0070  C4AF         LXP   :AF       ZERØ TØ -1
0071  930E         SUB   *PTR
0072  0128         IXR
0073  30C2         JAP   $-2
0074  8B0B         ADD   *PTR
0075  9A08         STA   V
0076  0030         TXA
0077  FE4B         JST   ØTT       PRINT DIGIT
0078  DA07         IMS   PTR
0079  DA05         IMS   T
```

```
0160  007A  F60B          JMP    Ø1
0161  007B  E201          LDX    S       RESTØRE XR
0162  007C  F71A          RTN    ØDEC    RETURN
0163  007D  0800  S       HLT            TEMP FØR XR
0164  007E  0800  V       HLT            VALUE
0165  007F  0800  T       HLT            CØUNT
0166  0080  0800  PTR     HLT            PØINTER
0167  0081  0082  STRT    DATA   TBL     TABLE ADDR
0168  0082  2710  TBL     DATA   10000,1000,100
      0083  03E8
      0084  0064
0169  0085  000A          DATA   10,1
      0086  0001
0170                      END
0000 ERRØRS
```

```
                          NAM   READ, PUNCH, CLEAR
                          EXTR  IKB, ØTT, BIPT, ØTL, CRLF, IER, ERR
0000                      REL   0
0000  0800        READ    ENT
0001  F900                JST   CRLF
      0000
0002  F900                JST   IER
      0000
0003  C030                CAI   '0'
0004  F203                JMP   REZE
0005  C0C7                CAI   'G'
0006  F204                JMP   RESN
0007  F900                JST   ERR
      0000
0008  E21F        REZE    LDX   IBC
0009  B21F                LDA   ZCT0
000A  F204                JMP   RDLP
000B  B21C        RESN    LDA   IBC
000C  8A1E                ADD   SN0
000D  0048                TAX
000E  B21B                LDA   ZCT1
000F  9A1C        RDLP    STA   CNT
0010  C68A                LAP   :8A
0011  F900                JST   ØTT
      0000
0012  F900                JST   BIPT
      0000
0013  2141                JAZ   $-1         SKIP LEADER
0014  F900        R1      JST   ØTT
      0000
0015  F900                JST   BIPT        READ TAPE
      0000
0016  C092                CAI   :92         END ØF LABEL
0017  F201                JMP   R2          YES
0018  F604                JMP   R1          NØ
0019  F900        R2      JST   BIPT        READ TAPE
      0000
001A  C0FF                CAI   :FF         FILE MARK
001B  F201                JMP   R3          YES
001C  F603                JMP   R2          NØ
001D  F900        R3      JST   BIPT
      0000
001E  1357                LLA   8
001F  9A0E                STA   TEMP
0020  F900                JST   BIPT
      0000
0021  A20C                IØR   TEMP
0022  8C00                ADD   @0
0023  9C00                STA   @0
0024  0128                IXR
0025  DA06                IMS   CNT
0026  F609                JMP   R3
0027  F727                RTN   READ
```

ORIGINAL PAGE IS
OF POOR QUALITY

```
0028        IBC     REF
0029  F010  ZCT0    DATA    -4030
002A  FF01  ZCT1    DATA    -255
002B  0EF1  SN0     DATA    3325
002C  0000  CNT     DATA    0
002D  0000  PNT     DATA    0
002E  0000  TEMP    DATA    0
                    *
                    * PUNCH
002F  0800  PUNCH   ENT
0030  F900          JST     CRLF
      0000
0031  F90C          JST     IER
      0000
0032  C0B0          CAI     '0'
0033  F203          JMP     PNZE
0034  C0C7          CAI     'G'
0035  F204          JMP     PNSN
0036  F900          JST     ERR
      0000
0037  E60F  PNZE    LDX     IBC
0038  B60F          LDA     ZCT0
0039  F204          JMP     PNLP
003A  B612  PNSN    LDA     IBC
003B  8E10          ADD     SN0
003C  0048          TAX
003D  B613          LDA     ZCT1
003E  9E12  PNLP    STA     CNT
003F  FA0D          JST     LEAD
0040  F900  P1      JST     IKB         ECHØ LABEL
      0000
0041  C092          CAI     :92         CTRL/TAPE
0042  F201          JMP     P2          YES
0043  F603          JMP     P1          NØ
0044  C6FF  P2      LAP     :FF         PUNCH FILE MARK
0045  F900          JST     ØTT
      0000
0046  B400  P3      LDA     @0          PUNCH BITS
0047  FA0D          JST     ØTW
0048  0128          IXR
0049  DE1D          IMS     CNT
004A  F604          JMP     P3
004B  FA01          JST     LEAD
004C  F71D          RTN     PUNCH
                    *PUNCH 5" ØF LEADER
004D  0800  LEAD    ENT
004E  C732          LAM     50
004F  9E22          STA     PNT
0050  0110          ZAR
0051  F900  L2      JST     ØTT
      0000
0052  DE25          IMS     PNT
0053  F602          JMP     L2
```

```
0054   F707            RTN    LEAD
                *
0055   0800    ØTW      ENT
0056   11D7            RRA    8
0057   F900            JST    ØTT
       0000
0058   1157            RLA    8
0059   F900            JST    ØTT
       0000
005A   F705            RTN    ØTW
               *CLEAR  PRØGRAM
005B   0800    CLEAR   ENT
005C   F900            JST    CRLF
       0000
005D   F900            JST    IER
       0000
005E   C0B0            CAI    '0'
005F   F203            JMP    CLZE
0060   C0C7            CAI    'G'
0061   F204            JMP    CLSN
0062   F900            JST    ERR
       0000
0063   E63B    CLZE    LDX    IBC
0064   B63B            LDA    ZCT0
0065   F204            JMP    CLLP
0066   B63E    CLSN    LDA    IBC
0067   8E3C            ADD    SN0
0068   0048            TAX
0069   B63F            LDA    ZCT1
006A   9E3E    CLLP    STA    CNT
006B   0110            ZAR
006C   9C00    CR      STA    @0
006D   0128            IXR
006E   DE42            IMS    CNT
006F   F603            JMP    CR
0070   F715            RTN    CLEAR
                       END
0000 ERRØRS
```

```
                        NAM    FPLØT
0000                    REL    0
0000   0800   FPLØT     ENT
0001   C70F             LAM    15
0002   9ABB             STA    NRØW
0003   B2D0             LDA    IBC
0004   9ABA             STA    IB
0005   0108             ZXR
0006   FBCF             JST    *CRLF
0007   FBD1             JST    *IER
0008   C0B0             CAI    '0'
0009   F221             JMP    FZRØ
000A   C0B1             CAI    '1'
000B   F222             JMP    FØNE
000C   C0B2             CAI    '2'
000D   F222             JMP    FTWØ
000E   C0B3             CAI    '3'
000F   F222             JMP    FTHRE
0010   C0B4             CAI    '4'
0011   F222             JMP    FFØUR
0012   C0B5             CAI    '5'
0013   F222             JMP    FFIVE
0014   C0B6             CAI    '6'
0015   F222             JMP    FSIX
0016   C0B7             CAI    '7'
0017   F222             JMP    FSEVE
0018   C0B8             CAI    '8'
0019   F222             JMP    FEIGH
001A   C0B9             CAI    '9'
001B   F222             JMP    FNINE
001C   C0C1             CAI    'A'
001D   F222             JMP    FTEN
001E   C0C2             CAI    'B'
001F   F222             JMP    FELE
0020   C0C3             CAI    'C'
0021   F222             JMP    FTWVE
0022   C0C4             CAI    'D'
0023   F222             JMP    FTHD
0024   C0C5             CAI    'E'
0025   F222             JMP    FFRTN
0026   C0C6             CAI    'F'
0027   F222             JMP    FFVTN
0028   C0C7             CAI    'G'
0029   F222             JMP    FSXTN
002A   FBAF             JST    *ERR
002B   0110   FZRØ      ZAR
002C   9A9C             STA    CALL
002D   F22A             JMP    FØØP1
002E   C601   FØNE      LAP    1
002F   F21E             JMP    FSTØ
0030   C602   FTWØ      LAP    2
0031   F21C             JMP    FSTØ
0032   C603   FTHRE     LAP    3
```

```
0033  F21A           JMP   FSTØ
0034  C604  FFØUR    LAP   4
0035  F218           JMP   FSTØ
0036  C605  FFIVE    LAP   5
0037  F216           JMP   FSTØ
0038  C606  FSIX     LAP   6
0039  F214           JMP   FSTØ
003A  C607  FSEVE    LAP   7
003B  F212           JMP   FSTØ
003C  C608  FEIGH    LAP   8
003D  F210           JMP   FSTØ
003E  C609  FNINE    LAP   9
003F  F20E           JMP   FSTØ
0040  C60A  FTEN     LAP   10
0041  F20C           JMP   FSTØ
0042  C60B  FEL E    LAP   11
0043  F20A           JMP   FSTØ
0044  C60C  FTWVE    LAP   12
0045  F208           JMP   FSTØ
0046  C60D  FTHD     LAP   13
0047  F206           JMP   FSTØ
0048  C60E  FFRTN    LAP   14
0049  F204           JMP   FSTØ
004A  C60F  FFVTN    LAP   15
004B  F202           JMP   FSTØ
004C  C610  FSXTN    LAP   16
004D  F200           JMP   FSTØ
004E  9A7A  FSTØ     STA   CALL
004F  0310           NAR
0050  9A79           STA   FRØW
0051  B26D           LDA   IB
0052  DA77  FRØNØ    IMS   FRØW
0053  F201           JMP   $+2
0054  F202           JMP   $+3
0055  8A75           ADD   H255
0056  F604           JMP   FRØNØ
0057  9A67           STA   IB
0058  B270  FØØP1    LDA   CALL
0059  2101           JAZ   $+2
005A  F204           JMP   $+5
005B  B26C           LDA   ZCT
005C  0150           IAR
005D  9A63           STA   CNT
005E  F203           JMP   $+4
005F  C7FF           LAM   255
0060  0150           IAR
0061  9A5F           STA   CNT
0062  B25C           LDA   IB
0063  9A5E           STA   IPB1
0064  B35D           LDA   *IPB1
0065  9A5E           STA   MAX
0066  DA5B  LØØP2    IMS   IPB1
0067  B35A           LDA   *IPB1
```

```
0068   D25B           CMS     MAX
0069   F201           JMP     $+2
006A   9A59           STA     MAX
006B   DA55           IMS     CNT
006C   F606           JMP     LØØP2
006D   0350           ARP
006E   9A56           STA     SCALE
006F   9A56           STA     RØUND
0070   B256           LDA     H50
0071   D252           CMS     MAX
0072   F202           JMP     $+3
0073   F20C           JMP     LØØP
0074   F20B           JMP     LØØP
0075   B24E           LDA     MAX
0076   0108           ZXR
0077   924F           SUB     H50
0078   0128           IXR
0079   31C2           JAG     $-2
007A   EA4A           STX     SCALE
007B   1200           RØV
007C   11A8           RRX     1
007D   3201           JØR     $+2
007E   0128           IXR
007F   EA46           STX     RØUND
0080   FB55   LØØP    JST     *CRLF
0081   FB54           JST     *CRLF
0082   C6BD           LAP     '='
0083   FB54           JST     *ØTL
0084   00CD           DATA    SF
0085   C6A0           LAP     ' '
0086   FB50           JST     *ØTT
0087   B23D           LDA     SCALE
0088   FB4C           JST     *ØDEC
0089   C601           LAP     1
008A   9A41           STA     RØNØ
008B   FB4A           JST     *CRLF
008C   FB49           JST     *CRLF
008D   B23E           LDA     RØNØ
008E   FB48           JST     *ØTT
008F   C7FF           LAM     255
0090   9A2F           STA     NCØL
0091   B22D           LDA     IB
0092   9A30           STA     IPB2
0093   FB42   LØØP1   JST     *CRLF
0094   B32E           LDA     *IPB2
0095   FB3F           JST     *ØDEC
0096   C6A0           LAP     ' '
0097   FB3F           JST     *ØTT
0098   C6B0           LAP     '0'
0099   FB3D           JST     *ØTT
009A   B328           LDA     *IPB2
009B   2192           JAL     CLØSE
009C   0108           ZXR
```

```
009D  9227         SUB    SCALE
009E  0128         IXR
009F  31C2         JAG    $-2
00A0  8A24         ADD    SCALE
00A1  00A8         DXR
00A2  D223         CMS    RØUND
00A3  F202         JMP    $+3
00A4  0000         NØP
00A5  0128         IXR
00A6  0030         TXA
00A7  2186         JAL    CLØSE
00A8  C6AA         LAP    '*'
00A9  0508         NXR
00AA  EA16         STX    CNT
00AB  FB2B         JST    *ØTT
00AC  DA14         IMS    CNT
00AD  F602         JMP    $-2
00AE  DA14  CLØSE  IMS    IPB2
00AF  0000         NØP
00B0  DA0F         IMS    NCØL
00B1  F61E         JMP    LØØP1
00B2  FB23         JST    *CRLF
00B3  B215         LDA    CALL
00B4  2101         JAZ    $+2
00B5  F206         JMP    FSH
00B6  C6FF         LAP    255
00B7  8A07         ADD    IB
00B8  9A06         STA    IB
00B9  DA12         IMS    RØNØ
00BA  DA03         IMS    NRØW
00BB  F628         JMP    LØØP1
00BC  FB19  FSH    JST    *CRLF
00BD  F7BD         RTN    FPLØT
00BE  0000  NRØW   DATA   0
00BF  0000  IB     DATA   0
00C0  0000  NCØL   DATA   0
00C1  0000  CNT    DATA   0
00C2  0000  IPB1   DATA   0
00C3  0000  IPB2   DATA   0
00C4  0000  MAX    DATA   0
00C5  0000  SCALE  DATA   0
00C6  0000  RØUND  DATA   0
00C7  0032  H50    DATA   50
00C8  F10F  ZCT    DATA   -3825
00C9  0000  CALL   DATA   0
00CA  0000  FRØW   DATA   0
00CB  00FF  H255   DATA   255
00CC  0000  RØNØ   DATA   0
00CD  D3C3  SF     TEXT   'SCALE FACTØR='
00CE  C1CC
00CF  C5A0
00D0  C6C1
00D1  C3D4
```

```
        00D2  CFD2
        00D3  BDA0
0209    00D4              IBC      REF
0210    00D5              ØDEC     REF
0211    00D6              CRLF     REF
0212    00D7              ØTT      REF
0213    00D8              ØTL      REF
0214    00D9              IER      REF
0215    00DA              ERR      REF
0216                               END
0000  ERRØRS
```

```
                         NAM   CRT
                         NAM   DISP
                         NAM   DISD
                         EXTR  RTDA
                         EXTR  RTTR
0000                     REL   0
0000  0800   CRT         ENT
0001  C70F               LAM   15
0002  9900               STA   NRØW
      0112
0003  49C4               SEN   24,4
0004  F601               JMP   $-1
0005  40C7               SEL   24,7
0006  0110               ZAR
0007  9900               STA   ØFFSET
      0113
0008  C601               LAP   1
0009  9900   DISP        STA   TR1
      0116
000A  3106               JAN   $+7
000B  B100               LDA   AD16
      0126
000C  8900               ADD   IBC
      0133
000D  9900               STA   IB
      0114
000E  0110               ZAR
000F  9900               STA   CALL
      0117
0010  F25F               JMP   MXMI
0011  B100               LDA   IBC
      0133
0012  9900               STA   IB
      0114
0013  0108               ZXR
0014  F900               JST   *CRLF
      8133
0015  F900               JST   *IER
      8134
0016  C0B0               CAI   '0'
0017  F221               JMP   ZERØ
0018  C0B1               CAI   '1'
0019  F222               JMP   ØNE
001A  C0B2               CAI   '2'
001B  F222               JMP   TWØ
001C  C0B3               CAI   '3'
001D  F222               JMP   THREE
001E  C0B4               CAI   '4'
001F  F222               JMP   FØUR
0020  C0B5               CAI   '5'
0021  F222               JMP   FIVE
0022  C0B6               CAI   '6'
0023  F222               JMP   SIX
```

```
0024   C0B7          CAI    '7'
0025   F222          JMP    SEVEN
0026   C0B8          CAI    '8'
0027   F222          JMP    EIGHT
0028   C0B9          CAI    '9'
0029   F222          JMP    NINE
002A   C0C1          CAI    'A'
002B   F222          JMP    TEN
002C   C0C2          CAI    'B'
002D   F222          JMP    ELE
002E   C0C3          CAI    'C'
002F   F222          JMP    TWVE
0030   C0C4          CAI    'D'
0031   F222          JMP    THD
0032   C0C5          CAI    'E'
0033   F222          JMP    FRTN
0034   C0C6          CAI    'F'
0035   F222          JMP    FVTN
0036   C0C7          CAI    'G'
0037   F222          JMP    SXTN
0038   FBFC          JST    *ERR
0039   0110   ZERØ   ZAR
003A   9ADC          STA    CALL
003B   F22E          JMP    LØØP1
003C   C601   ØNE    LAP    1
003D   F222          JMP    STØRE
003E   C602   TWØ    LAP    2
003F   F220          JMP    STØRE
0040   C603   THREE  LAP    3
0041   F21E          JMP    STØRE
0042   C604   FØUR   LAP    4
0043   F21C          JMP    STØRE
0044   C605   FIVE   LAP    5
0045   F21A          JMP    STØRE
0046   C606   SIX    LAP    6
0047   F218          JMP    STØRE
0048   C607   SEVEN  LAP    7
0049   F216          JMP    STØRE
004A   C608   EIGHT  LAP    8
004B   F214          JMP    STØRE
004C   C609   NINE   LAP    9
004D   F212          JMP    STØRE
004E   C60A   TEN    LAP    10
004F   F210          JMP    STØRE
0050   C60B   ELE    LAP    11
0051   F20E          JMP    STØRE
0052   C60C   TWVE   LAP    12
0053   F20C          JMP    STØRE
0054   C60D   THD    LAP    13
0055   F20A          JMP    STØRE
0056   C60E   FRTN   LAP    14
0057   F208          JMP    STØRE
0058   C60F   FVTN   LAP    15
```

```
0059   F206           JMP    STØRE
005A   C610   SXTN    LAP    16
005B   F204           JMP    STØRE
005C   0108   DISD    ZXR
005D   EAB8           STX    TR1
005E   E2D4           LDX    IBC
005F   EAB4           STX    IB
0060   9AB6   STØRE   STA    CALL
0061   0310           NAR
0062   9AB5           STA    RØWVA
0063   B2B0           LDA    IB
0064   DAB3   RØWNØ   IMS    RØWVA
0065   F201           JMP    $+2
0066   F202           JMP    $+3
0067   8ABB           ADD    H255
0068   F604           JMP    RØWNØ
0069   9AAA           STA    IB
006A   B2AC   LØØP1   LDA    CALL
006B   2101           JAZ    $+2
006C   F203           JMP    $+4
006D   B2AC           LDA    ZCT
006E   9AAC           STA    CNT
006F   F202           JMP    $+3
0070   C7FF   MXMI    LAM    255
0071   9AA9           STA    CNT
0072   B2A1           LDA    IB
0073   9AA8           STA    IBP1
0074   0110           ZAR
0075   9AA3           STA    MIN
0076   9AA8           STA    MAX
0077   B3A4   LØØP2   LDA    *IBP1
0078   D2A6           CMS    MAX
0079   F202           JMP    $+3
007A   9AA4           STA    MAX
007B   F203           JMP    $+4
007C   D2A1           CMS    MIN
007D   9AA0           STA    MIN
007E   0000           NØP
007F   DA9C           IMS    IBP1
0080   DA9A           IMS    CNT
0081   F60A           JMP    LØØP2
0082   0350           ARP
0083   9A9C           STA    SCALE
0084   9A9C           STA    RØUND
0085   B299           LDA    MAX
0086   9297           SUB    MIN
0087   9A97           STA    MAX
0088   B28D           LDA    TR1
0089   2106           JAZ    SCA
008A   B28C           LDA    CALL
008B   2101           JAZ    $+2
008C   F203           JMP    $+4
008D   B294           LDA    H100
```

```
008E  9A98          STA   TØTDØT
008F  F202          JMP   $+3
0090  B293   SCA    LDA   H200
0091  9A95          STA   TØTDØT
0092  B294          LDA   TØTDØT
0093  D28B          CMS   MAX
0094  F202          JMP   $+3
0095  F20C          JMP   LØØP
0096  F20B          JMP   LØØP
0097  B287          LDA   MAX
0098  0108          ZXR
0099  928D          SUB   TØTDØT
009A  0128          IXR
009B  31C2          JAG   $-2
009C  EA83          STX   SCALE
009D  1200          RØV
009E  11A3          RRX   1
009F  3201          JØR   $+2
00A0  0128          IXR
00A1  EA7F          STX   RØUND
00A2  B273   LØØP   LDA   TR1
00A3  210B          JAZ   MI
00A4  FB93          JST   *CRLF
00A5  FB92          JST   *CRLF
00A6  C6BD          LAP   '='
00A7  FB8F          JST   *ØTL
00A8  012C          DATA  SF
00A9  C6A0          LAP   ' '
00AA  FB8B          JST   *ØTT
00AB  B274          LDA   SCALE
00AC  FB8C          JST   *ØDEC
00AD  FB8A          JST   *CRLF
00AE  FB89          JST   *CRLF
00AF  B26E   MI     LDA   MIN
00B0  0310          NAR
00B1  0108          ZXR
00B2  926D          SUB   SCALE
00B3  0128          IXR
00B4  31C2          JAG   $-2
00B5  8A6A          ADD   SCALE
00B6  00A8          DXR
00B7  D269          CMS   RØUND
00B8  F202          JMP   $+3
00B9  0000          NØP
00BA  0128          IXR
00BB  EA6C          STX   X1
00BC  B26B   LØØP4  LDA   X1
00BD  9A6B          STA   X
00BE  C7FF          LAM   255
00BF  9A59          STA   NCØL
00C0  B253          LDA   IB
00C1  9A5B          STA   IBP2
00C2  B250   LØØP3  LDA   ØFFSET
```

```
00C3  8A65          ADD   X
00C4  9A66          STA   TØTØFF
00C5  B357          LDA   *IBP2
00C6  1200          RØV
00C7  1150          RLA   1
00C8  2207          JØS   NEG
00C9  11D0          RRA   1
00CA  0108          ZXR
00CB  9254          SUB   SCALE
00CC  0128          IXR
00CD  31C2          JAG   $-2
00CE  8A51          ADD   SCALE
00CF  F206          JMP   $+7
00D0  1400   NEG    SØV
00D1  11D0          RRA   1
00D2  0108          ZXR
00D3  8A4C          ADD   SCALE
00D4  00A8          DXR
00D5  20C2          JAN   $-2
00D6  9249          SUB   SCALE
00D7  00A8          DXR
00D8  D248          CMS   RØUND
00D9  F202          JMP   $+3
00DA  0000          NØP
00DB  0128          IXR
00DC  0030          TXA
00DD  9A4C          STA   DØTNØ
00DE  E24C          LDX   TØTØFF
00DF  49C4   DØT    SEN   24,4
00E0  F601          JMP   $-1
00E1  49C2          SEN   24,2
00E2  F601          JMP   $-1
00E3  6EC2          ØTX   24,2
00E4  B231          LDA   TR1
00E5  2108          JAZ   $+9
00E6  B230          LDA   CALL
00E7  2101          JAZ   $+2
00E8  F205          JMP   $+6
00E9  B240          LDA   DØTNØ
00EA  8A40          ADD   TØTØFF
00EB  0048          TAX
00EC  6EC2          ØTX   24,2
00ED  F20B          JMP   DØNE
00EE  B23B          LDA   DØTNØ
00EF  2109          JAZ   DØNE
00F0  3184          JAG   PØS
00F1  00A8          DXR
00F2  0150          IAR
00F3  9A36          STA   DØTNØ
00F4  F615          JMP   DØT
00F5  0128   PØS    IXR
00F6  00D0          DAR
00F7  9A32          STA   DØTNØ
```

```
00F8   F619             JMP    DØT
00F9   B22F   DØNE      LDA    X
00FA   8A2A             ADD    H256
00FB   9A2D             STA    X
00FC   DA20             IMS    IBP2
00FD   DA1B             IMS    NCØL
00FE   F63C             JMP    LØØP3
00FF   B216             LDA    TR1
0100   3104             JAN    $+5
0101   B215             LDA    CALL
0102   2101             JAZ    $+2
0103   F100             JMP    RTDA
       0000
0104   F100             JMP    RTTR
       0000
0105   B211             LDA    CALL
0106   2101             JAZ    $+2
0107   F203             JMP    FIN
0108   C60A             LAP    10
0109   8A09             ADD    ØFFSET
010A   9A08             STA    ØFFSET
010B   B217             LDA    H255
010C   8A07             ADD    IB
010D   9A06             STA    IB
010E   DA03             IMS    NRØW
010F   F653             JMP    LØØP4
0110   FB27   FIN       JST    *CRLF
0111   F100             RTN    CRT
       8000
0112   0000   NRØW      DATA   0
0113   0000   ØFFSET    DATA   0
0114   0000   IB        DATA   0
0115   0000   IBQ       DATA   0
0116   0000   TR1       DATA   0
0117   0000   CALL      DATA   0
0118   0000   RØWVA     DATA   0
0119   0000   NCØL      DATA   0
011A   F10E   ZCT       DATA   -3826
011B   0000   CNT       DATA   0
011C   0000   IBP1      DATA   0
011D   0000   IBP2      DATA   0
011E   0000   MIN       DATA   0
011F   0000   MAX       DATA   0
0120   0000   SCALE     DATA   0
0121   0000   RØUND     DATA   0
0122   0064   H100      DATA   100
0123   00FF   H255      DATA   255
0124   00C8   H200      DATA   200
0125   0100   H256      DATA   256
0126   0EF1   AD16      DATA   3825
0127   0000   TØTDØT    DATA   0
0128   0000   X1        DATA   0
0129   0000   X         DATA   0
```

```
0305   012A   0000   DØTNØ   DATA   0
0306   012B   0000   TØTØFF  DATA   0
0307   012C   D3C3   SF      TEXT   'SCALE FACTØR='
       012D   C1CC
       012E   C5A0
       012F   C6C1
       0130   C3D4
       0131   CFD2
       0132   BDA0
0308   0133          IBC     REF
0309   0134          IER     REF
0310   0135          ERR     REF
0311   0136          ØTT     REF
0312   0137          ØTL     REF
0313   0138          CRLF    REF
0314   0139          ØDEC    REF
0315                         END
0000 ERRØRS
```

PAGE 0001

```
                       NAM    MASKO
0000                   REL    0
0000  0001  MASKO      DATA   1
0001  0001             DATA   1
0002  0001             DATA   1
0003  0001             DATA   1
0004  FFFF             DATA   -1
0005  0001             DATA   1
0006  FFFF             DATA   -1
0007  0001             DATA   1
0008  0001             DATA   1
0009  FFFF             DATA   -1
000A  FFFF             DATA   -1
000B  0001             DATA   1
000C  FFFF             DATA   -1
000D  FFFF             DATA   -1
000E  FFFF             DATA   -1
000F  0001             DATA   1
0010  0001             DATA   1
0011  0001             DATA   1
0012  0001             DATA   1
0013  FFFF             DATA   -1
0014  0001             DATA   1
0015  FFFF             DATA   -1
0016  0001             DATA   1
0017  0001             DATA   1
0018  FFFF             DATA   -1
0019  FFFF             DATA   -1
001A  0001             DATA   1
001B  FFFF             DATA   -1
001C  FFFF             DATA   -1
                       END
0000 ERRØRS
```

```
0001                          NAM    IBC
0002  0000                    REL    0
0003  0000  0000  IBC         DATA   0000
0004                          END
0000 ERRORS
```

APPENDIX D


```
1      DEF FNR(X)=INT(100*X+0.5)/100
10     DIM Ø(255),F(255),X(255)
20     PRINT "SPECTRUM CØRRECTED FØR NEGETIVE DIP"
25     PRINT
26     PRINT
30     CALL (20)
40     CALL (5,Ø(0),256,2)
50     LET F(0)=Ø(0)
60     FØR N=1 TØ 255
70     LET I1=N-1
75     IF I1>0 THEN 85
80     LET I1=255
85     LET I2=N+1
90     IF I2<256 THEN 100
95     LET I2=I2-255
100    LET I3=N+24
105    IF I3<256 THEN 115
110    LET I3=I3-255
115    LET I4=N+25
120    IF I4<256 THEN 130
125    LET I4=I4-255
130    LET C=(Ø(I3)+Ø(I4)-Ø(I1)-Ø(I2))/20
140    LET F(N)=Ø(N)+C
150    NEXT N
160    PRINT "A: 1 FØR DISPLAY, 2 FØR GRAPH, 3 FØR TAPE"
170    PRINT "B: 0 FØR ØRIGINAL, 1 FØR FINAL"
180    PRINT
200    PRINT "A=";
210    INPUT A
220    PRINT "B=";
230    INPUT B
240    PRINT "RESØLUTIØN D=";
250    INPUT D
260    PRINT "INITIAL WAVE LENGTH L0=";
270    INPUT L0
280    PRINT
290    PRINT
300    IF A=3 THEN 730
310    LET Z=0
320    LET M=1E10
330    FØR N=1 TØ 255
```

```
350   IF B=1 THEN 400
360   LET X(N)=Ø(N)
370   GØTØ 410
400   LET X(N)=F(N)
410   IF X(N)>=M THEN 430
420   LET M=X(N)
430   IF X(N)<=Z THEN 450
440   LET Z=X(N)
450   NEXT N
460   IF M>=0 THEN 510
470   LET S0=255/(Z-M)
480   LET S1=48/(Z-M)
490   LET Y0=-M*S
500   GØTØ 540
510   LET S0=255/Z
520   LET S1=48/Z
530   LET Y0=0
540   PRINT "MAX=";Z;"MIN=";M
550   IF A=2 THEN 630
560   PRINT "SCALE FACTØR=";S0
570   FØR N=1 TØ 255
580   LET E=INT(S0*X(N)+0.5)
590   CALL (3,N,Y0,2,E)
600   NEXT N
620   GØTØ 160
630   PRINT "SCALE FACTØR="; S1
635   PRINT
636   PRINT
640   FØR N=1 TØ 255
650   LET E=INT(S1*X(N)+0.5)
660   LET L=L0+(N-1)*D
670   PRINT FNR(L);TAB(8);X(N)
715   NEXT N
730   IF B=0 THEN 760
740   IF B=1 THEN 780
750   GØTØ 200
760   CALL(6,Ø(0),256,2)
770   GØTØ 790
780   CALL(6,F(0),256,2)
790   CALL(6,0,0,3)
800   STØP
```

BIBLIOGRAPHY

1. Aitken, D.K., and Jones, B., (1972), Nature, 240, 230.
2. Allen, J.D., Jr., and Schweitzer, G.K., (1972, 1973), J. Electron Spectroscopy 1, 509.
3. Baumert, L.D., (1964), Digital Communication with Space Application, Prentice-Hall Inc., Canada, S.W. Golomb, Ed. pp.17-32.
4. Combes, M., Encrenaz, TH., Vapillon, L., and Ze'au, Y., (1974), Astron & Astrophys, 34, 33.
5. Colpa, J.P., and Keltelaar, J.A.A.,(1958), Mol. Phys., 1,14.
6. Cudaback, D.D., and Gaustad, J.E., (1971), 166, L49.
7. Day, K.L., (1974), Ap.J., 192, L15.
8. Decker, J.A., Jr., and Harwit, M., (1968), Appl. Opt., 7, 2205.
9. Decker, J.A., Jr., (1969), Appl. Opt., 8, 2552.
10. Decker, J.A., Jr., (1971), Appl. Opt., 10, 510.
11. Decker, J.A., Jr., (1974), Appl. Opt., 13, 1296.
12. Encrenaz, Th., (1972), Astron and Astrophys, 16, 237.
13. Fellgett, P., (1951), Cambridge Univ., PH.D. thesis.
14. Fellgett, P., (1958), J. Phys., 19, 187.
15. Fink, U., Larson, H.P., and Poppen, R.F., (1974), Ap.J., 187, 407.
16. Finkbeiner, D.T., II(1960), Introduction to Matrices and Linear Transformations, W.H. Freeman and Co., San Francisco.

17. Gamown, R.H., Gaustad, J.E., and Treffers, R.R., (1973), Ap.J., 175, 687.

18. Gillett, F.C., Low, F.J., and Stein, W.A., (1968), Ap.J., 154,677.

19. Gillett, F.C., Low, F.J., and Stein, W.A., (1969), Ap.J., 157, 925.

20. Gilman, R.C., (1969), Ap.J., 155, L185.

21. Golay M.J.E., (1949), J. Opt. Soc. Amer. 39, 437.

22. de Graauw, Th., Veltman, B.P. Th., (1970), Appl. Opt., 9, 2658.

23. Hall, M., Jr., (1967), Combinational Theory, Blaisdell Publ. Co., Waltham, Mass., 204.

24. Harwit, M., Phillips, P.G., Fine, T., and Sloane, N.J.A., (1970), Appl. Opt., 9, 1149.

25. Harwit, M., (1971), Appl. Opt., 10, 1415.

26. Harwit, M., (1973), Appl. Opt., 12, 285.

27. Harwit, M., Phillips, P.G., King, L.W., and Briotta, D.H., (1974a), Appl. Opt., 13, 2669.

28. Harwit, M., and Decker, J.A., Jr., (1974b), Progress in Optics XII, North-Holland.

29. Hirschfeld, T., and Wijntjes, G., (1973), Appl. Opt., 12, 2876.

30. Hirschfeld, T., and Wijntjes, G., (1974), Appl. Opt., 13, 1740.

31. Hirschy, V.L., and Aldridge, J.P., (1971), Rev. Sci. Inotrum. 42, 381.

32. Hotelling, H., (1944), Ann. Math. Stat. 15, 297.

33. Houck, J., Pollack, J.B., Schaack, D., Sagan, C., and Decker, J.A., (1973), Icarus, 18, 470.

34. Ibbett, R.N., Aspinall, D., Grainger, J.F., (1968), Appl. Opt., 7, 1089.

35. Ingersoll, A.P., submitted to space Sci. Rev. July, 1975.

36. Jacquinot, P., (1954), J.O.S.A., 44, 761.

37. Jacquinot, P., (1960), Rep. Prog. Phys., 23, 267.

38. Kittel, C., (1966), Introduction to Solid State Physics, John Wiley and Sons, N.Y., 548.

39. Kowalski, B.R., and Bender, C.F., (1973), Anal. Chem. 45, 2234.

40. Kranendonk, J.Van. and Kiss, Z.J., (1959), Can. J. Phys., 37, 1187.

41. Lacy, J.H., Larrabee, A.I., Wollman, E.R., Geballe, T.R., Townes, L.H., Bregman, J.D., and Rank, D.M., (1975), Ap. J., 198, L145.

42. Larson, N., Crosmun, R., and Taimi, Y., (1974), Appl. Opt., 13, 2662.

43. Lewis, J.S., and Prinn, R.G., (1970), Science, 169, 472.

44. Linsky, J.L., (1973), Ap.J., Supp., 216, 25, 163.

45. Low, F.J., and Swamy, K.S.K., (1970), Nature, 227, 1333.

46. Maas, R.W., Ney, E.P., and Woolf, N.J., (1970), Ap.J., letters, 160, L101.

47. McCord, T.B., and Adams, J.B., (1972), Icarus, 17, 585.

48. McElroy, M.B., (1973), Space Sci. Rev., 14, 460.

49. Mertz, L., (1965), Transformation in Optics, John Wiley and Sons, Inc., N.Y.

50. Mertz, L., (1976) Private communication.

51. Mertz, L., and Flamand, J., (1976), Private communication.

52. Morrison, D., and Sagan, C., (1967), Ap.J., 150, 1105.

53. Morrison, D., (1970), Spa. Sci. Rev., 11, 271.

54. Murcray, F.H., Murcray, D.G., and Williams, W.J., (1970), J. Geo. Res. 75, 14, 2662.

55. Murdock, T.L., (1974), Ap.J., 79, 1457.

56. Nelson, E.D., and Fredman, M.L., (1970), J.O.S.A., 60, 1664.

57. Oliver, C., and Pike, E., (1974), Appl. Opt., 13, 158.

58. Penman, (1976), Mon. Not. R. Astr.Soc., 175, 149.

59. Pettingill, G.H., and Dyce, R.B., (1965), Nature, 206, 1240.

60. Phillips, P.G., and Harwit, M., (1971), Appl. Opt., 10, 1415.

61. Planky, F.W., Winefordner, J.D., (1974), paper No.200, Pittsburgh Conference on Analytical Chemistry and Applied Spectroscopy.

62. Podolak, M., and Cameron, A.F.W., (1974), Icarus, 22, 123.

63. Pratt, W.K., Kane, J., and Andrew, H.C., (1969), Proc IEEE, 57, 58.

64. Putley, E.H., (1964), Phys, Stat. Solidi, 6, 571.

65. Rage and Sagan, C., (1977), in preparation.

66. Ridgway, S.T., (1974), Ap.J., 187, L41.

67. Sagan, C., and Salpeter, E.E., (1976), Ap.J., Suppl 76.

68. Saiedy, F., and Goody, R.M., (1959) R.A.S.M.N. 119, 213.

69. Salpeter, E.E., (1974a), Ap.J., 193, 579.

70. Salpeter, E.E., (1974b), Ap.J., 193, 585.

71. Sloane, N.J.A., Fine, T., Phillips, P.G., and Harwit M., (1969), Appl. Opt., 8, 2103.

72. Sloane, N.J.A., and Harwit, M., (1976), Appl. Opt., 15, 107.

73. Smith, L.G., (1949), J. Chem. Phys., 17, 139.

74. Soter, S.L., and Ulrichs, J., (1967), Nature, 214, 1315.

75. Stewart, J.E., (1970), Infrared Spectroscopy: Experimental Methods and Techniques, Marcel Dekper, Inc., N.Y.

76. Strobel, D.F., (1973), J. Atmos, Sci., 30, 489.

77. Swift, R.D., Wattson, R.B., Decker, J.A., Paganetti, R., and Harwit, M., (1976), Appl. Opt., 15, 1595.

78. Tai, M.H., Briotta, D.A., Kamath, N.S., and Harwit, M., (1975a), Appl. Opt., 14, 2533.

79. Tai, M.H., Harwit, M., and Sloane, N.J.A., (1975b), Appl. Opt., 14, 2678.

80. Terrile, R.J., and Westphal J.A., (1976), preprint.

81. Trafton, L.M., and Münch, G., (1969), J. Atm. Sci., 26, 813.

82. Treffers, R., and Cohen, M., (1974), Ap.J., 188, 545.

83. Vanasse, G.A., Sakai, H., (1967), Progress in Optics, 7, 298, E. Wolf, Ed., Wiley-Interscience, N.Y.

84. Vanasse, G.A., (1974), Application of Walsh Functions and Sequency Theory. The Institute of Electronic Engineering, Inc., New York, N.Y. 10017.

85. de Vancouleurs, G., (1964), Icarus, 3, 187.

86. Wallace, L., Caldwell, J.J., and Savage, B.D., (1972), Ap. J., 172, 755.

87. Wallace, L. Prather, M., and Belton, M.J.S., (1974), Ap.J., 193, 481.

88. Weidenschilling, S.J., and Lewis, J.S., (1973), Icarus, 20, 465.

89. Woolf, N.J., and Ney, E.P., (1969), Ap.J., 155, L181.

90. Wyatt, C., and Esplin, R., (1974), Appl. Opt., 13, 2651.